AD-A134 547 EFFECT OF BLADE STRUCTURAL PARAMETERS ON HELICOPTER 1/1
VIBRATIONAL CHARACTER..(U) WASHINGTON UNIV ST LOUIS MO
DEPT OF MECHANICAL ENGINEERING D A PETERS OCT 83
UNCLASSIFIED ARO-14585.4-EG DAAG29-80-C-0092 F/G 1/3 NL

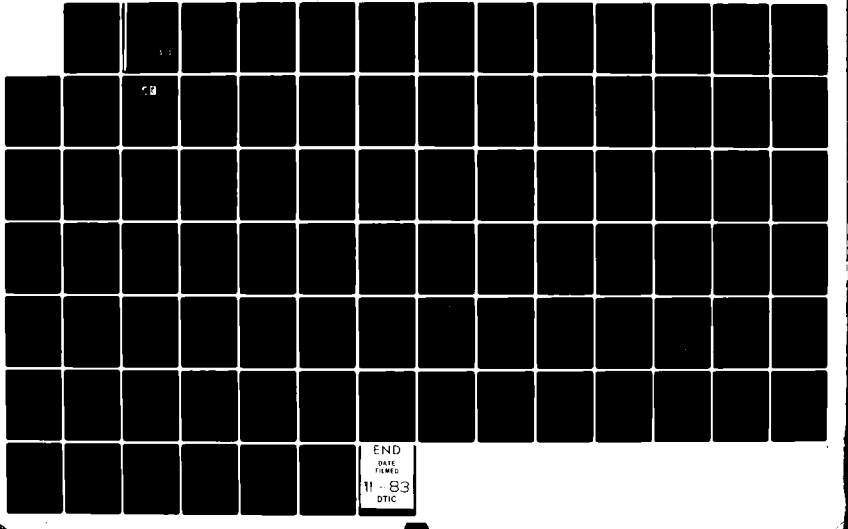

END
DATE FILMED
11-83
DTIC

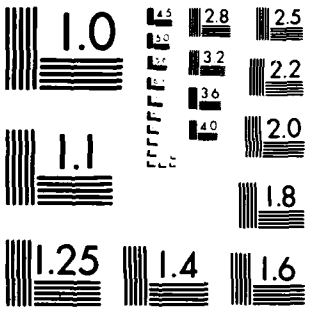

MICROCOPY RESOLUTION TEST CHART
NATIONAL BUREAU OF STANDARDS 1963-A

(12) ARO 14585.4-EG and 17067.8-EG

EFFECT OF BLADE STRUCTURAL PARAMETERS ON HELICOPTER VIBRATIONAL CHARACTERISTICS

Final Technical Report
Report No. 3

by

David A. Peters
Principal Investigator

October 1983

U. S. Army Research Office
Grant Nos.: DAAG-29-77-G-0103
DAAG-29-80-C-0092

Washington University
School of Engineering and Applied Science
St. Louis, Missouri

Approved for Public Release
Distribution Unlimited

EFFECT OF BLADE STRUCTURAL PARAMETERS ON HELICOPTER VIBRATIONAL CHARACTERISTICS

Final Technical Report
Report No. 3

by

David A. Peters
Principal Investigator

October 1983

U. S. Army Research Office
Grant Nos.: DAAG-29-77-G-0103
DAAG-29-80-C-0092

Washington University
School of Engineering and Applied Science
St. Louis, Missouri

The view, opinions, and/or findings contained in this report are those of the author(s) and should not be construed as an official Department of the Army position, policy, or decision, unless so designated by other documentation.

SECURITY CLASSIFICATION OF THIS PAGE (When Data Entered)

REPORT DOCUMENTATION PAGE		READ INSTRUCTIONS BEFORE COMPLETING FORM
1. REPORT NUMBER 3	2. GOVT ACCESSION NO. AD A134541	3. RECIPIENT'S CATALOG NUMBER
4. TITLE (and Subtitle) Effect of Blade Structural Parameters on Helicopter Vibrational Characteristics		5. TYPE OF REPORT & PERIOD COVERED Final Report 1 March 1977-August 1983 6. PERFORMING ORG. REPORT NUMBER
7. AUTHOR(s) David A. Peters		8. CONTRACT OR GRANT NUMBER(s) DAAG-29-77-G-0103 DAAG-29-80-C-0092
9. PERFORMING ORGANIZATION NAME AND ADDRESS Department of Mechanical Engineering Washington University, Campus Box 1185 St. Louis, MO 63130		10. PROGRAM ELEMENT, PROJECT, TASK AREA & WORK UNIT NUMBERS NA
11. CONTROLLING OFFICE NAME AND ADDRESS U.S. Army Research Office Post Office Box 12211 Research Triangle Park, NC 27709		12. REPORT DATE October 1983 13. NUMBER OF PAGES 72
14. MONITORING AGENCY NAME & ADDRESS(if different from Controlling Office) Office of Naval Research Branch Office Chicago 536 South Clark Street Chicago, IL 60605		15. SECURITY CLASS. (of this report) Unclassified 15a. DECLASSIFICATION/DOWNGRADING SCHEDULE NA

16. DISTRIBUTION STATEMENT (of this Report)

Approved for public release; distribution unlimited.

17. DISTRIBUTION STATEMENT (of the abstract entered in Block 20, if different from Report)

NA

18. SUPPLEMENTARY NOTES

The view, opinions, and/or findings contained in this report are those of the author(s) and should not be construed as an official Department of the Army position, policy, or decision, unless so designated by other documentation.

19. KEY WORDS (Continue on reverse side if necessary and identify by block number)

Helicopter, Vibration, Structures

20. ABSTRACT (Continue on reverse side if necessary and identify by block number)

See Page i

DD FORM 1 JAN 73 1473 EDITION OF 1 NOV 65 IS OBSOLETE

Unclassified

SECURITY CLASSIFICATION OF THIS PAGE (When Data Entered)

Abstract (Block 20)

This final report covers 6 1/2 years of ARO-sponsored research into the fundamental mechanisms of rotor vibrations. This research effort has spanned several areas of vibration analysis including structural coupling, rotor-body interaction, dynamic stall, and the computational problems associated therewith (especially rotor trim). There were 16 graduate assistants with the project. Four received doctor's degrees, eight received master's degrees, and four are now working on degrees. Publications from the project include eight technical papers, nine theses, two technical reports, four invited lectures, and eleven presentations at student paper conferences. The main body of this report consists of reprints of some of these papers.

Table of Contents

		Page No.
1.	Introduction.	1
2.	Statement of Problem.	2
3.	Scientific Personnel and Degrees.	3
4.	Publications and Reports.	4
5.	Summary of Results.	8

EFFECT OF BLADE STRUCTURAL PARAMETERS ON HELICOPTER VIBRATIONAL CHARACTERISTICS

1. INTRODUCTION

This document represents the Final Technical Report on two Army Research Office Grants, DAAG-29-77-G-0103 and DAAG-29-80-C-0092, each of which is entitled as per the title of this report. The first proposal was sent on 8 July 1976, and the award began on March 1, 1977. This was to be a three-year proposal. However, the principal investigator spent a summer at the Army Aeromechanics Laboratory; and a no-cost extension was consequently granted to 30 June 1980 (a 40-month period). The second proposal was sent on 1 July 1979 and the grant was awarded on 1 July 1980. Again, the grant period was initially three years; but a no-cost extension was granted to 31 August 1983 (a 38-month period). Thus, the two grants together span a period of 78 months, or 6 1/2 years.

Because of the continuing nature of the second grant, the Army Research Office waived the Final Report for the first grant with the understanding that a final comprehensive report would be submitted at the end of the second grant. (Reference ARO letter dated 23 June 1980 DRXRO-PR, P-14585-E, P-17067-E.) Therefore, this present document is the comprehensive report that covers the entire period. This report treats the two grants as a single unit, and no attempt is made to discriminate work done before July 1980 from work done after July 1980.

2. Statement of Problem

The major objectives of our research project have been as follows:

1) Discover the basic relationships between structural parameters and the blade vibrational characteristics.

2) Determine the degree of sophistication that is required to adequately model the more important mechanisms.

3) Develop efficient computational methods suitable to solving the rotor trim and vibration problem.

Along these lines, our work has taken a "building block" approach to these objectives. In other words, the statement of work in each proposal outlines small research tasks, each of which studies a particular aspect in detail. When two or more of these tasks are completed, the results are combined together to produce the next level of analysis. At each step, the lessons learned in the previous steps are used to simplify the analysis as much as possible before combining with another analysis.

In the area of blade structural vibrations, two separate branches have been pursued. One is the modeling of blade structural response. This has progressed from rigid blade to elastic flap-lag to elastic flap-lag-torsion. The second branch has dealt with problems of rotor-body coupling. Here, we have progressed from a vertical model to vertical-roll-pitch to a complete 9-degree-of-freedom elastic fuselage. We have studied both modal and finite-element approaches.

In the area of aeroelastic modeling, we have been working on the application of simple dynamic stall models to improve the estimation of aerodynamic loads. There are many sophisticated stall tools that do not lend themselves to practical research calculations, but we have limited ourselves to methods that lend themselves to linearization.

One area of our work that greatly expanded over original estimates is the study of rotor trim methods. We have applied trim methods over the entire spectrum of possible strategies. These include harmonic balance, numerical integration, automatic pilot, Newton-Raphson, periodic shooting, and Floquet techniques.

Finally, because of the close relationship between stability, vibration, and transition matrices, we have studied efficient calculation and use of the Floquet transition matrix. In all of the above areas, there is a strong synergistic relationship among the areas. Each task has fed the other tasks in terms of applications and solutions.

3. Scientific Personnel and Degrees

In addition to the principal investigator, 16 students have worked on the project during the past 6 1/2 years. Of these 16 students, 12 received advanced degrees and three are still working on their degrees. Of the 12 degree recipients, four took positions with the U. S. Army or helicopter industry, four took positions in the U. S. aerospace industry, and four have continued here to work on more advanced degrees. Below is a listing of these students.

Name	Degree	Date	Present Status
Harry Woehrle	M.S.	12-77	U.S. Army
Daniel Schrage	D.S.	7-78	U.S. Army
Abraham Eipe	D.S.	12-79	Douglas Aircraft
Amir Izadpanah	M.S.	12-79	Working on D.S.
Byung Kim	M.S.	5-80	Working on D.S.
Timothy Ko	M.S.	5-80	Working on D.S.
Tom Hsu	D.S.	12-80	Sundstrand
S-Y Chen	D.S.	8-81	Kaman Aerospace
H-S Chen	M.S.	12-81	MTS Corp.
Jon Rogers	M.S.	5-82	U.S. Army
Dan Rudy	M.S.	5-83	Emerson Space Div.
M-S. Huang	M.S.	5-83	Working on D.S.
Tim Ryan	M.S.	8-83	McDonnell Aircraft
James O'Malley	M.S.	5-84	U.S. Army
Swami Karunamoorthy	-	-	Working on D.S.
Sirajul Iqbal	-	-	Unknown

4. Publications and Reports

Throughout this project, we have published the results of our research in several media. First, we have published technical papers in refereed journals and in conference proceedings. Second, we have produced Master's and Doctoral theses. Third, we have published ARO interim reports. Fourth, we have participated in the annual Robert R. Lichten paper contest. In the eight years of this contest, Washington University students have won the National Award four times. The most recent of these was for work on the ARO grant. Below is a list of the pertinent publications.

Technical Papers

1. Schrage, D. P. and Peters, D. A., "Comparison of the Effect of Structural Coupling Parameters on Flap-Lag Forced Response and Stability of a Helicopter Rotor Blade in Forward Flight," Army Science Conference, West Point, New York, June, 1978.

   Schrage, D. P. and Peters, D. A., "Effect of Structural Coupling Parameters on the Flap-Lag Forced Response of a Rotor Blade in Forward Flight Using Floquet Theory," Fourth European Rotorcraft and Powered Lift Aircraft Forum, Stresa, Italy, September 1978; Vertica, Vol. 3, No. 6, June 1979.

2. Hsu, T-K and Peters, D. A., "Coupled Rotor/Airframe Vibration Analysis by a Combined Harminic-Balance, Impedance-Matching Method," 36th Annual National Forum of the American Helicopter Society, May 1980, JAHS, Vol. 27, January 1982.

3. Peters, David A. and Kum, Byung S., "Control Settings for a Trimmed, Stalled Rotor by an Automatic Feedback System," AIAA Dynamics Specialists' Conference, Atlanta, Georgia, April 1981, AIAA Paper No. 81-0617-CP.

   Peters, D. A., Kim, Byung S., and Chen, H-S, "Calculation of Trim Settings for a Helicopter Rotor by an Optimized Automatic Control," Journal of Guidance and Control, 1983.

4. Peters, David A. and Izadpanah, Amir, "Helicopter Trim by Periodic Shooting with Newton-Raphson Iteration," 37th Annual Forum of the American Helicopter Society, New Orleans, Louisiana, May 1981, Paper 81-23.

5. Roger, Jon P., "Application of a Dynamic Stall Model to Dynamic Analysis of Rotor Blades," Proceedings of the 38th Annual National Forum of the American Helicopter Society, Proceedings of the 8th European Rotorcraft Forum, 1982, Journal of the AHS, 1984.

6. O'Malley, James P., Izadpanah, Amir, and Peters, David A., "Comparison of Three Numerical Trim Methods for Rotor Airloads," Ninth European Rotorcraft Forum, Stresa, Italy, September 13-15, 1983; Vertica 1984.

Theses

1. Schrage, D. P., Effect of Structural Parameters on the Flap-Lag Forced Response of a Rotor Blade in Forward Flight, Doctor of Science Thesis, Washington University, May 1978.

2. Eipe, Abraham, Effect of Blade Flexibility, Structural Parameters, and Trim Conditions on Rotor Loads, Doctor of Science Thesis, Washington University, December 1979.

3. Izadpanah, Amir, Calculation of Helicopter Trim and Air Loads by the Method of Periodic Shooting, Master of Science Thesis, Washington University, December 1979.

4. Kim, Byung, Helicopter Rotor Trim by an Automatic Feedback System, Master of Science Thesis, Washington University, May 1980.

5. Ko, Timothy, Use of Tapered, Twisted Finite Elements for Dynamic Analysis of Helicopter Rotors, Master of Science Thesis, Washington University, May 1980.

6. Hsu, Tung-Kuang, Coupled Rotor Airframe Vibration Analysis by a Combined Harmonic-Balance, Impedance-Matching Method, Doctor of Science Thesis, Washington University, August 1981.

7. Rogers, Jon P., Application of an Analytic Stall Model to Dynamic Analysis of Rotor Blades, Master of Science Thesis, Washington University, May 1982.

8. Rudy, Daniel J., Three Interpretations of a Dynamic-Stall Model with Applications to Rotor Blade Flapping Response, Master of Science Thesis, Washington University, May 1983.

9. Huang, Ming-Sheng, Analysis of Helicopter Vibrations with Inplane Degrees of Freedom, Master of Science Thesis, Washington University, August 1983.

Contractor Reports

1. Peters, David A. and Schrage, Daniel P., "Effect of Blade Structural Parameters on the Flap-Lag Response of a Rotor Blade in Forward Flight," Interim Technical Report No. 1, ARO Grant DAAG-29-77-G-0103, July 1978.

2. Peters, D. A. and Chen, H-S, "Optimization of Auto-Pilot Equations for Rapid Estimation of Helicopter Control Settings, Interim Technical Report No. 1, ARO Grant DAAG-29-80-C-0092, November 1981.

Invited Lectures

1. Peters, David A., "Some Mathematical Approaches for Prediction of Rotorcraft Vibrations," presented at the ARO Rotorcraft Vibration Workshop, NASA Ames Research Center, February 1978.

2. Peters, David A., "Some Aspects of Rotor Trim," presented at the ARO Workshop on Unified Equations, February 1979.

3. Peters, David A., "Helicopter Research at Washington University, Flutter and Dynamics Council, Denver, Colorado, November 1982.

4. Peters, David A., "The Importance of Steady and Dynamic Inflow on the Stability of Rotor-Body Systems," ITR Methodology Assessment Workshop, Ames Research Center, June 1983.

Lichten Presentations

1. Hsu, Tung-Kuang, "Effect of Rotor-Body Coupling on Helicopter Vibration," 1979.

2. Kim, Byung S., "Helicopter Trim by an Automatic Pilot," 1980.

3. Ko, Timothy, "Use of Tapered, Twisted, Finite Elements for Rotor Blades," 1980.

4. Chen, S-Y, "Dynamic Analysis of a Two-Bladed, Teetering Rotor on a Flexible Pylon," 1980.

5. Roger, Jon, "Application of an Analytic Stall Model to Dynamic Analysis of Rotor Blades," 1982.

6. O'Malley, James, "Application of Periodic Shooting to an Existing Air Loads Program," 1982.

7. Izadpanah, Amir, "The Convergence of a Periodic Shooting Algorithm for Rotor Trim," 1982.

8. Rudy, Daniel, "Three Interpretations of the ONERA Dynamic-Stall Model," 1983.

9. Ort, Jack, "Application of Hamilton's Law of Varying Action to Calculation of the Floquet Transition Matrix," 1983.

10.* Karunamoorthy, S., "Derivation of a Hierarchy of Elastic Blade Equations for Helicopter Vibration Analysis," 1983.

11.* Huang, M-S, "Analysis of Helicopter Vibrations with Inplane Degrees of Freedom," 1983.

---

*Also presented at the AIAA Student Conference, U.S. Air Force Academy, Colorado Springs, April 14-15, 1983.

5. Summary of Results

We here follow the suggestion of Reporting Procedures for Contractors and Grantees of the U.S. Army Research Office, ARO Form 18, and present the major results of our work in the form of reprints. Results not presented here appear in the interim reports of these grants. The first of these showed that elastic coupling could be used to lower inplane loads, pitch-flap coupling could be used to lower flap loads, and pitch-lag coupling could then be used for stability margins. The second of these showed that rotor trim could be obtained by an automatic pilot in only five rotor revolutions.

The reprints given here represent summaries of the other major areas of research. The first paper, by Tom Hsu, summarizes the work on rotor-body coupling. The second paper, by Jon Rogers, summarizes the work on dynamic stall. Finally, the paper by O'Malley, Izadpanah, and Peters summarizes the trim studies.

Coupled Rotor/Airframe Vibration Analysis by a Combined Harmonic-Balance, Impedance-Matching Method

T-K Hsu*
Graduate Student

D.A. Peters
Professor

Washington University, St. Louis, Mo.

A coupled rotor/airframe vibration analysis is performed by the matching of rotor and fuselage impedances. The rotor impedance for b blades is calculated from the periodic-coefficient equations of a single blade in forward flight. Three flapping modes are included, and the equation is solved by harmonic balance. The fuselage impedance, including structural damping, is calculated for 3 rigid-body and 3 elastic modes in plunge, roll, and pitch. The results show that the effect of hub motions on rotor loads is greatest for relatively stiff rotors, and is not well-approximated by lumped-mass or purely inertial rotor models.

Notation

$\begin{Bmatrix} a \\ b \end{Bmatrix}_F$	= cosine and sine harmonics of F
a	= slope of lift curve
A_{ij}	= elements of portion of $[Z]$
b	= number of blades
$\hat{C}_T$	= conventional thrust coefficient, thrust/$\rho\pi r^2 R^4$
C_T, C_L, C_M	= vibratory portion of nondimensional thrust, roll, and pitch moment over σa.
$\hat{C}_T, \hat{C}_L, \hat{C}_M$	= steady portion of thrust, roll, and pitch moment over σa
$[F]$	= vector of harmonics of C_T, C_L, C_M
g	= nondimensional acceleration of gravity, $g/\Omega^2 R$
g_v, g_L, g_m	= plunge, roll, and pitch structural damping
$[G]$	= fuselage receptance
$[H]$	= hub receptance
p	= first flap frequency/Ω
r_{gm}, r_{gL}	= radius of gyration of fuselage in pitch, roll, divided by R
R	= rotor radius, m
w	= fuselage vertical motion, m
$\bar{w}_F$	= w/R nondimensional vertical motion
$\bar{x}$	= distance along fuselage, tail to nose, divided by R
z	= hub vertical displacement
z_f	fuselage generalized coordinates, Eq. 3
$[z]$	= vector of harmonics of z, α_s, α_c
$[z_F]$	= vector of harmonics of z_f, α_{sf}, α_{cf}
$[Z]$	= rotor impedance
α_c, α_{cf}	= pitch angle of hub, fuselage, positive nose up, rad
$\hat{\alpha}_c$	= steady hub pitch angle, rad
α_s, α_{sf}	= roll angle of hub, fuselage, positive advancing side down, rad
γ	= Lock number
λ	= inflow ratio
ρ	= ratio of distributed beam mass to total beam mass
μ	= advance ratio
σ	= rotor solidity
$[\theta]$	= control derivatives
$\{\theta\}$	= vector of control variables
$\theta_0, \theta_s, \theta_c$	= collective and cyclic pitch, rad
ψ	= azimuth angle, nondimensional time, $\psi = \Omega t$
ω	= swashplate excitation frequency divided by Ω
ω_2, ω_3	= second and third flap frequencies, nondimensionalized by Ω
$\bar{\omega}_{xy}$	= frequency of "y" motion with "x" boundary condition, divided by Ω; $y = v, m, L$ — plunge, pitch, roll $x = c, f$ — cantilevered, free
Ω	= rotor speed, rad/sec

Introduction

THE concept of performing a coupled rotor/airframe vibration analysis by impedance matching goes back at least 15 years, Ref. 1. That reference points out two important facts. First, a coupled rotor/airframe analysis can be performed in a rigorous manner by separate calculation of rotor and fuselage impedances followed by a matching of forces and displacements at the hub. Second, the rotor impedance need only be calculated for a single blade and then appropriately transformed to apply to any number of blades. Ten years later, the method of impedance-matching (formulated a little differently from Ref. 1) was used to illustrate an important phenomenon.[2] Namely, rotor loads calculated for a fixed-hub condition cannot always be applied as simple forcing functions to a fuselage model. The reason for this is that the resultant fuselage motions cause the hub to translate and rotate which, in turn, can alter the expected loads. This alteration is not just a small correction, but can be an order-of-magnitude change. The role of rotor impedance has been futher studied by Hohenemser[3] with very interesting conclusions that pertain to fuselage design. In particular, he notes

Presented at the 36th Annual National Forum of the American Helicopter Society, Washington, D.C., May 1980.

*Presently at Sunstrand Corp., Rockford, Illinois.

that under certain conditions it may be desirable to tune a fuselage frequency to the blade passage frequency in order to eliminate hub loads. Hohenemser outlines a method of computing the complete rotor impedance by finite elements and transfer matrices. Numerical values of the effect of hub motions on rotor loads are only given for simplified rotor models, however. Other work on the importance of hub impedance has appeared in the literature, for example Ref. 4; but this other work does not bear directly on the results presented here.

The interesting conclusions of Refs. 2 and 3 have raised some fundamental questions about coupled rotor/body vibration analyses:

1) If hub motions have such a large effect on loads, why do present methods (which neglect this effect) show reasonable correlation?

2) How sophisticated a blade model is necessary for a realistic model of rotor impedance?

a) Can aerodynamic terms be neglected due to the high frequency (-4/rev)?

b) Can a constant-coefficient or hover approximation be used?

c) How many blade modes are necessary?

d) Must pitch-thrust, roll-thrust, and pitch-roll coupling be included?

3) Which terms in the impedance matrix are most responsible for the effects of hub motions on rotor loads?

It should be emphasized that the effects listed above (aerodynamics, periodic coefficients, blade modes, coupling) have all been used previously in the calculation of the fixed-hub loads; but these terms have been omitted in the calculation of the rotor impedance. It is the purpose of this paper to study the modeling of rotor impedance and to answer the above questions.

Rotor Model

The rotor model used here is that of Ref. 5 but without reversed flow. The blade is assumed uniform and is described in terms of modal coordinates in flapping only. The periodic-coefficient equations are solved by harmonic balance to give a solution of the form

$$[F] = [\theta]\{\theta\} + [Z]\{z\} \tag{1}$$

where $\{F\}$ is the vector of the harmonics of loads, $\{\theta\}$ is the vector of controls, and $\{z\}$ is the vector of harmonics of hub motions;

$$\{F\} = \begin{Bmatrix} \begin{Bmatrix} a \\ b \end{Bmatrix}_{C_T} \\ \begin{Bmatrix} a \\ b \end{Bmatrix}_{C_L} \\ \begin{Bmatrix} a \\ b \end{Bmatrix}_{C_M} \end{Bmatrix}, \qquad \{\theta\} = \begin{Bmatrix} \theta_0 \\ \theta_s \\ \theta_c \\ \setminus \end{Bmatrix},$$

$$\{z\} = \begin{Bmatrix} \begin{Bmatrix} a \\ b \end{Bmatrix}_z \\ \begin{Bmatrix} a \\ b \end{Bmatrix}_{\alpha_s} \\ \begin{Bmatrix} a \\ b \end{Bmatrix}_{\alpha_c} \end{Bmatrix} \tag{2}$$

and where z is plunge, α_s is the roll angle, and α_c is the pitch angle of the hub. The matrix $[\theta]$ represents the rotor loads with a fixed hub, and the matrix $[Z]$ represents the effect of hub motions on rotor loads (i.e., the impedance). The efficiency of the above procedure is one of the advantages of the harmonic balance approach. The calculation of $[\theta]$ and $[Z]$ in Eq. (1) need be performed for a single blade only. Subsequently, the corresponding matrices for a b-bladed rotor can be found by elimination of all harmonics (i.e. rows and columns) that are not integer multiples of b. (Complete details are in Ref. 5).

The impedance matrix $[Z]$ is the most critical item of the rotor analysis because it represents the crucial effect of hub motions on rotor loads. In Ref. 2, this rotor impedance includes the aerodynamic terms for a rigid, hovering rotor and the inertial terms for a rotor mass lumped at the hub (i.e. an infinitely rigid rotor). In the numerical results of Ref. 3, aerodynamic terms are not included; but the inertial terms are found with the assumption that only one-half of the rotor mass is lumped at the hub and that the remaining mass is suspended on a spring of sufficient stiffness to model correctly the first flapping frequency. One of the purposes of this present study is to compare the results calculated under these assumptions with results calculated from the complete, aeroelastic rotor impedance.

It should be noted here that the present method of calculation of rotor impedance has some experimental verification. Figure 1 shows data for rotor response due to swashplate oscillation compared with harmonic-balance results, Ref. 6. The swashplate responses are sufficiently similar to shaft responses to indicate that the present method is reasonably accurate in the frequency range of interest. The peaks in the curve are the resonances at $p \pm 1$.

Fuselage Model

The fuselage is modeled by 6 modes—a rigid-body and an elastic degree of freedom in each of the directions plunge, pitch, and roll. The plunge model, shown in Fig. 2, is a uniform beam with a lumped mass added at the center. The beam deflection is expressed in terms of two comparison functions that multiply two generalized coordinates, z and z_f

$$w(x,t) = Rz(t) + R(x - \tfrac{1}{2})^2 z_f(t) \tag{3}$$

where z is the hub motion, z_f is 4 times the elastic tip deflection, and x is the nondimensional distance along the

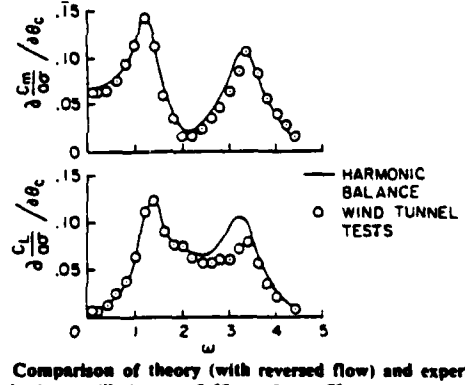

Fig. 1 Comparison of theory (with reversed flow) and experiment for swash-plate oscillation: $p = 2.32$, $\gamma = 5$, $\mu = .78$.

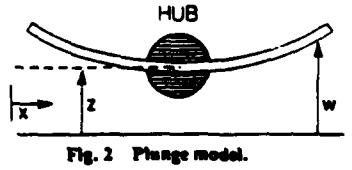

Fig. 2 Plunge model.

beam. The nondimensional equations of motion are

$$\begin{bmatrix} 1 & \rho/12 \\ 20/3 & 1 \end{bmatrix} \begin{Bmatrix} \ddot{z} \\ \ddot{z}_f \end{Bmatrix} + \begin{bmatrix} 0 & 0 \\ 0 & \bar{\omega}_{cv}^2 \end{bmatrix} \begin{Bmatrix} z \\ z_f \end{Bmatrix} = \begin{Bmatrix} C_T \\ 0 \end{Bmatrix} \frac{g}{\hat{C}_T} \quad (4)$$

where ρ is the ratio of distributed beam mass to total beam mass, $\bar{\omega}_{cv}^2$ is the natural frequency of the fuselage when cantilevered at the hub, $\hat{C}_T$ is the steady thrust required to support the fuselage, and g is the nondimensional acceleration of gravity $g/\Omega^2 R$. The parameters ρ and $\bar{\omega}_{cv}^2$ completely determine the free natural frequency of the fuselage, $\bar{\omega}_{fv}$.

$$\bar{\omega}_{fv}^2 = \frac{9}{9 - 5\rho} \bar{\omega}_{cv}^2 \quad (5)$$

Structural damping is included by multiplication of the stiffness matrix by g_s to obtain a damping matrix.

Although Eq. (4) describes a beam model of the fuselage, the equations are completely analogous to those for the much simpler model of two lumped masses connected by a spring, as is used in Refs. 2 and 3. In fact, the fuselage impedance of Ref. 2 is matched by $\rho = .94$, $g = .02$. Thus, there is no fundamental difference between the vertical fuselage model of Refs. 1 and 2 and that of this work. By extension, one may also argue that the fuselage impedance used here should be little different from a single-mode impedance obtained from more complicated, finite-element fuselage models.

The roll and pitch model used here is illustrated in Fig. 3 for the case of pitch. The fuselage is considered rigid in pitch but connected to the rotor hub through a torsional spring. Only rotational motions are included, and hub or fuselage lateral motion is reasonably neglected. The resultant equations, although not given here, are exactly analogous to Eq. (4) with α_s (or α_c) taking the place of z_f; and C_L (or C_M) taking the place of C_T. A lumped inertia at the hub includes transmission mass and hub mass, but not blade mass or rotor moment of inertia. Details of the model may be found in Ref. 7.

The fuselage impedance for plunge, pitch, and roll is found by substitution of the appropriate Fourier series for z, z_f, α_c, α_{cf}, α_s, α_{sf}, C_T, C_L, and C_M into the hub equations followed by a simple harmonic-balance solution.

$$\begin{Bmatrix} \{z\} \\ \{z_F\} \end{Bmatrix} = \begin{bmatrix} [H] \\ [G] \end{bmatrix} \{F\} \quad (6)$$

Here, $[H]$ and $[G]$ are receptances (inverse of impedance).

As before, only integer-multiple harmonics of the blade number ($b, 2b, \ldots$) are retained. Furthermore, higher harmonics may be truncated as deemed appropriate.

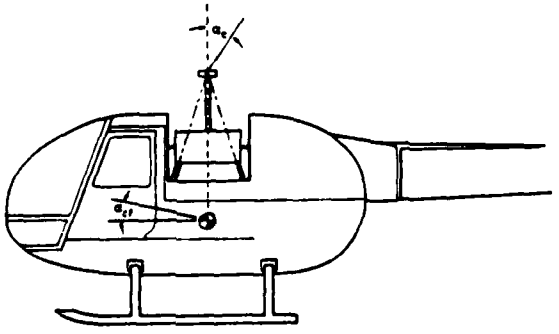

Fig. 3 Pitch-roll model.

Impedance Matching

The combined rotor/fuselage vibrations may be obtained by the matching of impedances from Eq. (1) with those of Eq. (6). This implies the matching of harmonics of both loads $\{F\}$ and displacements $\{z\}$ at the interface. Therefore, we have

$$\{F\} = [\theta]\{\theta\} + [Z][H]\{F\} \quad (7)$$

or

$$\{F\} = (I - [Z][H])^{-1}[\theta]\{\theta\} \quad (8)$$

Thus, the hub loads including blade motions, $\{F\}$, are obtained from the fixed-hub loads, $[\theta]\{\theta\}$, by the appropriate use of fuselage receptance $[H]$ and rotor impedance $[Z]$. The related hub motions (all harmonics) follow immediately from Eq. (6).

The efficiency of the calculation in Eq. (8) should be emphasized here. First, we note that calculation of rotor impedance is by far the most difficult portion of the calculation. Once $[Z]$ and $[\theta]$ are calculated for a given rotor, however, changes in fuselage properties $[H]$ can be made with only a minor effort. Thus, large-scale investigations into the effects of fuselage frequency can be performed with a very small computational effort. When the coupled rotor-fuselage response is done in one computation, on the other hand, the computational effort can become forbidding. Another efficient aspect of Eq. (8) is its potential for rotor trim. A given $\hat{C}_T$, $\hat{C}_L$, and $\hat{C}_M$ (the a_0 portions of $\{F\}$) can be easily matched by solving Eq. (8) for θ_0, θ_S, and θ_C (the first three terms of $\{\theta\}$). This solution involves only the inversion of a 3×3 matrix.

Coupled Response

We now apply the foregoing theory to the calculation of vibrations. To begin, we look at the coupled rotor-fuselage response of a system with the following baseline parameters.

Rotor: 4 blades, $P = 1.12$, $\omega_1 = 2.5$, $\omega_3 = 4.5$, $\gamma = 8$, $\hat{C}_T = .0144$, $\hat{C}_L = 0$, $\hat{C}_L = 0$, $\hat{C}_M = 0$, $\mu = .3$, $\hat{\alpha}_c = .07$, $\sigma = .07$, $a = 5.73$, $\lambda = .032$, $\hat{C}_T = .0058$, $\hat{C}_T/\sigma = .083$

Fuselage: $r_{gm} = .37$, $r_{gL} = .14$, $\bar{\omega}_{fL} = 1.18\bar{\omega}_{fm}$, $\bar{\omega}_{fv} = 1.53$, $\bar{\omega}_{fv} = 1.45\bar{\omega}_{cv}$, $\bar{\omega}_{fm} = 10.0\bar{\omega}_{cm}$, $\bar{\omega}_{fL} = 3.04$, $\bar{\omega}_{fL} = 4.47\bar{\omega}_{cl}$, $g_v = g_m = g_L = .02$.

Frequencies with subscript "c" denote cantilevered modes in which the hub degree of freedom (i.e. z, α_s, or α_c) is constrained but the remainder of the fuselage is free to move elastically. Frequencies with subscript "f" denote free modes for which neither the hub nor the fuselage is fixed. For all of the results to follow, the parameters are as above unless otherwise noted.

The first results to be shown are the 4/rev components of thrust, roll moment, and pitch moment versus the unconstrained (free) roll and pitch frequencies $\bar{\omega}_{fL}$ and $\bar{\omega}_{fm}$, Figs. 4-6. Results are presented for $p = 1.03$, 1.06, 1.09, and 1.12. Also shown are similar curves, labelled "feedback neglected," which give the fixed-hub loads. Several interesting characteristics of these curves should be noted. First, the effect of rotor-body diminishes as $\bar{\omega}_{fm}$ (and $\bar{\omega}_{fL}$) become large. Therefore, for this case, the rigid-body motion is not playing a significant role. Second, the effect of coupling dramatically increases as the flapping frequency increases. This indicates that the rotor inertia plays an important roll, but that the inertia is isolated from the 4/rev when p is very close to 1.00. Third, the roll frequency greatly affects the vertical loads, C_T. This implies that aerodynamic coupling is vitally important and cannot be neglected. Fourth, the roll (or pitch) moments show peaks when the roll frequency, $\bar{\omega}_{fL}$ (or the pitch frequency, $\bar{\omega}_{fm}$) is near 3.7/rev; but they show *valleys* when these frequencies are at 4.0/rev. Thus, as

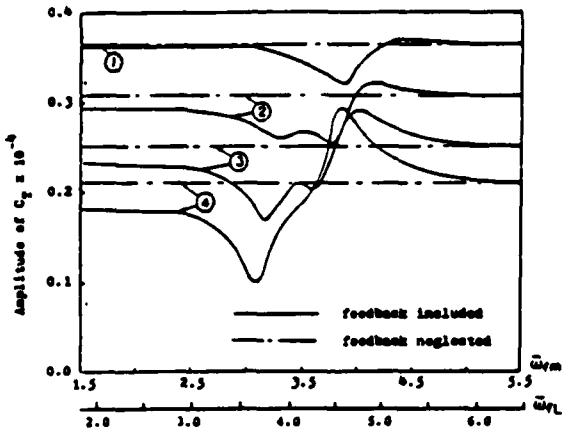

Fig. 4 4/rev vertical loads as a function of pitch (and roll) frequency; 1) through 4) refer to $p = 1.03$, 1.06, 1.09, and 1.12 respectively; $\omega_{fL} = 1.18\omega_{fm}$.

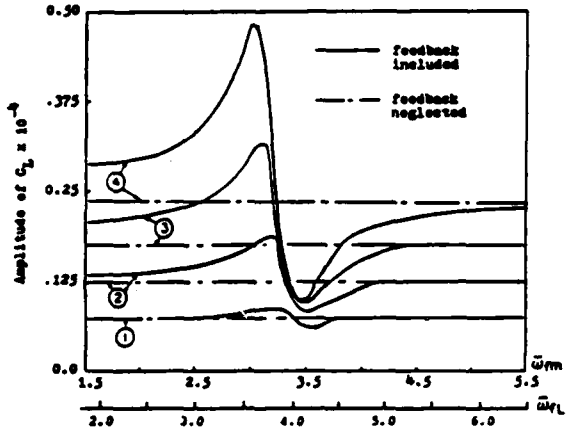

Fig. 5 4/rev roll loads as a function of pitch (and roll) frequency; 1) through 4) refer to $p = 1.03$, 1.06, 1.09, and 1.12 respectively; $\omega_{fL} = 1.18\omega_{fm}$.

predicted in Ref. 3, designing right on a blade-passage frequency does lower hub loads. However, as we shall see later, this does not necessarily mean a lowering of fuselage vibrations.

We now look at the effect of damping on these results. Figure 7 gives C_M versus ω_{fm} at $p = 1.12$ for two values of structural damping g. (Percent critical damping is roughly $g/2$ for these cases.) Magnitude and phase are both plotted. Several things are noteworthy. First, we see that with only .002 damping, the pitch moment goes to zero, at $\omega_{fm} = 4.0$ as predicted in Ref. 3. Also noted are peaks at points for which ω_{fm} or ω_{fL} is 3.7. Thus, with small damping, the pitch-roll coupling is apparent (two peaks) while at large damping it is less noticeable (one peak). The phase behavior is also interesting and shows that significant phase shifts do occur near 4/rev. (The phase here is taken as the arctangent of the $\sin 4\psi$ component divided by the $\cos 4\psi$ component of C_M). In Fig. 8, we see the behavior of the fuselage pitch angle for the identical range of frequencies. The curves reveal three important behaviors. First of all, the uncoupled analysis predicts a peak at $\omega_{fm} = 4.0$ whereas the coupled analysis shows the peak at $\omega_{fm} = 3.7$. This is indicative of the fact that the natural frequency with the rotor is different from the frequency without the rotor. Second, although the pitching moment is essentially zero at $\omega_{fm} = 4.0$, $g_m = .002$, the response at

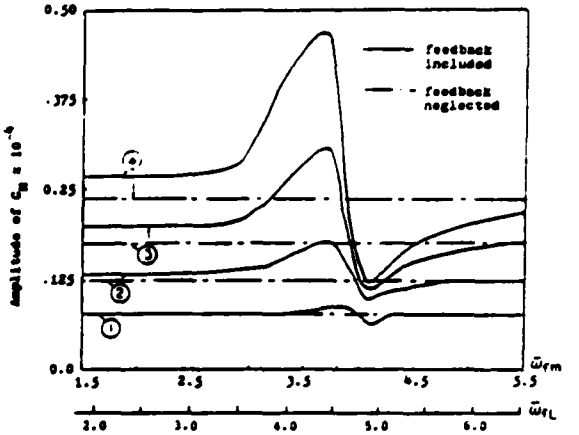

Fig. 6 4/rev pitch loads as a function of pitch (and roll) frequency; 1) through 4) refer to $p = 1.03$, 1.06, 1.09, and 1.12 respectively; $\omega_{fL} = 1.18\omega_{fm}$.

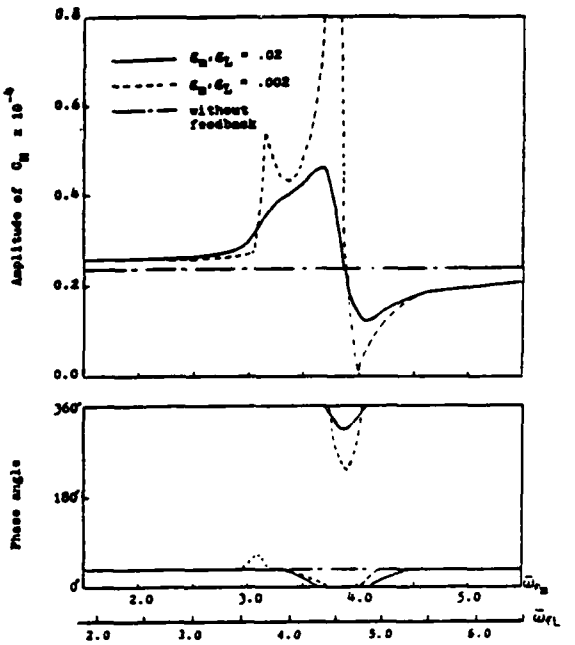

Fig. 7 4/rev pitch loads as a function of pitch (and roll) frequency and damping; $p = 1.12$, $\omega_{fL} = 1.18\,\omega_{fm}$.

$\omega_{fm} = 4.0$ is very high. Therefore, setting C_M to zero by tuning to 4/rev does not minimize vibrations and would probably not be a good design choice.

The physical interpretation of this is as follows. First, as the natural frequency approaches 4.0, the receptance of the fuselage goes to infinity (for zero damping) as is the case with all oscillators. Second, since H approaches infinity in equations (6) and (7), F must approach zero (as pointed out in Ref. 3). However, even though the force goes to zero, the response does not go to zero. This can be seen from Eq. (1) which shows that $F = 0$ does not imply $Z = 0$. Thus the zero force and infinite receptance combine to create a finite response. Also, the phase angle here is very important in that fuselage vibrations will be a combination of pitch and plunge. Thus, relative phasings are crucial. A final look at the effect of damping is given in Fig. 9, which shows fuselage plunge amplitude versus pitch frequency. The importance of dam-

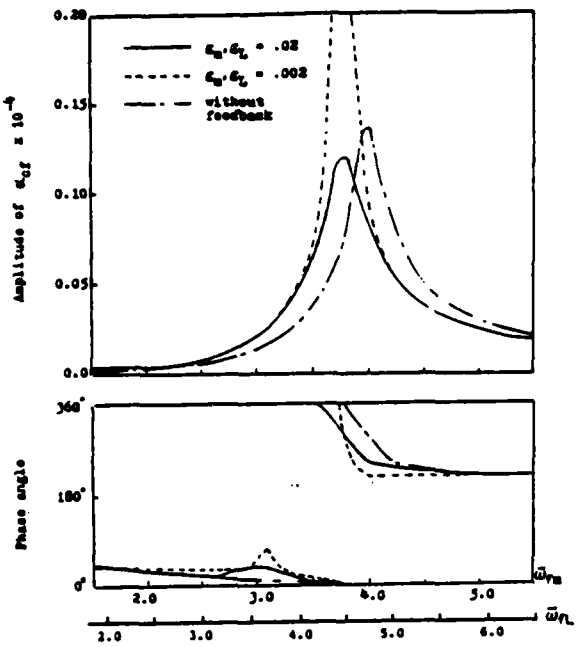

Fig. 8 Fuselage pitch angle as a function of pitch (and roll) frequency and damping; $p = 1.12$, $\omega_{f_L} = 1.18\,\omega_{f_m}$.

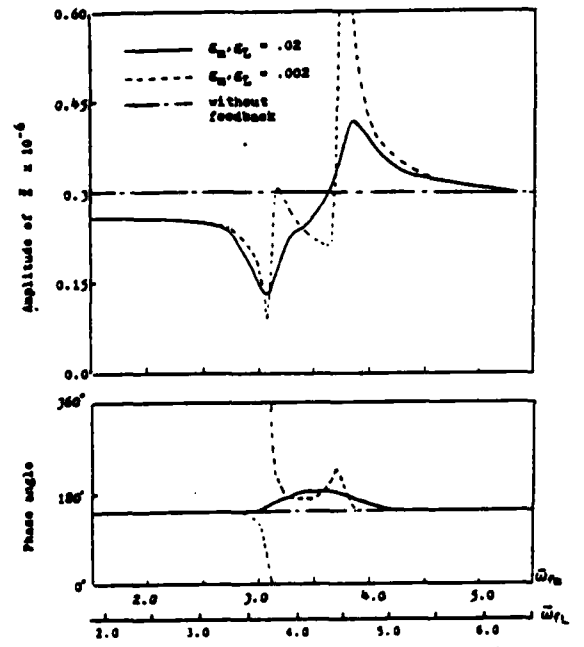

Fig. 9 Fuselage plunging as a function of pitch (and roll) frequency and damping; $p = 1.12$, $\omega_{f_L} = 1.18\,\omega_{f_m}$.

ping and the strong coupling between pitch and plunge are clearly evident. Thus, the result without the effect of hub motions on loads is inadequate.

The preceding results have centered on the effect of pitch and roll frequency. We now turn to the effect of vertical (or plunge) frequency, ω_{f_v}. Figure 10 shows the 4/rev C_T as a function of ω_{f_v}. The large differences between curves with and without the "feedback" of hub motions is due primarily to the effect of pitching and roll frequency, as seen previously in

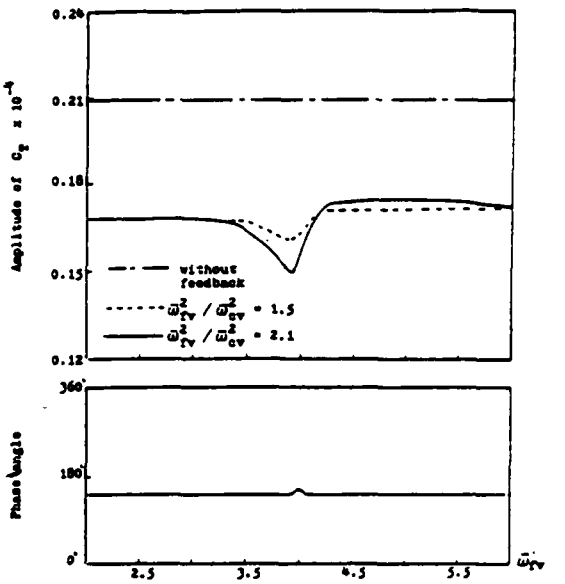

Fig. 10 4/rev vertical loads as a function of fuselage vertical frequency.

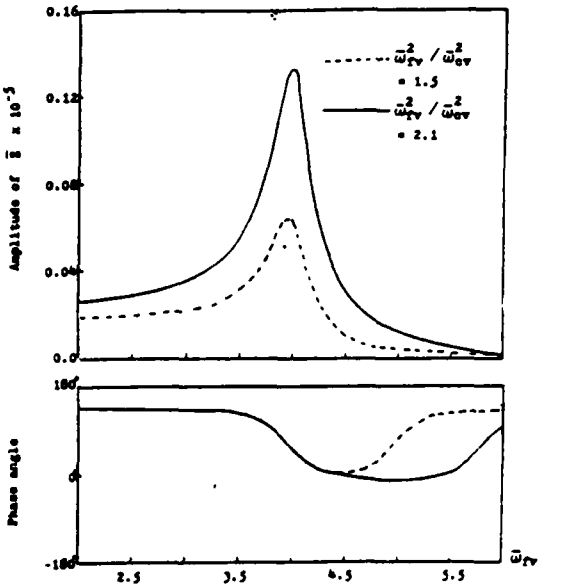

Fig. 11 Vertical hub motion as a function of fuselage vertical frequency.

Fig. 4. However, the effect of elastic, vertical motions is also seen to be significant, as indicated by the local decrease in C_T near $\omega_{f_v} = 4.0$. Two curves with feedback are shown. The solid curve corresponds to 94% of the fuselage mass distributed along the beam and 40% lumped at the hub. The phase angle is fairly constant in either case. Figure 11 shows the vertical hub motion for the same parameter range. As might be expected, the hub motion is greater when less mass is lumped at the hub. Although C_T shows a minimum near $\omega_{f_v} = 4.0$, $\bar{z}$ shows a pronounced peak at $\omega_{f_v} = 4.0$. Figure 12 gives the total vertical motion along the fuselage versus ω_{f_v} ($\bar{x} = .5$ is the hub). The curve for $\omega_{f_v} = 4.0$ is dashed simply for clarity. The curves show that not only does the hub motion peak near $\omega_{f_v} = 4.0$, but the tip motion also peaks. The symmetry of the

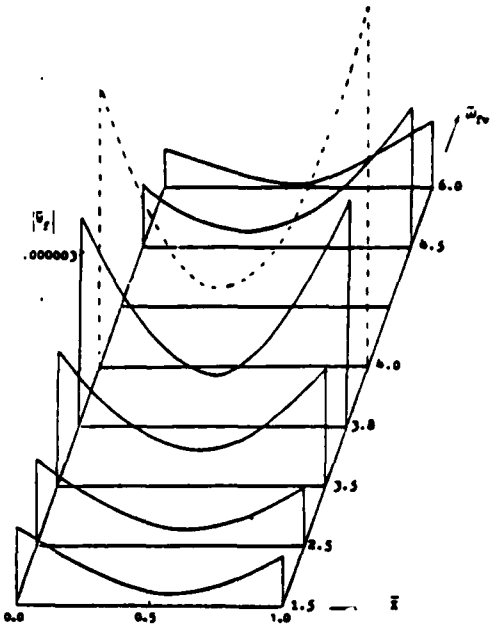

Fig. 12 Fuselage vertical motion as a function of fuselage vertical frequency.

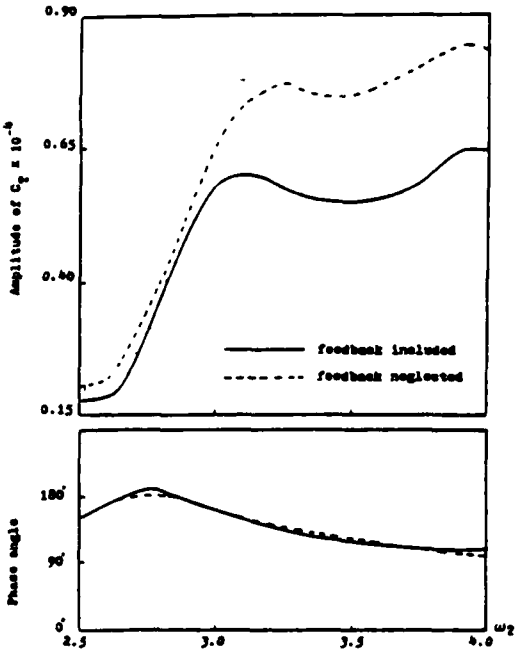

Fig. 13 4/rev vertical loads as a function of blade second and third flap mode frequency; $\omega_3 = 1.8\,\omega_2$.

curves about $\bar{x}=0.5$ indicates, for this case, the relative dominance of hub vertical terms over pitch terms, since both effects add to give the vertical motion along the beam. Although not shown here, the vibratory pitch and roll moments are virtually unchanged by $\bar{\omega}_{fv}$.

So far, we have investigated the effects of the first blade flapping frequency and the effects of several fuselage parameters. We now look at the effect of the blade second flap frequency, ω_2, Fig. 13. (The third flap frequency, ω_3, is varied as $1.8\,\omega_2$.) The second flap frequency is seen to greatly

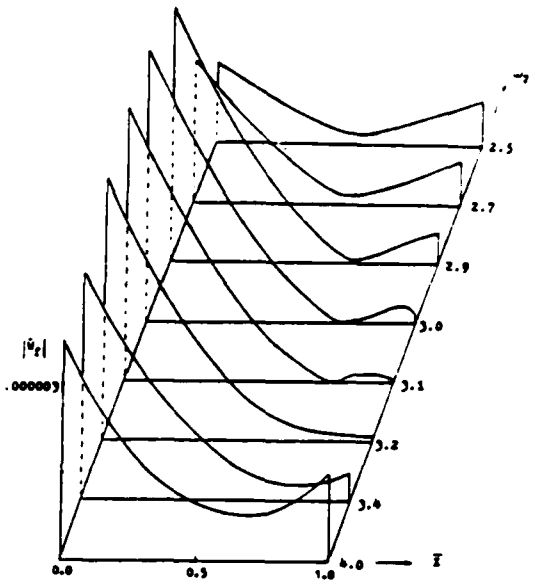

Fig. 14 Fuselage vertical motion as a function of blade second and third flap mode frequency; $\omega_3 = 1.8\,\omega_2$.

affect the 4/rev thrust response. There is a dramatic rise in 4/rev C_T between $\omega_2 = 2.5$ (about the lowest value physically possible) and $\omega_2 = 3.0$. The effect at $\omega_2 = 3.0$ indicates a response of the cyclic flapping modes at $(\omega_2 + 1)$. A second peak is seen at $\omega_2 = 4.0$ and indicates coupling with a coning mode. For $\omega_2 > 3.0$, the effect of hub motions is significant. Figure 14 gives a more detailed account of how fuselage motions at various points along the beam are affected by ω_2. The large dissymmetries for $\omega_2 > 2.5$ indicate that pitch moments are playing a dominant role. A near anti-node is noted at $\bar{x} = .8$ when ω_2 is near 3.0.

Elements of Rotor Impedance

Now that we have taken a general look at the effect of rotor/body coupling on loads and vibrations, we are in a position to determine which terms in the rotor impedance matrix are the primary contributors to these effects. The rotor impedance matrix $[Z]$ is a rather complicated array, and we need to consider it in detail before going on. In general, $[Z]$ represents the response of every sine and cosine harmonic of C_T, C_L, and C_M to every sine and cosine harmonic of the motions $\bar{z}$, α_s, and α_c. For simplicity, let us momentarily consider only C_T due to $\bar{z}$ for a b-bladed rotor. We will also neglect harmonics of order 3b and higher. This yields

$$\begin{Bmatrix} a_0 \\ a_b \\ a_{2b} \\ b_b \\ b_{2b} \end{Bmatrix}_{C_T} = \begin{bmatrix} A_{00} & A_{01} & A_{02} & A_{03} & A_{04} \\ A_{10} & \underline{A_{11}} & A_{12} & \underline{A_{13}} & A_{14} \\ A_{20} & A_{21} & A_{22} & A_{23} & A_{24} \\ A_{30} & \underline{A_{31}} & A_{32} & \underline{A_{33}} & A_{34} \\ A_{40} & A_{41} & A_{42} & A_{43} & A_{44} \end{bmatrix} \begin{Bmatrix} a_0 \\ a_b \\ a_{2b} \\ b_b \\ b_{2b} \end{Bmatrix}_{\bar{z}} \tag{9}$$

where A_{ij} are the elements of $[Z]$. In general, elements with zero subscripts are not relevant because higher harmonic motion has little effect on steady loads, and steady motions (with the exception of α_c) do not effect higher harmonic loads.

The dominant terms in Eq. (9) are those terms that relate the various harmonics at the fundamental blade-passage frequency, b/rev.

These terms are A_{11}, A_{13}, A_{31}, and A_{33}. For a purely constant-coefficient system, these terms would obey the equalities $A_{11}=A_{33}$, $A_{31}=-A_{13}$. For a periodic-coefficient system, however, these equalities do not necessarily hold. The numerical results of our work have shown, however, that the equalities are good approximations for $b\geq 3$ (rotors with 3 or more blades). For two-bladed rotors, on the other hand, the equalities are definitely not valid. These observations could lead one to believe that a constant-coefficient approximation might be valid for calculation of rotor impedance when $b\geq 3$. No such approximation is used here, however. We will say more about constant-coefficients shortly.

In order to gain a better understanding of the effects of rotor impedance, pertinent coefficients are defined in the following manner. For example, for $b=3$ in Eq. (9), the relationship between 3/rev C_T and 3/rev z is summarized by the following coefficient.

$$C_{T3}/z_3 = \sqrt{\tfrac{1}{2}(A_{11}^2+A_{13}^2+A_{31}^2+A_{33}^2)} \tag{10}$$

Similarly, the relationship between 6/rev C_T and 3/rev z is summarized as

$$C_{T6}/z_3 = \sqrt{\tfrac{1}{2}(A_{21}^2+A_{23}^2+A_{41}^2+A_{43}^2)} \tag{11}$$

Parallel definitions apply for other harmonics, for other loadings (C_M and C_L), and for other hub motions (α_s and α_c). An interesting aspect of the coupling between different harmonics, as in Eq. (11), is that such coupling would be identically zero in a constant-coefficient system. The results to follow, however, show that significant magnitudes can occur for such terms. Therefore, attempts at a constant-coefficient approximation for rotor impedance in forward flight may not be valid in the presence of significant higher-harmonic loads. Thus, the tentative conclusion of this work is that a constant-coefficient approximation is valid for $b\geq 3$ provided that 2b/rev loads are negligible with respect to b/rev loads.

Figure 15 provides a typical plot of the 3/rev impedance elements averaged as in Eq. (10). The solid lines are the exact values versus advance ratio, and the dashed lines are values calculated from inertial effects only (aerodynamics neglected as in a vacuum). The couplings between vertical and roll-pitch (C_{L3}/z_3, C_{M3}/z_3, C_{T3}/α_{s3}, C_{T3}/α_{c3}) are zero for the vacuum calculation. Several interesting observations can be made from this figure and comparisons with the results in Figs. 4-14. First, as previously mentioned, the vertical frequency does not affect roll and pitch vibrations. Therefore, C_{L3}/z_3 and C_M/z_3 must not significantly contribute to the role of rotor impedance on vibrations. Also, the fact that roll and pitch frequencies do affect thrust indicates that C_{T3}/α_{s3} and C_{T3}/α_{c3} are important terms. It further follows that the vacuum approximation, which gives zero for these terms, would not be adequate. Furthermore, this shows that not even the hover impedance, which also shows zero coupling, would be adequate to model this important thrust-roll-pitch coupling.

There are two interesting aspects of Fig. 15 which bear on the presentation of subsequent results. First, we note that C_{L3}/z_3 and C_{M3}/z are comparable in magnitude to the complementary terms C_{T3}/α_{s3} and C_{T3}/α_{c3}. Nevertheless, we have found that the z derivatives have negligible effect on roll and pitch whereas the α derivatives have a large effect on thrust. The reason for this is that plunge magnitudes are generally much smaller than roll and pitch magnitudes. Therefore, since the C_L and C_M derivatives with z have little effect or response, they will not be shown in subsequent graphs. The second interesting aspect of Fig. 15 is the fact that $C_{L3}/\alpha_{s3}\approx C_{M3}/\alpha_{c3}$ and $C_{M3}/\alpha_{s3}\approx C_{L3}/\alpha_{c3}$. These approximate equalities have been found to hold for all parameters and at all harmonics. Therefore, the two roll-moment derivatives will not be shown in subsequent graphs, as they may be inferred from the pitch-moment derivatives.

One last note on Fig. 15 is the variation in curves with μ. Curves linear with μ imply an effect due to coupling terms of the type $\mu\sin\psi$ or $\mu\cos\psi$. Higher-order curvature represents the coupling effects of higher powers of μ and higher harmonics of ψ. It is interesting that the pitch and roll derivatives, although constant with μ, are not well approximated by a vacuum analysis. The error is 20% for C_{M3}/α_{c3} and 50% for C_{M3}/α_{s3}.

The five essential elements of the impedance matrix, averaged as in Eq. (11), are shown in Fig. 16 for a representative configuration for the 3/rev loads due to 6/rev motions and 6/rev loads due to 6/rev motions. The parabolic characteristic of the thrust/roll couplings indicates the effect of higher-harmonic periodic coefficients. The total effect of these terms on 3/rev response, however, is dependent on the amount of 6/rev motion of z, α_s, and α_c. The counterpart derivatives, 6/rev loads due to 3/rev motions, are almost identical.

Figure 17 provides the impedance terms for 4/rev loads due to 4/rev motion. The curves are qualitatively similar to those for 3/rev, Fig. 15; but the magnitude of thrust/roll and thrust/pitch coupling is larger for this case. Another difference between Figs. 15 and 17 is that the C_{T4}/z_4 derivative is

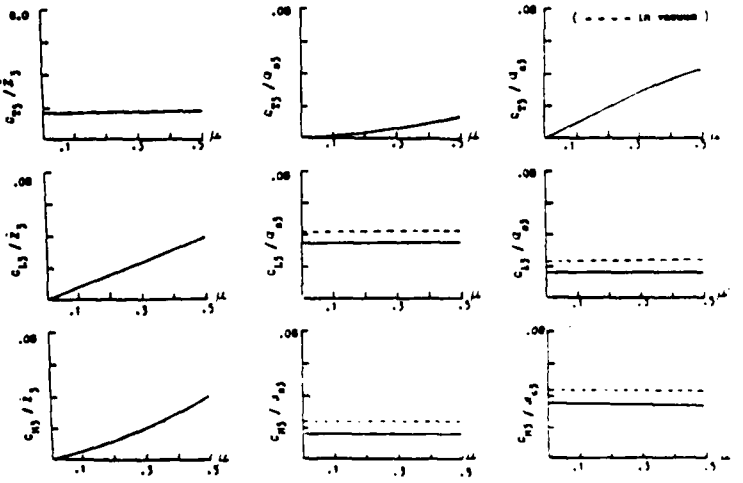

Fig. 15 Elements of impedance matrix, 3/rev components; $\rho=1.15$, $\omega_2=3.7$, $\omega_3=8.8$, $\alpha=8.2$.

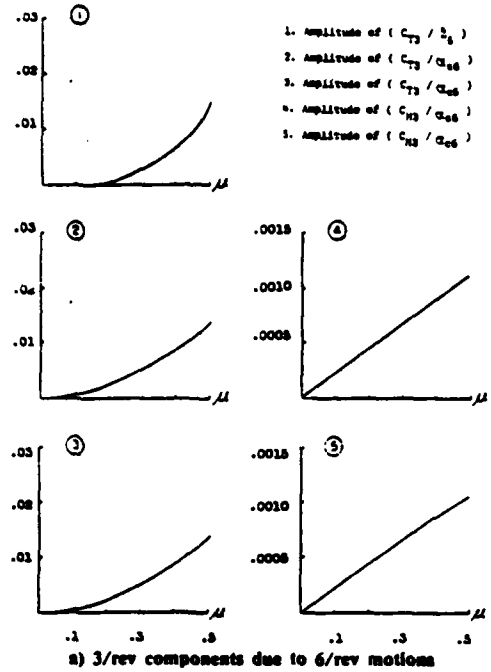

a) 3/rev components due to 6/rev motions

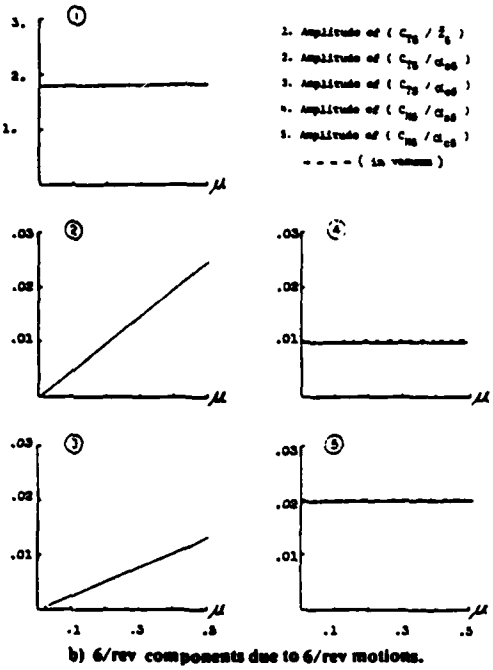

b) 6/rev components due to 6/rev motions.

Fig. 16 Elements of impedance matrix; $p = 1.15$, $\omega_2 = 3.7$, $\omega_3 = 8.8$, $\gamma = 8.2$.

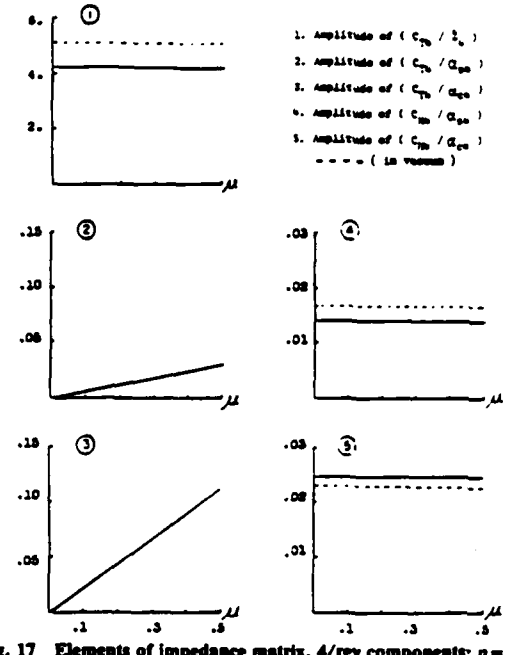

Fig. 17 Elements of impedance matrix, 4/rev components; $p = 1.15$, $\omega_2 = 3.7$, $\omega_3 = 8.8$, $\alpha = 6.2$.

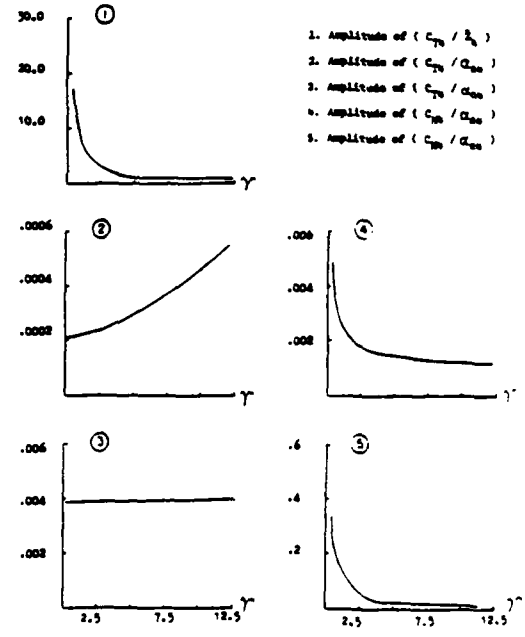

Fig. 18 Elements of impedance matrix, 4/rev components as a function of Lock number, $\mu = .3$, $p = 1.15$ (single flap mode).

much larger than its 3/rev counterpart and is not well-approximated by the vacuum calculation. This increase in aerodynamic effect is present despite a lower Lock number in Fig. 17 than in Fig. 15.

The direct effect of Lock number can be seen in Fig. 18. The flapping frequency is the same as in Fig. 17, but only a single, straight-line mode is used. Curves which approach ∞ as γ approaches zero indicate inertial effects. It should be pointed out the C_{T_4} refers to the fourth harmonic of $\hat{C}_T/\sigma a$. Therefore, γ going to zero implies "a" going to zero and $\hat{C}_T/\sigma a$ going to infinity. (Vacuum curves on previous plots assume $\hat{C}_T/\sigma a$ normalized on a nominal value of "a" which remains constant in a vacuum). The curves that remain finite as $\gamma \to 0$ show entirely aerodynamic effects.

It may be recalled that Figs. 4, 5, and 6 indicate a strong effect of flapping frequency on the coupled rotor/fuselage response. Figure 19a provides plots of impedance elements versus flapping frequency for a 4-bladed rotor. Several interesting conclusions can be drawn. First, the $C_{T_4}/\dot{z}_4$ derivative is not a strong function of p in this frequency

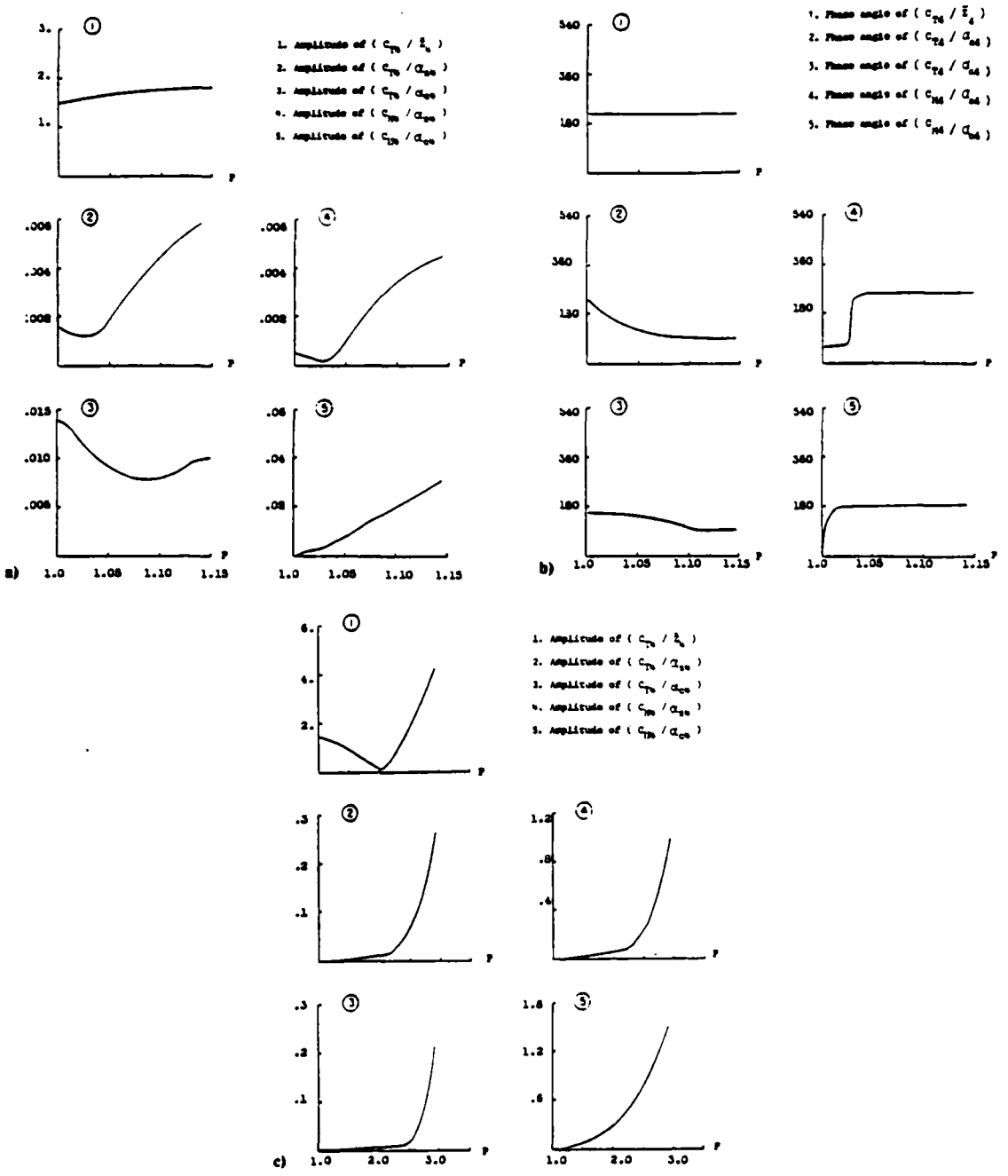

Fig. 19 Elements of impedance matrix, 4/rev components as a function of flapping frequency; $\mu = .3$, $\alpha = 8.0$, $\omega_2 = 2.5$, $\omega_3 = 4.5$. a) 4/rev components magnitude for $1.00 \le p \le 1.15$; b) 4/rev components phase for $1.00 \le p \le 1.15$; c) 4/rev components magnitude for $1.0 \le p \le 3.0$ (single flap mode).

range. Therefore, the large effect of p on C_T in Fig. 4 must be attributed to the coupling terms C_{T_4}/α_{s_4} and C_{T_4}/α_{c_4} which are dependent on p. It must also be pointed out, however, that $C_{T_4}/\bar{z}_4$ is stongly dependent on flap frequency at higher values of p, Fig. 19c. In fact, for a single rigid mode and for a uniform blade, $C_{T_4}/\bar{z}_4$ drops to zero at $p=2$ (the blade becomes an absorber) and increases dramatically beyond that. Thus, analyses that assume a lumped rotor mass ($p=\infty$) cannot be expected to give accurate rotor impedance. Another interesting aspect of Fig. 19a is the complex behavior of several elements of $[Z]$ as p is varied. This indicates complex dynamic interactions between aerodynamic and inertial terms. Calculations at higher values of p show that these interactions are strongly p-dependent even for $p>2$. Similar conclusions hold for phase angles, Fig. 19b.

The final figure to be considered here is the effect of second flap frequency on the rotor impedance, Fig. 20. The motivation here results from the strong effect of ω_2 seen in Fig. 13. There are several noteworthy points in Fig. 20. First, we note the total inadequacy of the vacuum approximation. The infinite peaks of that approximation (at $\omega_2 = 3.0$, $\omega_2 = 3.0$, and $\omega_2 = 4.0$) are simply not realized in the presence

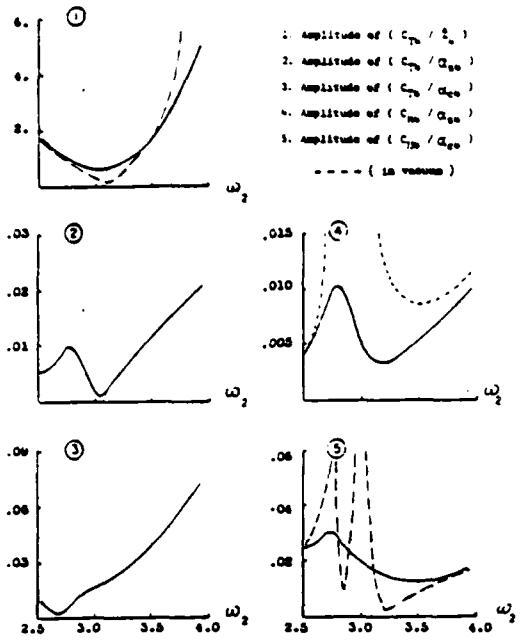

Fig. 20 Elements of impedance matrix, 4/rev components as a function of blade second and third flap mode frequencies; $\omega_3 = 1.8\ \omega_2$, $\mu = .3$, $\gamma = 8.0$, $\rho = 1.12$.

of aerodynamic damping. This is a companion result to that of Fig. 7. The earlier figure shows that results without structural damping are invalid, and Fig. 20 shows that results without aerodynamic damping are invalid, even when ω_2 is not directly at a resonance point. On the other hand, despite the large effect of damping, the resonance and antiresonance effects of higher modes are still clearly seen in the results, although diminished. Thus, higher modes play a large role in rotor impedance.

Conclusions

Detailed calculations of rotor impedance in flapping only have been calculated for a wide range of rotor parameters. These impedances have been used to calculate the coupled rotor/airframe response of helicopters. The theory, and several hundred figures showing the results, can be found in Ref. 7. A few of the more interesting curves have been presented here. The conclusions of these results are:

1) Hub motions can greatly affect hub loads with the most dramatic effects being for relatively stiff rotors.

2) There is a very large affect of pitch and roll motions on vertical response, but little effect of vertical motion on pitch and roll response.

3) Stuctural damping in the fuselage plays a dominant role, with as little as 1% critical damping changing the entire character of the fuselage vibrations.

4) Higher-frequency flap modes can greatly affect the coupled response and can alter the relative contributions of pitch and plunge motions.

5) Vacuum, lumped mass, and hover approximations of the rotor impedance are entirely inadequate.

6) A constant-coefficient approximation to rotor impedance may be valid under certain conditions, but must be used with caution when higher-harmonic loads are present, due to significant cross-harmonic coupling.

7) The effects of Lock number, first flapping frequency, and higher flapping frequencies are strongly interdependent and depend upon a complicated balance of inertial and aerodynamic terms.

Acknowledgement

This work was sponsored by the United States Army Research Office, ARO Grant No. DAAG29-77-G-0103.

References

[1]Gestenberger, Walter and Wood, Edward, R., "Analysis of Helicopter Aeroelastic Characteristics in High-Speed Flight," *AIAA Journal*, Vol. 1, No. 10, October 1964.

[2]Staley, J.A. and Sciarra, J.J., "Coupled Rotor/Airframe Vibration Prediction Methods," *Rotocraft Dynamics*, NASA SP-352, 1974.

[3]Hohenemser, Kurt H. and Yin, Sheng-Kuang, "The Role of Rotor Impedance in the Vibration Analysis of Rotorcraft," *Fourth European Powered Lift Aircraft Forum*, Stresa, Italy, September 1978.

[4]Viswanthan, S.P. and Meyers, A.W., "Reduction of Helicopter Vibration through Control of Hub Impedance," *Journal of the American Helicopter Society*, Vol. 25, No. 4, October 1980, pp. 5-12.

[5]Peters, David A. and Ormiston, Robert A., "Flapping Response Characteristics of Hingeless Rotor Blades by a Generalized Harmonic Balance Method," *NASA TN D-7856*, February 1975.

[6]Kuczynski, W.A. and Sissingh, G.J., "Characteristics of Hingeless Rotors with Hub Moment Feedback Controls Including Experimental Rotor Frequency Response," NASA CR 114427, January 1972.

[7]Hsu, T-K, "Coupled Rotor/Airframe Vibration Analysis by a Combined Harmonic-Balance, Impedance-Matching Method," Doctor of Science Thesis, Washington University in St. Louis, May 1981.

APPLICATION OF AN ANALYTIC STALL MODEL TO TIME-HISTORY AND EIGENVALUE ANALYSIS OF ROTOR BLADES*

Jon P. Rogers**
Graduate Student
Washington University
St. Louis, Missouri

Presented February 3, 1982

Revised April 11, 1983

*Co-Winner of the 1982 Robert L. Lichten Award

**Presently with the U.S. Army Aviation Research and Development Command, Directorate for Advanced Systems, St. Louis, Missouri

Abstract

A dynamic analysis of a single-section model of helicopter blade is performed including an analytic model of dynamic stall. This stall model, a simplified version of the model introduced by Tran and Petot[1], characterizes the lift force on the blade section throughout both the linear and non-linear regimes of angle of attack. The resultant, nonlinear blade equations are solved by numerical integration for the periodic, forced response. Perturbation equations, written for small disturbances about this equilibrium, provide eigenvalue and stability information by means of Floquet theory.

Notation

a = linear static lift curve slope, per degree

$\bar{a}$ = linear static lift curve slope, per radian

a_i = coefficients of the non-linear static lift curve polynomial

b = blade element semi-chord, equal to c/2, m

c = blade element chord, m

$\bar{C}$ = phase shift parameter

C_z = total lift coefficient, lift measured normal to free stream, $C_{z_1} + C_{z_2}$

C_{z_1} = lift coefficient in linear regime

C_{z_2} = lift coefficient in non-linear regime

C_{z_ℓ} = static lift coefficient in linear regime

C_{z_s} = static lift coefficient, approximate expression

C_{z_o} = actual static lift coefficient

ΔC_z = difference between the extended linear static lift coefficient (C_{z_ℓ}) and the actual static lift coefficient (C_{z_o})

d = blade element span, m

I_y = mass moment of inertia of blade section about center of rotation, $kg\text{-}m^2 = mx^2$

$\bar{k}$ = reduced frequency $\bar{k} \equiv \omega b/\Omega x$

k = ratio of semi-chord to radial position $\equiv b/x$

k_β = blade flapping restraint spring, N-m/rad, Figure 5

M = Mach number

m = mass of blade section, kg

p = non-dimensional blade flapping frequency, per revolution, $\sqrt{1+k_\beta/\Omega^2 I_y}$

Δ = apparent mass parameter, equation (2)

t = time, sec

$u(\theta)$ = unit step function

U = forward velocity of rotor center, m/sec

V = average blade element velocity, $V = \Omega x$, m/sec

x = distance from center of rotation, m

α = damping parameter, equation (2)

β = blade flapping angle, deg

γ = Lock number based on equivalent blade damping, $8\rho\bar{a}bdx^3/I_y$

$\bar{\gamma}$ = natural frequency parameter, equation (2)

δ = parameter relating lift and airfoil pitch rate, equation (2)

λ = system eigenvalue

θ = total aerodynamic angle of attack, deg

θ_o = mean angle of attack (collective pitch minus inflow angle), deg

θ_s, θ_c = cyclic pitch, deg

θ_{cr} = airfoil angle of attack at which lift departs from linearity, deg

$\tilde{\theta}$ = amplitude of airfoil oscillation, deg

λ = time delay parameter, equation (2)

$\bar{\mu}$ = local advance ratio at blade section, $U/\Omega x$

μ = equivalent advance ratio of uniform blade, $\mu = .75\bar{\mu}$

τ = reduced time, $\tau = \Omega x t/b$

ψ = azimuth angle, $\psi = \Omega t = k\tau$

Ω = rotor speed, rad/sec

ω = airfoil frequency of pitch oscillation, rad/sec

$(^{*}),(^{**})$ = $\partial/\partial\tau$, $\partial^2/\partial\tau^2$ (derivatives with respect to reduced time, τ)

$(\ )_F$ = periodic, forced response of ( )

$(\ )_P$ = perturbation to ( )

Introduction

The phenomenon of dynamic stall is known to be important for the dynamic analysis of helicopter rotors in forward flight, Reference 2. Consequently, a great deal of effort has gone into the development of analytic methods that will predict the behavior of both rotor lift and section pitching moment during dynamic stall. The most general methods available are based on tabulated data in a three-dimensional array (angle of attack, reduced pitch rate, reduced pitch acceleration) with an appropriate correction for local Mach number, References 3 and 4. Other methods of analysis have attempted to replace the large arrays of tabulated data with analytic expressions. References 5, 6, and 7 outline a method in which dynamic stall is treated as in impulse loading that occurs when stall is encountered and that decays following the stall event. References 8 and 9 describe a method based on a dynamic (or equivalent) angle of attack. The appropriate lift coefficient is chosen as the smaller of two formulas, based on this equivalent angle. Similar work has included a more detailed analysis to predict the onset of stall, Reference 10. This work also includes a time delay factor to account for the finite time required to shed vorticity.

Other work in dynamic stall has concentrated on the reduction of the large volumes of lift and moment data (i.e. the three-dimensional tables) to compact analytic expressions. In Reference 11, dynamic stall data is represented in terms of 47 parameters that synthesize the measured data. In Reference 12, this same method is extended (by the introduction of an equivalent angle of attack) to include arbitrary time variations in pitching motions. The equivalent angle of attack is based on Duhamel's integral with the Wagner function chosen as the unit step response to pitch. The results indicate good agreement with measurements.

In Reference 1, an alternative method is introduced for the calculation of dynamic stall; and that method is the subject of this paper. The model in Reference 1 describes the lift and moment coefficients in terms of ordinary differential equations. The equations are of first order in the linear regime, and they are of third order in the nonlinear regime. They include an analytic approximation to the static lift and pitching moment data as well as 12 coefficients (6 for lift, 6 for moment) that are chosen based on experimental data. These coefficients are identified as functions of angle of attack by parameter identification applied to $\pm$ 1° oscillations about each mean angle of attack at various reduced frequencies. The resultant, identified equations are used to simulate lift and moment for $\pm$ 6° oscillations about various mean angles of attack; and these show good correlation for angles of attack up to 23°. Reynold's number effects are included implicitly (as in other stall models) implicitly from the Reynold's number of the data base. Mach number can be included in a similar manner or from a local Mach number correction. In Reference 13, this stall model is applied to the dynamic response of a helicopter blade including stability and forced response.

The work reported in this paper is part of a larger research effort to study the stall model of Reference 1 in several ways. First, we wish to study the dynamic characteristics of the stall model including the relative importance of the parameters. Second, we wish to study the implementation of the model on helicopter problems. Of particular interest is the ease with which differential equations can be incorporated into conventional rotor analyses. (Such equations are easily linearized to obtain conventional stability information.) Third, we wish to study the physical basis of the theory including its extension to include unsteady free stream, very large

angles of attack, and plunge (as well as pitch) motions. This present paper is based on the work in Reference 14 but addresses only the lift response for a single, rotating blade section. This study of the sectional properties provides the foundation for the continuing work being done with the model (e.g. Reference 15) in which an entire blade is considered. Despite the fact that the model in question has already been applied to an entire rotor blade in Reference 13, we believe that much basic research still needs to be done to better understand the model and to more consistently apply it to rotor problems. We emphasize that the purpose of this paper is not to assess the accuracy of the method with respect to other dynamic stall models. Rather, the purpose of the paper is to study the basic behavior of this model, as defined in References 1 and 13.

Stall Model

The analytical stall model presented here is that of Reference 1. The model consists of three equations that relate the lift coefficient of an airfoil to its angle of attack as follows

$$\overset{*}{C}_{z_1} + \lambda C_{z_1} = \lambda C_{z_\ell} + (\lambda\Delta+\delta)\,\overset{*}{\theta} + \Delta\overset{**}{\theta} \tag{1}$$

$$\overset{**}{C}_{z_2} + 2\alpha\bar{\gamma}\overset{*}{C}_{z_2} + \bar{\gamma}^2(1+\alpha^2)\,C_{z_2} = -\bar{\gamma}^2(1+\alpha^2)\left[\Delta C_z + \bar{C}\,\frac{\partial \Delta C_z}{\partial \theta}\,\overset{*}{\theta}\right] \tag{2}$$

$$C_z = C_{z_1} + C_{z_2} \tag{3}$$

where C_{z_1} and C_{z_2} are the lift coefficients in the linear and non-linear regions of angle of attack, Θ is the total aerodynamic angle of attack of the airfoil, C_{z_ℓ} is the static lift coefficient in the linear region of angle of attack, ΔC_z is the difference between the extended linear lift curve ($C_{z_\ell} = a\Theta$) and the actual static lift curve (C_{z_o}), and C_z is the resulting total lift coefficient. The parameters $\lambda, \Delta, \delta, \alpha, \bar{\gamma}, \bar{C}$ are functions of blade angle of attack alone (for a given airfoil, Reynolds number, and Mach number) and must be determined from wind tunnel tests by parameter identification.

The parameters in equation (1) have direct physical interpretations in terms of classical, unsteady aerodynamics, Reference 16. The parameter λ is the time-delay parameter associated with the lift deficiency function. It provides for changes in magnitude and phase of the lift. The parameter δ represents lift due to pitch rate. The parameter Δ is the apparent mass term. The parameters in equation (2) are associated with the stall phenomenon. In particular, α is a damping parameter: $\bar{\gamma}$ is the frequency

of the stall response, and $\bar{C}$ is a phase shift parameter associated with the stall response.

The above parameters have been identified for an 0A212 airfoil at 0.3 Mach number, Reference 17. The static values (C_{z_ℓ}, ΔC_z, $\partial \Delta C_z / \partial \Theta$) are approximated in Reference 1 by polynomial approximations. The other parameters are found as functions of mean angle attack from experimental data at $\pm$ 1° oscillations about each mean angle. (The identified parameters are later verified by comparisons with data at $\pm$ 6° oscillations.) Since the tests were performed over a range of reduced frequencies, the resultant parameters are independent of reduced frequency. Thus, $\bar{k} = \omega b / \Omega x$ does not enter explicitly into the equations. It only enters indirectly (for harmonic excitation) through the $\overset{*}{C}_z$ and $\overset{*}{\Theta}$ terms. Thus, the equations are applicable to arbitrary blade motion and not just simple harmonic motion.

The above stall parameters are represented by simplified functions of Θ that approximate the true, identified values. These functions are given by Reference 17.

$$\lambda = 0.2 \tag{4}$$

$$\mathcal{A} = 5\pi/180 \tag{5}$$

$$\delta = \frac{\partial C_{z_\ell}}{\partial \Theta} - \frac{\pm\pi}{180}\left[1 + 1.43\ \Delta C_z\right] \tag{6}$$

$$\bar{\gamma} = 0.10 + 0.023\ (\Theta - 13°)\ u(\Theta - 13°) \tag{7}$$

$$\alpha = 0.105 / \bar{\gamma} \tag{8}$$

$$\bar{C} = 2 - 5.1 \tan^{-1}\{1.21(\Theta - 13°)\}\ u(\Theta - 13°) \tag{9}$$

The static lift curve of the 0A212 airfoil is presented in Figure 1. The curve is defined in the linear region by the equation

$$C_{z_s} = 7.1 \frac{\pi}{180}\theta \qquad \text{for} \qquad \theta \leq \theta_{cr} \tag{10}$$

and in the non-linear region by the seventh order polynomidal

$$C_{z_s} = \sum_{i=0}^{7} a_i(\theta-10°)^i \qquad \text{for} \qquad \theta \geq \theta_{cr} = 10° \qquad (11)$$

where the a_i are given in Reference 17 as

$$\begin{aligned} a_o &= 1.24 \\ a_1 &= 0.124 \\ a_2 &= -0.0630597 \\ a_3 &= 0.01395201 \\ a_4 &= -0.0017390851 \\ a_5 &= 0.00012451913 \\ a_6 &= -4.6849257 \times 10^{-6} \\ a_7 &= 7.087973 \times 10^{-8} \end{aligned} \qquad (12)$$

As mentioned earlier, the above stall model(with the appropriate parameters) has been applied to correlate large oscillation wind tunnel test data. The results, given in Reference 1, are very encouraging. They show that the model is indeed capable of describing the major dynamic stall characteristics of airfoils.

It should be noted here that the polynomial in equation (11) diverges for $\Theta > 30°$, as seen in Figure 1. Therefore, for the work presented here, C_{z_s} is held constant at 0.126 for $\Theta \geq 26°$.

Equations (1)-(3) comprise a description of dynamic stall that is amazingly simple to use. The model is composed of differential equations that describe lift in a context similar to the manner in which the other differential equations describe blade motions. C_{z_1} and C_{z_2} are always present (no switching on or off is necessary); but, in the linear regime, ΔC_z is zero so that C_{z_2} has

no excitation (it decays to zero on its own). Similarly, the C_{z_1} equation is always operative; but, in the unstalled region, it becomes a linear equation. It is the ease of utility of this model that provides the motivation to study it.

Verification and Simplification of Stall Model

The first step in the present application of the stall model to rotor dynamic analysis is to verify the validity of the model by reproduction of the previously published lift hysteresis loops. Thus the stall model, equations (1)-(3), has been transformed into a computer code that uses a Runge-Kutta method of numerical integration for solution. Figure 2 shows the results of this analysis in the form of C_z versus Θ. The mean angle of attack, oscillatory angle of attack, and blade parameters were chosen to match the examples given in Reference 1 in order to facilitate the comparison. The results of our computations generally duplicate the published data of Reference 1 for mean angles of attack of 11° or less. The hysteresis loops tend to take on an ellipsoidal appearance when angle-of-attack excursions do not exceed the static stall angle of attack. As slightly higher mean angles of attack are encountered, the loops tend to take on figure eight shapes; and at mean angles of attack well above stall, the loops are more erratic. For mean angles of attach between 12° and 14°, however, oscillations appear in the return portion of the present lift curves; and these are not found in the published data of Reference 1. Numerical convergence tests on the solution have revealed that these oscillations do indeed occur from the correct numerical solution of equations (1)-(3). However, if a relatively course step size is used in the integration, the oscillations are effectively filtered out of the response; and the smooth curves of Reference 1 appear. We have verified this by numerical experiments with validated integration codes. It may be that such an unconscious filtering occurs in Reference 1, thus explaining the lack of oscillations in those results.

The oscillations in the return strokes of Figure 2 are rather interesting from a theoretical standpoint in that similar oscillations appear in some experimental data, such as that reported in Reference 12. In other frequency-response tests, however, data are often averaged over many hysteresis loops. This averaging (along with the frequency-response characteristics of instrumentation) sometimes can mask such oscillations. Thus, they do not always appear in published data. However, the presence of these oscillations in the data of Reference 12, and in the model of Reference 1, may indicate that the oscillations in Figure 2 represent a true simulation of a physical phenomenon.

The next step in the research reported here, is to study the stall model for possible simplifications. A natural candidate for simplification is the elimination of some of the time derivative terms involving $\ddot{\theta}$ and $\dot{\theta}$ (apparent mass and angular rate terms). These terms are good candidates for elimination on at least two counts. First, they are almost always eliminated in simplified rotor-blade analyses; and, second, their retention (especially $\ddot{\theta}$) results in a cumbersome complication in the state variable equations for rotor flapping. Therefore, it is useful to study the effects of $\dot{\theta}$ and $\ddot{\theta}$ terms on the stall model. In the first study, the lift hysteresis loops are generated with $\Delta, \bar{C}, \delta = 0$ in equations (1) and (2) (no $\dot{\theta}$ or $\ddot{\theta}$ terms). Figure 3 shows C_z versus θ for $\tilde{\theta} = 6°$ and at four typical mean angles of attack. The resulting plots are not at all similar to the original results presented in Figure 2. Therefore, the stall model is oversimplified by elimination of all three parameters. Further investigation, however, shows that setting only the parameter Δ to 0 produces a much smaller effect on the hysteresis loops. An example is given in Figure 4 which gives C_z versus θ with the $\Delta = 0$,

$k = .05$. Similar runs have been made for $0 \leq \Theta_o \leq 17°$ and $.05 \leq k \leq .15$. These all show that A can be deleted from the stall model without a major change in the response. One might argue that only the $\ddot{\theta}$ should be removed from equation (1) with A remaining on the $\dot{\theta}$ term. As it turns out, however, A is only 12% of the total $\dot{\theta}$ term $(A\lambda+\delta)$ so that either approximation would be valid, although including the $\dot{\theta}$ will be slightly more accurate. In the remainder of this paper, the stall model of Tran and Petot, equations (1)-(3), will be used with the parameter A set to zero. This will be referred to as the "simplified stall model."

that the typical section in Figure 5 is at the 3/4 blade radius. Thus, we have the definitions

$$\mu_1 = \frac{3U}{4\Omega X} \quad , \quad \bar{\mu}_1 = \frac{U}{\Omega X} \quad , \quad \mu_1 = \frac{3}{4}\bar{\mu}_1$$

where μ is the dynamic equivalent to the advance ratio of a uniform blade, and $\bar{\mu}$ is the local advance ratio at the blade section.

The above definitions give flapping equations of the following form. (Details are given in Reference 14.)

$$\beta'' + k^2\rho^2\beta = \frac{\gamma'}{8} k^2 \frac{C_z(\theta,\tau)}{a}\left(1+\bar{\mu}_1 \sin k\tau\right)^2 \qquad (15)$$

Several aspects of equation (15) are noteworthy. First, the equation results directly from Newton's laws applied to the blade model in Figure 5 with lift given by the lift coefficient multiplied by $1/2\,\rho(V + U\sin\Psi)^2$. Second, the equation is written in terms of reduced time, τ, rather than in terms of real time, t, or azimuth angle, Ψ. The transformation from τ to either t or Ψ is easily made, however, by the definitions of these parameters.

$$\tau \equiv \frac{\Omega X}{b} t \quad , \quad k \equiv \frac{b}{X} \quad , \quad \Psi = k\tau = \Omega t \qquad (16a,b)$$

We have followed the suggestion of References (1) and (13) in using only the mean portion of velocity, ΩX, in the reduced time. (For further discussion of this assumption see Reference 15.) Note that the definition of k in equation (16b) is independent of any frequency. It is simply a measure of the ratio of blade chord to radial position. A final comment on equation (15) is with respect to the parameters "a" and "$\bar{a}$". The parameter a is the nominal lift-curve slope used in the definition of γ', with one alteration. In γ', we use

Rotor Blade Model

The rotor blade model used in the dynamics application of the simplified stall model is presented in Figure 5. The model consists of a single blade section located at a radial position x from the center of rotation. A single blade section is used to facilitate investigation of the model. Since any blade can be considered as a composite of such sections, this analysis forms the foundation for future work with an entire blade, for example Reference 15. Three virtual forces act on the blade element: 1) the centrifugal force, F_3, 2) the D'Alembert Force, $m\ddot{x}$, and 3) the normal lift force, L, which is a function of angle of attack, θ, and reduced time, τ. The blade is allowed to flap with angle, β, and is restrained in the flapping direction by a root spring, k_β. The angular velocity of the blade element about the hub is Ω. Physical dimensions of the element are c (the chord), d (the span), and b (the semi-chord).

Obviously, the model depicted in Figure 5 is far from an actual helicopter rotor blade. However, please recall that we wish to study the behavior of the stall model for a typical section. It follows, that we would like the model in Figure 5 to be the dynamic equivalent of a uniform rotor blade. This will give the most realistic response and the most valuable comparisons. Dynamic equivalence in hover is obtained by the definitions

$$\gamma' = 8\rho \bar{a} b d x^3 / I_\gamma \quad , \quad \rho^2 = \sqrt{1 + \frac{K_\beta}{\Omega^2 I_\gamma}} \qquad (13a,b)$$

Although this γ' may look cosmetically different from the conventional definition of Lock number, it is actually the exact dynamic equivalent. Similarly the best forward-flight equivalence is found under the assumption

that the typical section in Figure 5 is at the 3/4 blade radius. Thus, we have the definitions

$$\mu_1 = \frac{3U}{4\Omega X} \quad , \quad \bar{\mu} = \frac{U}{\Omega X} \quad , \quad \mu = \frac{3}{4}\bar{\mu}$$

where μ is the dynamic equivalent to the advance ratio of a uniform blade, and $\bar{\mu}$ is the local advance ratio at the blade section.

The above definitions give flapping equations of the following form. (Details are given in Reference 14.)

$$\beta'' + k^2\rho^2\beta = \frac{\gamma'}{8} k^2 \frac{C_z(\theta,\tau)}{a}(1+\bar{\mu}\sin k\tau)^2 \qquad (15)$$

Several aspects of equation (15) are noteworthy. First, the equation results directly from Newton's laws applied to the blade model in Figure 5 with lift given by the lift coefficient multiplied by $1/2\,\rho(V + U\sin\Psi)^2$. Second, the equation is written in terms of reduced time, τ, rather than in terms of real time, t, or azimuth angle, Ψ. The transformation from τ to either t or Ψ is easily made, however, by the definitions of these parameters.

$$\tau \equiv \frac{\Omega X}{b} t \quad , \quad k \equiv \frac{b}{x} \quad , \quad \Psi = k\tau = \Omega t \qquad (16a\text{-}c)$$

We have followed the suggestion of References (1) and (13) in using only the mean portion of velocity, ΩX, in the reduced time. (For further discussion of this assumption see Reference 15.) Note that the definition of k in equation (16b) is independent of any frequency. It is simply a measure of the ratio of blade chord to radial position. A final comment on equation (15) is with respect to the parameters "a" and "$\bar{a}$". The parameter a is the nominal lift-curve slope used in the definition of γ', with one alteration. In γ', we use

"$\bar{a}$" as "per radian" to conform with conventional definitions. In the denominator of equation (15), however, we use "a" as "per degree". This effectively converts β to degrees in the equation.

The simplified stall model enters equation (15) in that "$C_z(\theta, \tau) = C_{z_1} + C_{z_2}$" is described by equations (1)-(3), the stall model under investigation. Of importance here is the fact that C_z is a function of θ and $\overset{*}{\theta}$ which, in turn, are functions of β and $\overset{*}{\beta}$. In particular, the total aerodynamic angle of attack and its derivative can be approximated by the expressions

$$\theta = \theta_o + \theta_s \sin(k\tau) + \theta_c \cos(k\tau) - \left[\frac{\overset{*}{\beta}/k + \bar{\mu}\beta\cos(k\tau)}{1 + \bar{\mu}\sin(k\tau)}\right] \tag{17}$$

$$\overset{*}{\theta} = \theta_s k\cos k\tau - \theta_c k\sin k\tau - \left[\frac{\overset{**}{\beta}/k + \mu\overset{*}{\beta}\cos(k\tau) - \mu\beta k\sin(k\tau)}{1 + \mu\sin(k\tau)}\right] + \left[\frac{\mu\overset{*}{\beta}\cos(k\tau) + \mu^2\beta k\cos^2(k\tau)}{(1 + \mu\sin(k\tau))^2}\right] \tag{18}$$

where we have assumed $\tan\theta \approx \theta$ in determining the angle of attack due to β. (This assumption breaks down, however, for $\bar{\mu} > .3$ as is discussed in Reference 15.) Equation (17) implies more than just a coupling between the β and C_z equations. It also implies a nonlinearity in the system beyond the loss of lift in stall. To be precise, we recall that some of the coefficients of the C_z equation (δ, $\bar{\gamma}$, α, and $\bar{G}$) depend explicitly on θ, equations (6)-(9). Equation (17), therefore, implies more than just a time variation of these parameters; it also implies a nonlinear dependence with β.

One will also notice that the induced flow does not appear explicitly in equation (17). Recall, however, that we are dealing only with a single section. Thus, any radial variation of induced flow does not enter the problem. It follows that the induced flow can be considered as part of Θ_0, Θ_s, and Θ_c with no loss of generality. The values of Θ_s and Θ_c used in this present analysis are based on approximate trim formulas developed in Reference 14, which are based on a harmonic balance of the flapping equations in the unstalled regime with Θ_s and Θ_c chosen so as to set the first-harmonic flapping to zero. For small k, these formulas are well approximated by

$$\Theta_s = -\frac{8}{3}\mu\,\Theta_0 \tag{19}$$

$$\Theta_c = \frac{\gamma}{6}\frac{\mu}{p^2}\Theta_0 - \frac{8k}{3\lambda}(1-\delta/a)\mu\,\Theta_0 \tag{20}$$

In the results presented here, the quasi-steady version of equation (20) is used (k = 0) with little loss of accuracy. It is emphasized, however, that equations (19) and (20) do not eliminate cyclic flapping when the blade section is stalled. A discussion of trim under stalled conditions is given in Reference 15.

Before proceeding to numerical results, there are some aspects of the theory of Reference (1) that need further comment. First, the model of Reference 1 does not distinguish between angle of attack due to blade pitch and angle of attack due to vertical velocity components. Both are treated identically in equations (17) and (18). It is evident from Reference 18, however, that these ought to be treated differently in the $\dot{\theta}^*$ term.

Reference 18 convincingly shows that $\overset{*}{\theta}$ should only include the rotation of the airfoil with respect to the air mass. Thus, only the geometric pitch rate should be included. Furthermore, Reference 18 shows that the component of Ω along the blade, $\Omega \sin\beta$, should also be included. Thus, a more consistent $\overset{*}{\theta}$ would be

$$\overset{*}{\theta} = \theta_s k \cos(k\tau) - \theta_c k \sin(k\tau) + k\beta \qquad (21)$$

A second aspect of the model of Reference (1) is that the theory and experiments of Reference 1 are for a constant free stream, although the authors suggest that the theory may be extended to unsteady free stream by use of the average velocity (in defining reduced time) and by implementation of the unsteady velocity in both the lift expression, $C_z(V + U \sin\Psi)^2$, and in the angle of attack. Again, however, the linear, unsteady aerodynamic theory in Reference 19 shows that this is <u>not</u> the best way to extend unsteady aerodynamics to the case of oscillatory free stream. (In particular, extension to unsteady free stream must be done for the circulation equations and not for lift coefficient.) Nevertheless, in the work here we apply the stall model in exactly the way suggested in Reference 1. The errors introduced by the above anomalies are treated in Reference 15 and in ongoing research. A third aspect of the Tran and Petot model deals with the apparent mass terms. If $A\overset{**}{\theta}$ is retained in the equations, then $\overset{**}{\theta}$ introduces $\overset{***}{\beta}$, as can be seen by inspection of equation (18). This necessitates an extra state variable, $\overset{**}{\beta}$, in the system equations. Thus, there is an advantage to neglect this term as we have done.

As a final comment on the model of Reference 1, we note that the model is identified for a nonrotating airfoil. One might expect differences in the lift for rotating and nonrotating airfoils in the same way that Loewy's theory differs from Theodorsen's (as function of thrust and number of blades), Reference 20.

However, there is nothing in the theory to imply that the parameters could not be just as well identified for a rotating airfoil. Thus, we proceed with the study and apply the parameters of equation (4)-(9) to a rotor-blade section.

Time History Solutions

The combined set of simplified-stall-model and blade-dynamic equations form a fifth-order system (2nd order β, 1st order C_{z_1}, 2nd order C_{z_2}). State variables are introduced into this system ($y_1 = \beta$, $y_2 = \dot{\beta}$, $y_3 = C_{z_1}$, $y_4 = C_{z_2}$, $y_5 = \dot{C}_{z_2}$) and the resulting equations are solved by use of a predictor-corrector numerical integration. The time history is begun with zero initial conditions and is continued over a sufficient number of cycles to ensure that all transients have decayed. (Usually, six to ten cycles are sufficient to obtain convergence.) The forced response of the combined stall-model, blade-dynamics system is calculated initially for the following baseline parameters

$$M = 0.30,\ k = 0.05,\ \gamma = 6.0,\ p = 1.0,\ \bar{\mu} = 0.20 \qquad (22a\text{-}e)$$

The choice, k = .05, implies b/x = .05. Later on, variations will be made in $\bar{\mu}$ and k. The pitch angle θ_o is specified as 10° so that the airfoil will oscillate well into the linear and non-linear portions of the lift curve. Thus, the effect of dynamic stall on the response of the airfoil can be seen.

Figure 6 presents the results for the combined stall-model, blade-dynamics system with the above baseline parameters. In Figure 6a, the lift coefficient is plotted versus θ. A typical "figure 8" plot is obtained. However, in contrast to the earlier plots, this curve is complicated by the fact that θ includes blade flapping contributions and is not purely simple harmonic. Figure 6b presents the blade flapping response. The response for an analysis without stall is also given for comparison. We notice that the unstalled rotor is almost exactly trimmed (no once-per-rev in β) whereas the stalled blade is not completely trimmed. (There is a significant once-per-rev component.) This results from the fact that we are using approximate trim formulas.

The average value of β for the unstalled case is .13 radians, and the average value for the stalled case is .10 radians. This drop in β can be attributed to the overprediction of lift by the linearized model. Figure 6c depicts the variation of θ with azimuth angle for both the stalled and unstalled models. For the unstalled case, the variation in θ is completely due to θ_s and θ_c, $\hat{\theta} = \sqrt{\theta_s^2+\theta_c^2} = \pm 4^\circ$, since β has little unsteady component. For the stalled case, θ_s and θ_c remain the same, but the cyclic flapping adds another $\pm$ 2° to the angle of attack yielding $\hat{\theta} = \pm 6^\circ$ (even deeper into stall). An interesting aspect of the curves in Figure 6 is the 90° phase lag between stall and the drop in flapping. Under unstalled, trimmed conditions, the variations in θ exactly counter the variations in free stream to give a uniform lift and uniform β. When stall is introduced, however, there is a large drop in C_z at the maximum θ. (Compare linear and stall models in Figure 6a.) Figure 6c shows that this drop occurs nearly at Ψ = 270°, when θ is maximum. The resultant drop in β, however, occurs about 90° later at Ψ = 360°. This is the well-known gyroscopic effect that causes the tip path of a rotor to respond 90° out of phase with the lift. Similar analyses have been performed over a range of advance ratios, μ, and nondimensional semi-chord, k. These all show the same general trends as in Figure 6, Reference 14.

In the above paragraphs, we considered the forced response of the coupled stall model and rotor model. We now wish to turn to another aspect of dynamic analysis that is very important, the calculation of transient response characteristics. First, we will treat transient response in hover, μ = 0. Although this may seem somewhat less interesting than the transient response in forward flight, it forms the foundation necessary to understand the forward flight transients (as investigated in the next section). To begin, we give the blade an initial angle of attack with β, $\overset{*}{\beta}$, C_{z_1}, C_{z_2}, and $\overset{*}{C}_{z_2}$ all set to zero; and we solve numerically to investigate the transient build-up of lift

and coning. Figure 7 presents such results for three different step inputs. First, Figure 7a gives results for $\Theta_o = 10°$. (Since no stall occurs for $\Theta < 10°$, this figure is typical of all lower values of Θ_o.) A typical, linear transient response is observed with a decay near the expected value, $e^{-k\gamma/16}$. At a higher angle of attack, however, ($\Theta_o = 12°$ in Figure 7b), the transients do not completely decay. Instead, there is a small limit cycle that remains. This indicates a mild instability in the coupled stall-flap equations. When the blade stalls, β begins to drop which changes the angle of attack causing an increase in lift. The flapping angle, β, consequently responds causing a new stall cycle. Figure 7c shows that this stall instability is more pronounced at $\Theta_o = 14°$ (a larger limit cycle). Reference 14 provides simultaneous plots of C_{z_1} and C_{z_2} which can be used with Figure 7 to obtain a more complete picture of the coupled lift-rotor instability.

Eigenvalue Analysis of Linearized Equations

To investigate the model behavior further, both in hover and forward flight, we wish to write perturbation equations that will describe the coupled rotor-stall model. On the surface, one might wonder why a linearized perturbation analysis is necessary when one already has the numerical solution of the differential equations. Dynamic analysis over the years, however, has shown again and again that brute-force, numerical solutions of differential equations do not provide the insight of linearized eigenvalue analysis. An eigenvalue analysis provides specific damping, frequency, and mode shape data that is indispensable for the understanding of dynamic phenomena. It is for this reason that the analog and digital response programs of the 1960's gave way to linearized Floquet analysis techniques in the 1970's, Reference 21. It was simply impossible to efficiently extract the necessary insight from time histories alone. Thus, dynamic analysis must encompass eigenvalue analysis as well as forced response.

For the model considered in this paper, the perturbation equations must be written about a periodic equilibrium that describes the forced response. In other words, the perturbation equations describe how the system behaves when it is perturbed away from the normal position. (This is exactly the kind of information that is necessary to study gust response, rotor-body stability, or control derivatives of a helicopter.) In order to obtain these equations, we substitute the following perturbation expansions into equations (1), (2) and (15) where subscript F implies the periodic, forced response of each variable and subscript P implies the infinitesimal perturbation value.

$$C_{z_1} = (C_{z_1})_F + (C_{z_1})_P \tag{23a}$$

$$C_{z_2} = (C_{z_2})_F + (C_{z_2})_P \tag{23b}$$

$$\beta = (\beta)_F + (\beta)_P \tag{23c}$$

$$\Theta = (\Theta)_F + (\Theta)_P \tag{23d}$$

As a result, each of the parameters that depend upon Θ implicitly also takes on expansions.

$$\delta = (\delta)_F + (\delta)_P \tag{24a}$$

$$\bar{\gamma} = (\bar{\gamma})_F + (\bar{\gamma})_P \tag{24b}$$

$$\bar{c} = (\bar{c})_F + (\bar{c})_P \tag{24c}$$

Substitution of equations (23) and (24) into equations (1), (2), and (5) yields a set of $(\ )_F$ terms which by definition cancel since $(\ )_F$ is the forced solution. The remaining terms yield a set of linear differential equations in $(\ )_P$ quantities. Nonlinear terms in $(\ )_P$ are automatically eliminated due to the infinitesimal nature of the perturbation quantities, $(\ )_P$. Some $(\ )_F$ terms remain, however, as coefficients of the $(\ )_P$ quantities. This introduces additional periodic coefficients in the equations. A similar perturbation process is performed in Reference 13 to obtain linearized periodic-coefficient equations. However, several of the perturbation terms have been inadvertently omitted in Reference 13. For example, in the C_{z_1} equation the perturbation of the $\delta\dot{\Theta}^*$ term should be

$$\left[(\delta)_F + (\delta)_P\right]\left[(\dot{\Theta}^*)_F + (\dot{\Theta}^*)_P\right] =$$

$$(\delta)_F(\dot{\Theta}^*)_F + (\delta)_F(\dot{\Theta}^*)_P + (\delta)_P(\dot{\Theta}^*)_F + (\delta)_P(\dot{\Theta}^*)_P \tag{25}$$

The $(\ )_F(\ )_F$ term is not part of the perturbation equations, the $(\ )_p(\ )_p$ term is negligible, but the second and third terms are the perturbation quantities. Equations (6) can be used to express $(\delta)_p$ in terms of the perturbation quantity, $(\beta)_p$.

$$(\delta)_p = \frac{-4\pi}{180}(1.43)\left.\frac{\partial \Delta C_z}{\partial \Theta}\right|_{\Theta=\bar{\Theta}}(\Theta)_p \tag{26a}$$

where

$$(\Theta)_p = \frac{-(\dot{\beta})_p/k + \bar{\mu}(\beta)_p\cos(k\tau)}{1+\bar{\mu}\sin(k\tau)} \tag{26b}$$

The term $(\delta)_p(\dot{\theta})_F$ is omitted from R_{N_1} and S_{N_1} in equation (11) of Reference 13. Similarly, terms involving $(\bar{V})_p$ and $(\bar{C})_p$ are omitted from the C_{z_2} equation in Reference 13. The correct perturbation equations, given in Reference 14, contain these necessary terms.

Results of Eigenvalue Analysis

We now apply the linearized equations obtained in Reference 14 (as described above) to study the behavior of the coupled stall-model, flapping eigenvalues. We emphasize here that, due to the coupling of flapping and lift, the eigenvalues and eigenvectors of the system represent coupled modes with β, C_{z_1}, and C_{z_2} all participating. Nevertheless, one of these three is usually predominant so that each mode can be identified. To begin, we examine the case $\mu = 0$. For this case, the equilibrium values $(\ )_F$ are constant, which results in a set of constant-coefficient equations. The eignevalue analysis of these equations results in the root locus plot of Figure 8. For $0° < \Theta_o < 10°$, the equations are completely linear and the classical, rigid-blade eigenvalues are obtained. The real part of the

flapping eigenvalue $\left(-\frac{\gamma}{16} k\right)$ is the flap damping, and the imaginary part of the eigenvalue $\left(\pm k \sqrt{1-(\gamma/16)^2} \right)$ is the damped flap frequency. Eigenvalues also exist for the C_{z_1} and C_{z_2} equations. These are plotted in Reference 14. As Θ_o is increased beyond 10°, the frequency and damping of the flapping modes decrease due to the smaller slope of C_{z_s}, as seen in Figure 1. By $\Theta_o = 12°$, the damping is nearly neutrally stable. It is this neutral stability that is manifested in Figure 7b as a weak limit cycle. At $\Theta_o = 13°$, full stall is encountered and the flapping eigenvalues make an abrupt change of direction. They quickly become unstable. It is this instability that is manifested in Figure 7c as a strong limit cycle. Thus, we see that the time history behavior is in agreement with the perturbation eigenvalues.

We next turn to the eigenvalue analysis in forward flight. Here, the equilibrium quantities $(\beta)_F$, $(\Theta)_F$, $(C_{z_1})_F$, and $(C_{z_2})_F$ are periodic. They are stored in files, based on the forced response, and then passed to the periodic coefficients in the Floquet analysis. Figure 9 presents results for the entire system as a function of advance ratio for an unstalled case. The real part of each eigenvalue is plotted. The C_{z_2} eigenvalue is the damping of the stall mode. Because the blade is unstalled, this stall eigenvalue is uncoupled from the system and remains fixed at $-\alpha = -.10$. There is a significant amount of coupling, however, between the transient behavior of C_{z_1} and that of β. The flapping eigenvalue splits into two branches at $\bar{\mu} = 0.79$. This is typical of periodic-coefficient systems, e.g. Reference 21.

Figure 10 presents the effect of higher collective pitch on the damping at $\bar{\mu} = 0.25$. At $\Theta_o = 6°$, the blade begins to experience significant stall on the retreating side. Because of this, the flapping and stall eigenvalues begin to interact with each other in a marked way. Both eigenvalues split,

and the flap damping decreases to about 1/2 of its original value at $\Theta_o = 8°$. The type of damping calculation provided in Figure 10 is possible because of the ease of implementation of the stall model of Reference 1 and because of its amenability to linearization.

Summary and Conclusions

The dynamic response of a single section of rotor blade has been calculated including an analytic stall model developed in Reference 1. In this present research, the model is verified and simplified; and the resultant flapping-stall equations are solved both by time history methods and by linearized, eigenvalue analysis. The conclusions of these dynamic analyses are:

1) The simplified stall model can be incorporated into a rotor dynamic analysis by the addition of three state variables at each section. (Four are required for the complete stall model.) One such typical section is analyzed here.
2) The coupled blade-aerodynamic equations for a single section are easily analyzed for time history or for eigenvalue analysis, the latter being effected by a straightforward linearization.
3) The perturbation eigenvalue analysis gives results with direct physical interpretation with respect to the time history solution.
4) Further research is necessary to understand how to correctly apply the model to an entire blade with unsteady free stream and with both pitch and plunge motions.

References

[1]Tran, C.T. and Petot, D., "Semi-Empirical Model for the Dynamic Stall of Airfoils in View to the Application to the Calculation of Responses of a Helicopter Blade in Forward Flight," Vertica, Vol. 5, 1981, pp 35-53.

[2]McCroskey, W.J., "The Phenomenon of Dynamic Stall," NASA TM-81264, March 1981.

[3]Arcidiacono, P.J., Carta, F.O., Casellini, L.M., and Elman, H.L., "Investigation of Helicopter Control Loads Induced by Stall Flutter," USAAVLABS TR 70-2, March 1970.

[4]Carta, F.O. and Carlson, R.G., "Determination of Airfoil and Rotor Blade Dynamic Stall Response," Journal of the American Helicopter Society, Vol. 1o, No. 2, April 1973, pp 31-39.

[5]Ham, Norman D. and Garelick, Melvin S., "Dynamic Stall Considerations in Helicopter Rotors," Journal of the American Helicopter Society, Vol. 13, No. 2, April 1968.

[6]Johnson, Wayne, "The Effect of Dynamic Stall on the Response and Airloading of Helicopter Rotor Blades," Journal of the American Helicopter Society, Vol. 14, No. 2, April 1969.

[7]Johnson, Wayne, "Comparison of Three Methods for Calculation of Helicopter Rotor Blade Loading and Stresses Due to Stall," NASA TN D-7833, November 1974.

[8]Tarzanin, F.J., Jr., "Prediction of Control Loads Due to Blade Stall," Journal of the American Helicopter Society, Vol. 17, No. 2, April 1977.

[9]Gormont, Ronald E., "A Mathematical Model of Unsteady Aerodynamics and Radial Flow for Application to Helicopters," USAAMRDL TR 72-67, May 1973.

[10]Beddoes, T.S., "Onset of Leading Edge Separation Effects under Dynamic Conditions and Low Mach Number," Proceedings of the 34th Annual National Forum of the American Helicopter Society, Paper 78-63, May 1978.

[11]Bielewa, R.L., "Synthesized Unsteady Airfoil Data with Applications to Stall Flutter Calculations," Proceedings of the 31st Annual National Forum of the American Helicopter Society, Preprint No. 935, May 1975.

[12]Gangwani, Santu T., "Predictions of Dynamic Stall and Unsteady Airloads for Rotor Blades," Proceedings of the 37th Annual National Forum of the American Helicopter Society, Preprint No. 81-1, May 1981.

[13]Tran, C.T. and Falchero, D., "Application of the ONERA Dynamic Stall Model to a Helicopter Blade in Forward Flight," Vertica, Vol. 6, 1982, pp 219-239.

[14]Rogers, Jon P., Application of an Analytic Stall Model to Dynamic Analysis of Rotor Blades, Master of Science Thesis, Washington University in St. Louis, May 1982.

[15]Rudy, Daniel J., Comparison of Rotor Blade Flapping Response with Three Different Dynamic Stall Models, Master of Science Thesis, Washington University in St. Louis, May 1983.

[16]Bisplinghoff, Raymond L., Ashley, Holt, and Halfman, Robert L., Aeroelasticity, Addison-Wesley, Reading, Mass., 1955, pp 272-293.

[17]Tran, C.T. and Petot, D., Private Communication to Prof. David A. Peters dated July 21, 1981, and Internal ONERA Report, to be published.

[18]Johnson, Wayne, "Application of Unsteady Airfoil Theory to Rotary Wings," Journal of Aircraft, Vol. 17, No. 4, April 1980, pp 285-286.

[19]Greenberg, J.M., "Airfoil in Sinusoidal Motion in a Pulsating Stream," NACA TN-1326, June 1947.

[20]Loewy, R.G., "A Two Dimensional Approach to the Unsteady Aerodynamics of Rotary Wings," Journal of Aerospace Science, Vol. 24, 1957, pp 82-98.

[21]Peters, D.A. and Hohenemser, K.H., "Application of the Floquet Transition Matrix to Problems of Lifting Rotor Stability," Journal of the American Helicopter Society, Vol. 16, No. 2, April 1971.

Acknowledgment

The author would like to extend his sincerest gratitude to Dr. David Peters for his guidance and moral support during this research.

This work was sponsored by the United States Army Research Office, Grant No. DAAG-29-80-C-0092. The view, opinions, and/or findings contained in this report are those of the author and should not be construed as an official Department of the Army position, policy, or decision, unless so designated by other documentation.

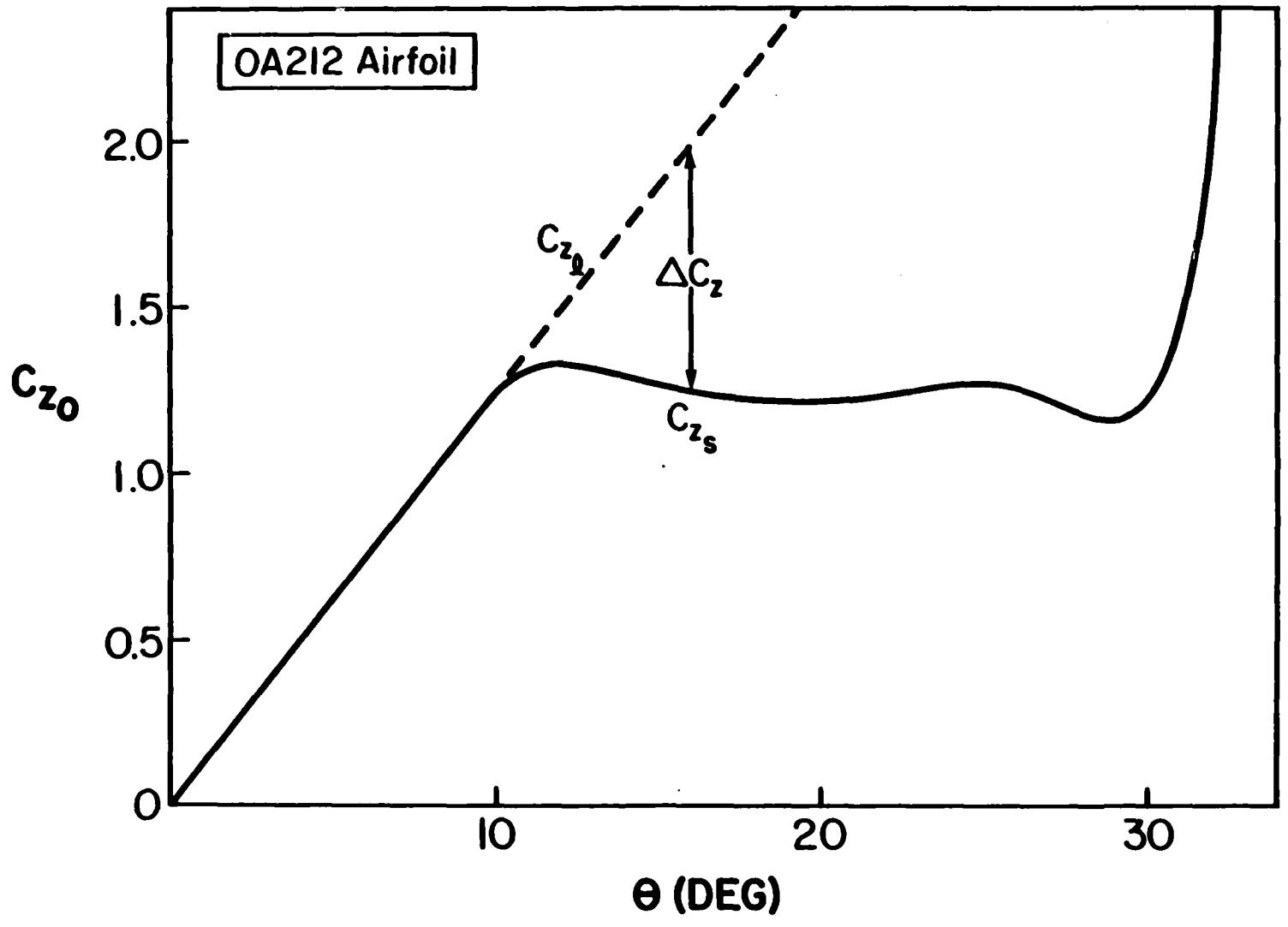

Figure 1. Difference between the Linearized Lift Coefficient and the Actual, Nonlinear Static Lift Coefficient

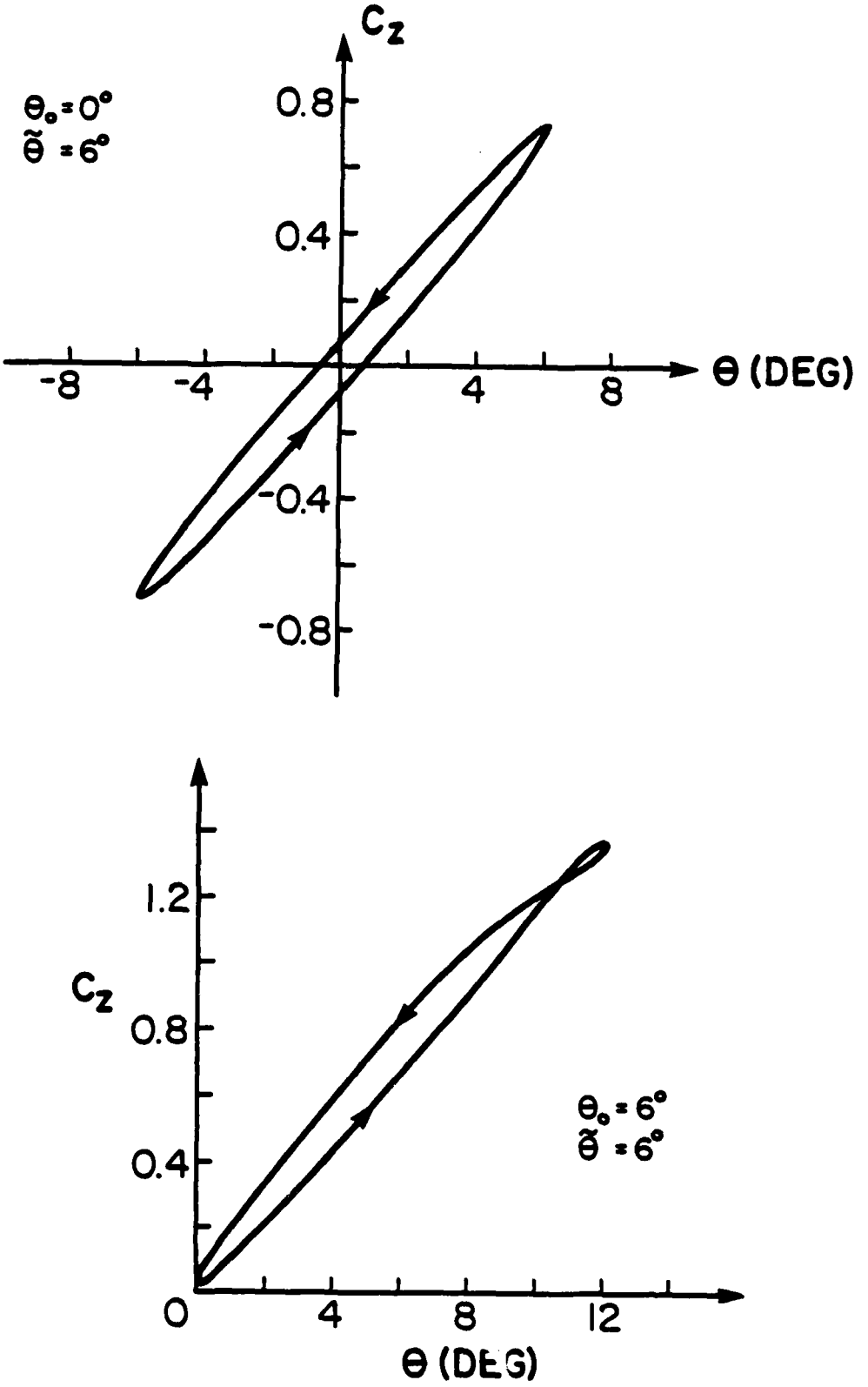

Figure 2. Lift Hysteresis Loops at Various Mean Angles of Attack, M = .30, k = .05

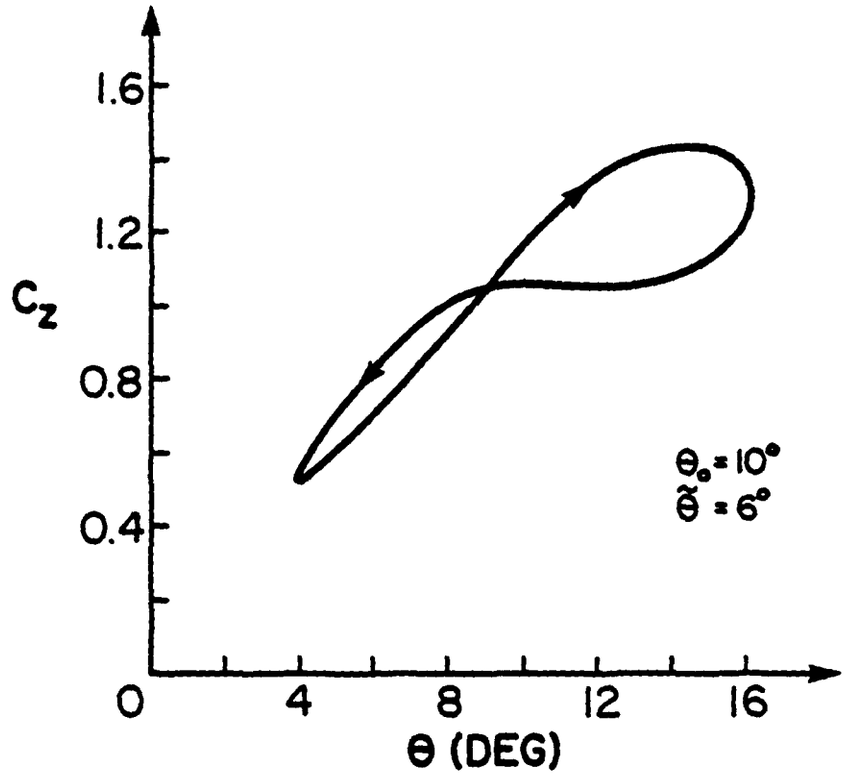

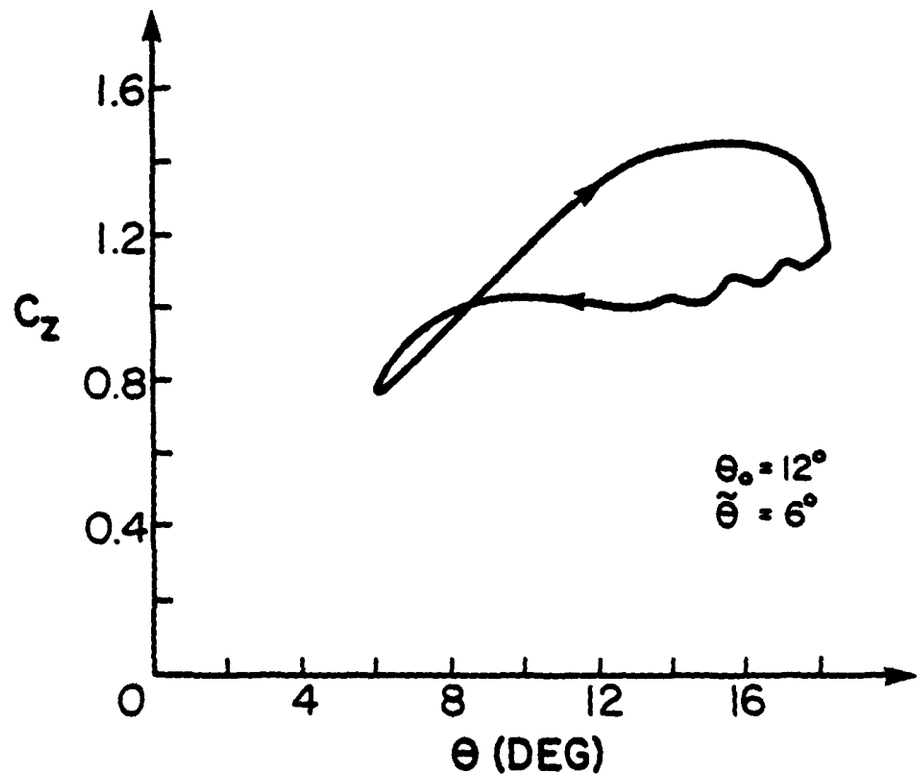

Fig. 2 continued

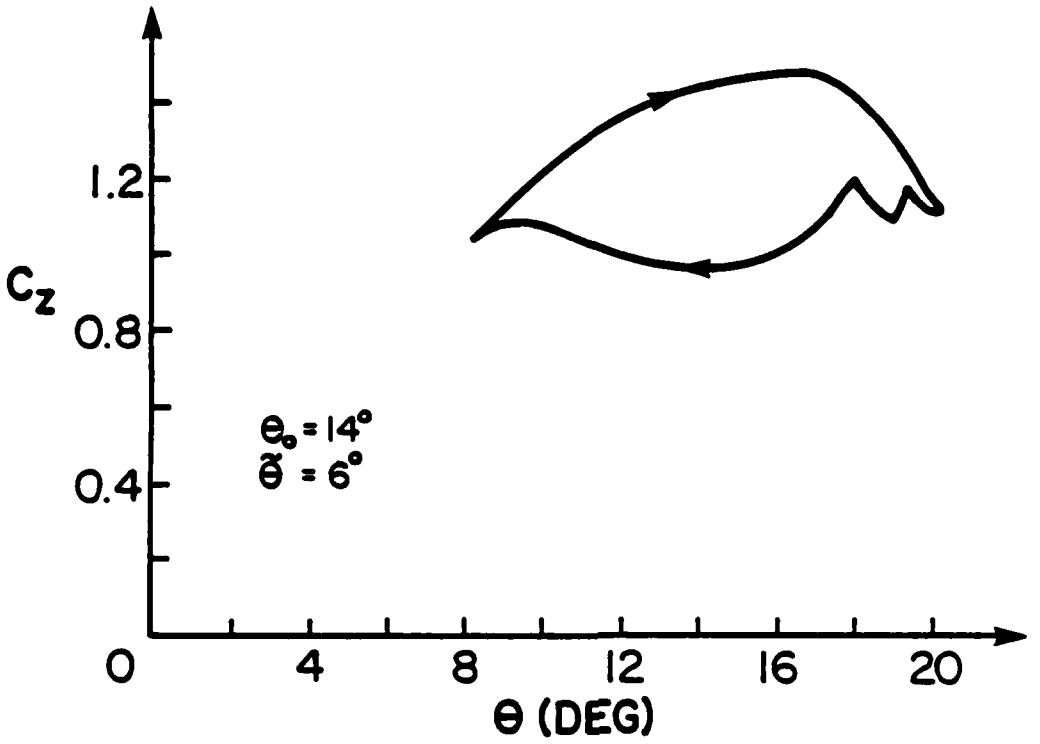

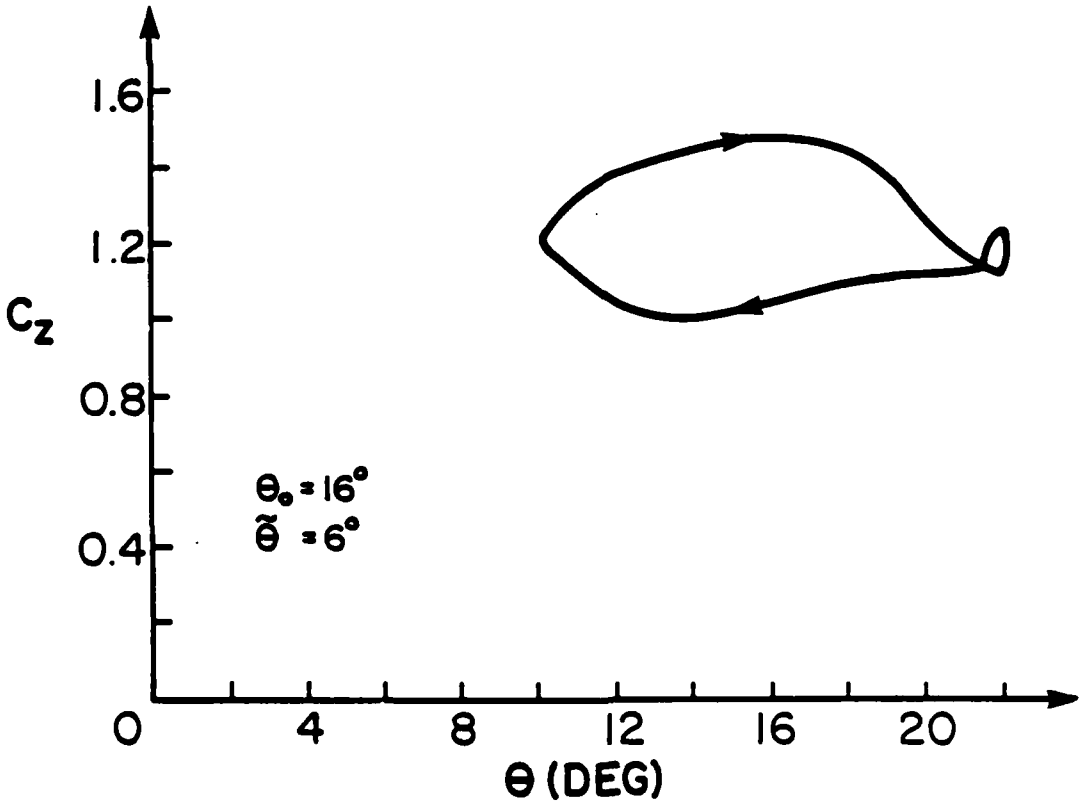

Fig. 2 continued

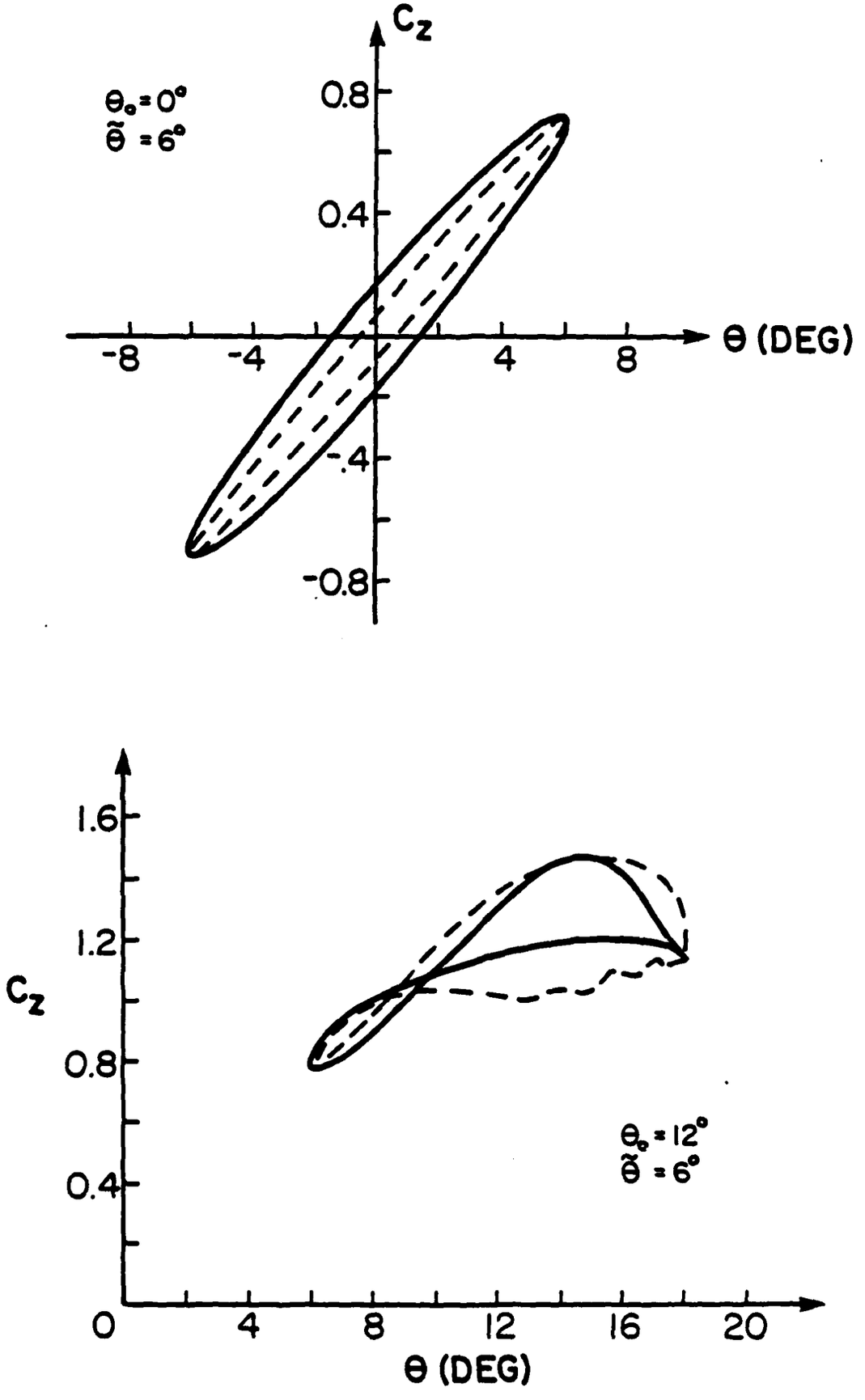

Figure 3. Effect of $\overset{*}{\theta}$ and $\overset{**}{\theta}$ Terms on Lift, k = .05

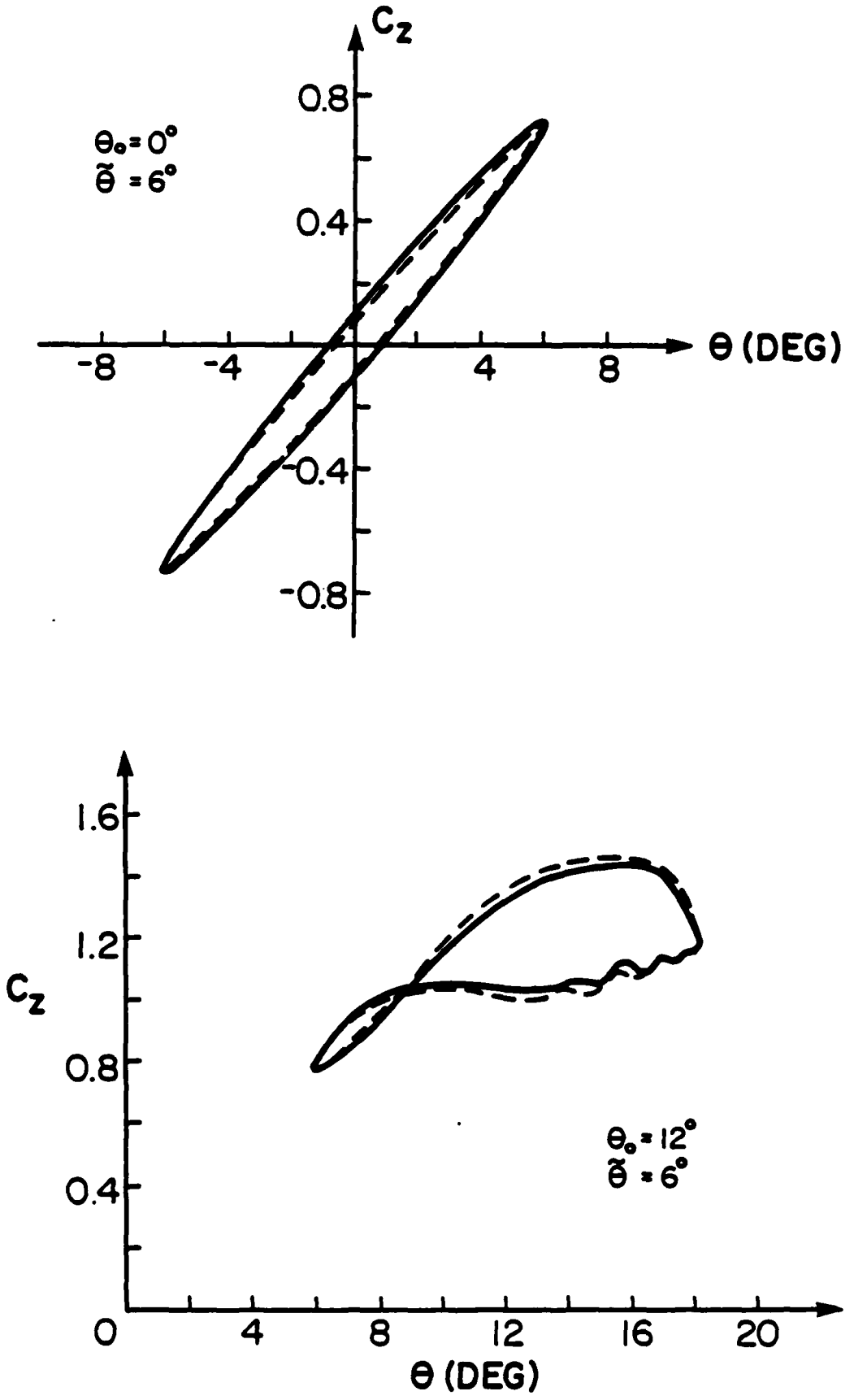

Figure 4. Effect of Apparent Mass Terms on Lift, k = .05

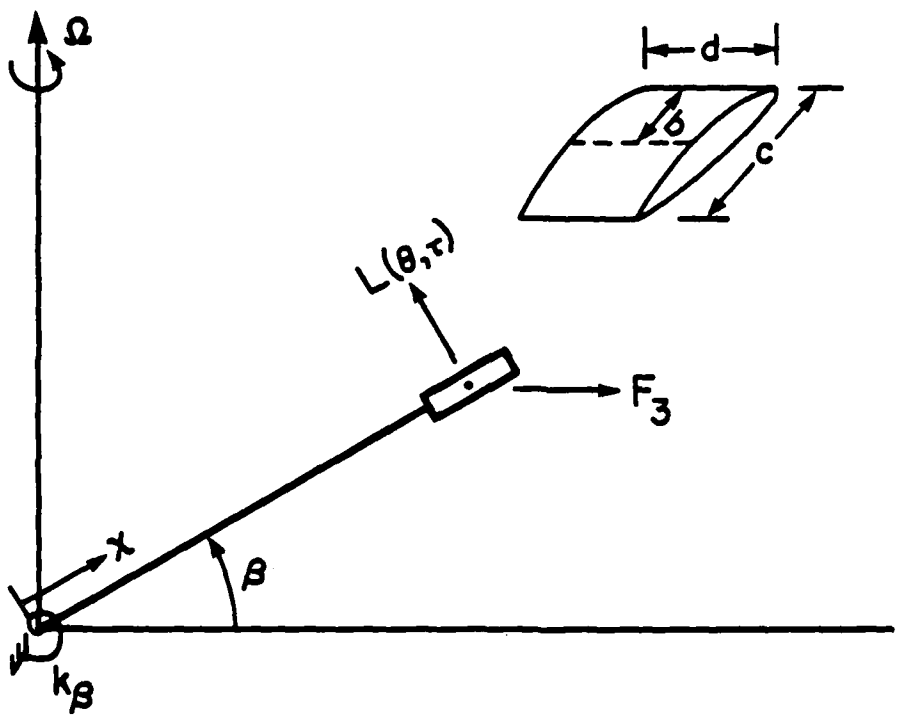

Figure 5. Rotor Blade Model

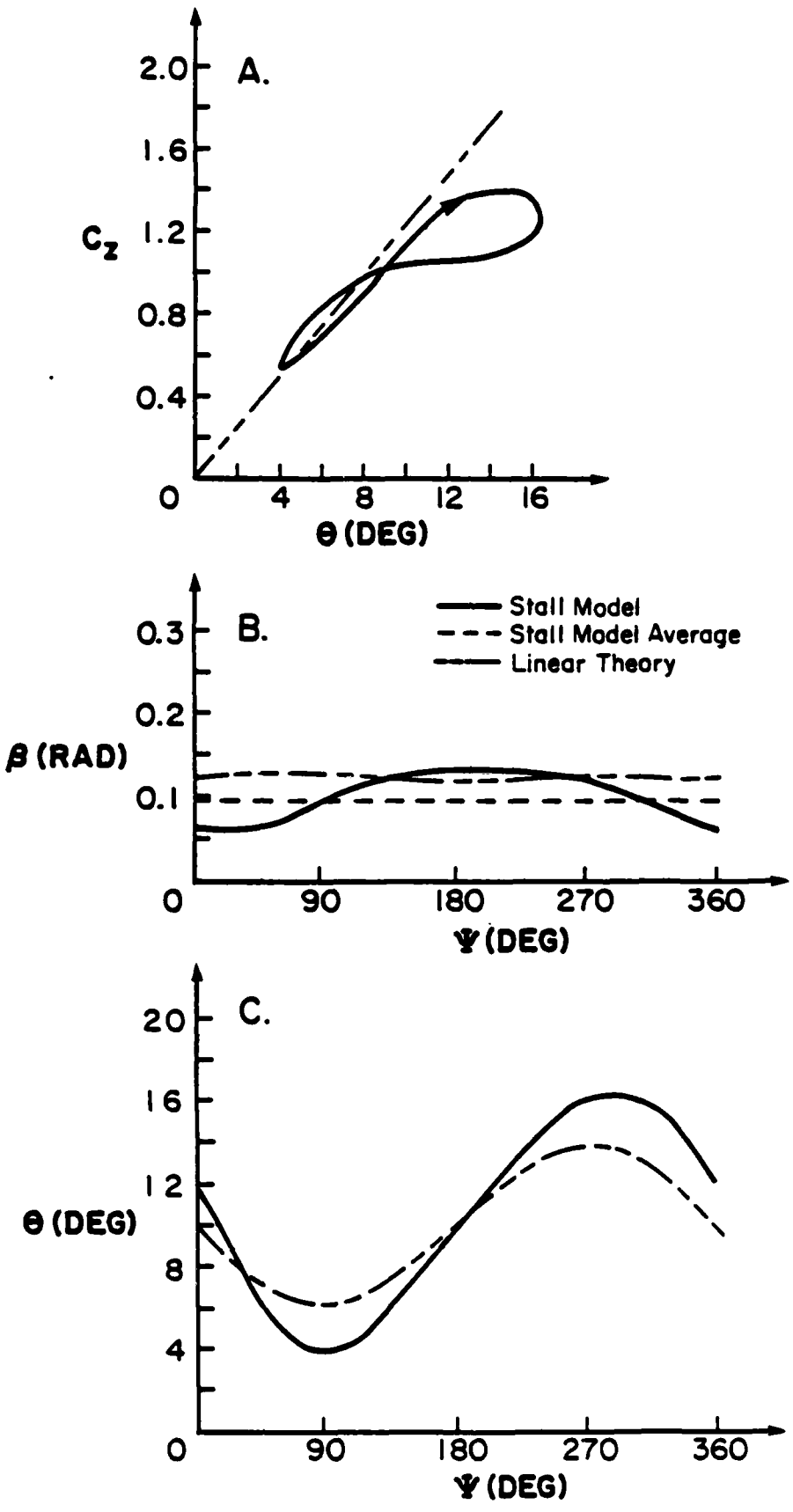

Figure 6. Forced Response of Baseline Configuration

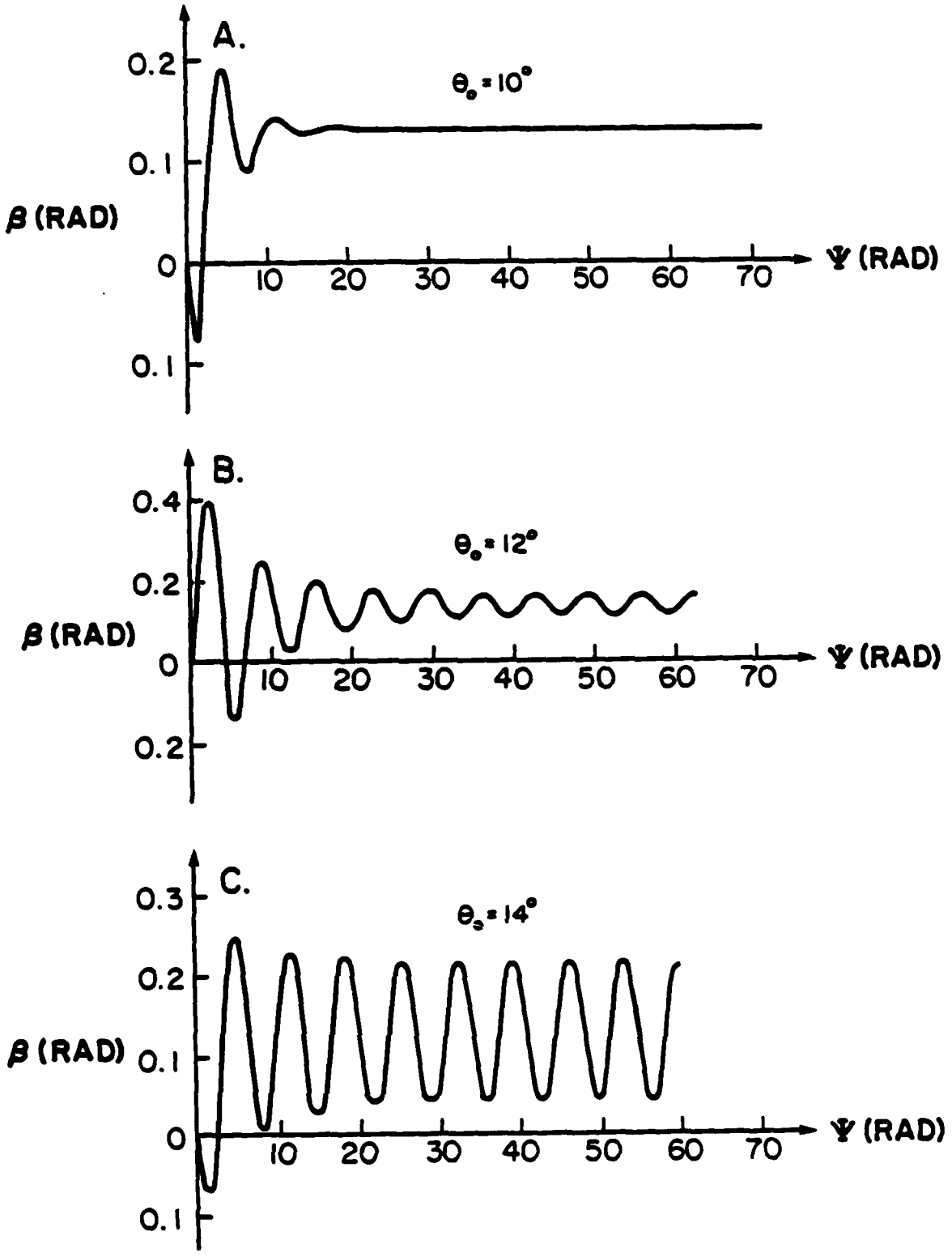

Figure 7. Hover Transients, k = .05, γ = 6, P = 1.0, μ = 0.0

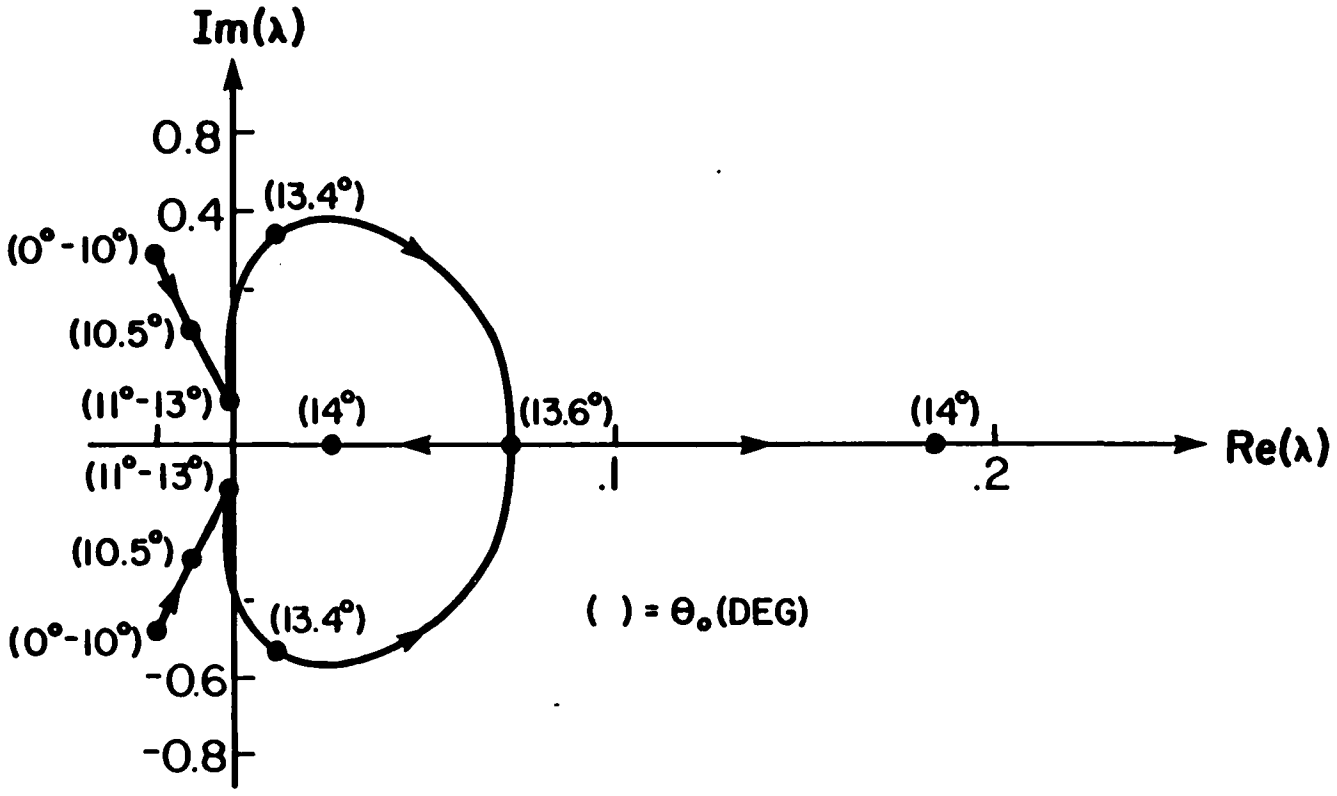

Figure 8. Flap Eigenvalue Root Locus, k = .05, γ = 6, P = 1.0, μ = 0.0

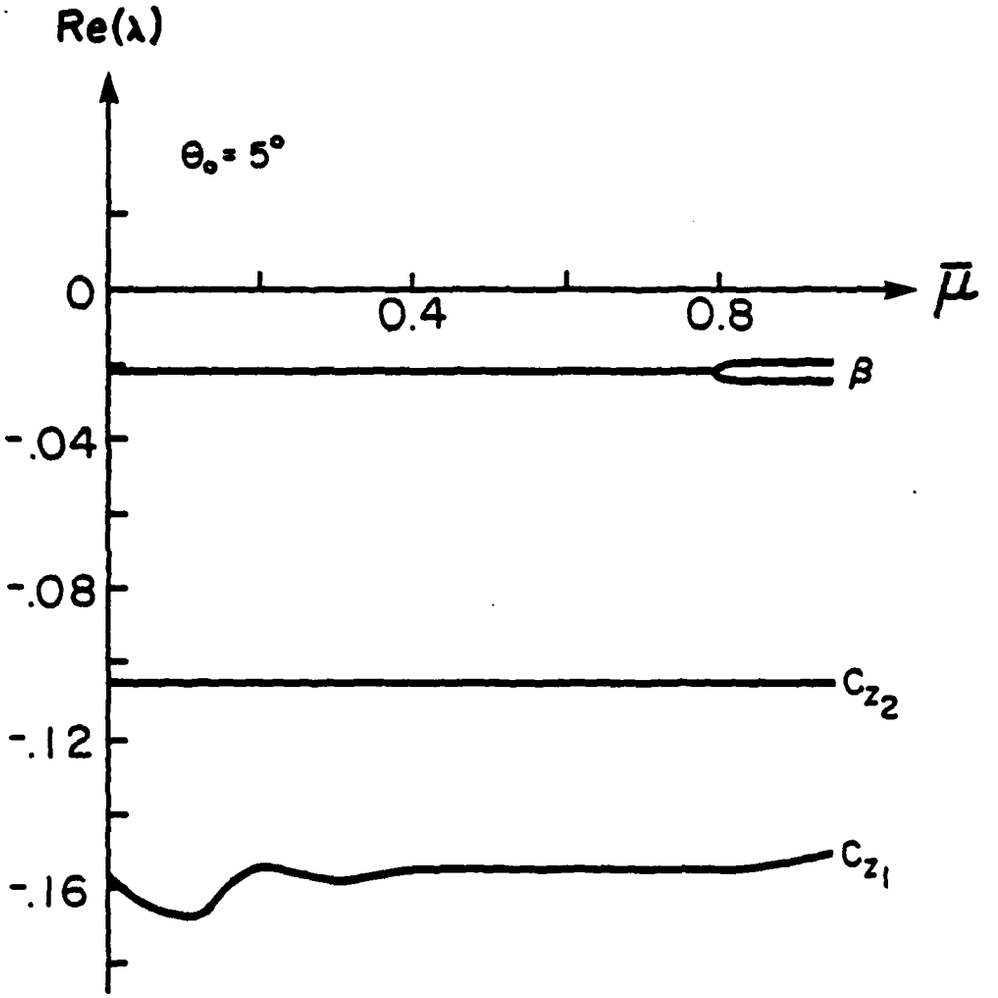

Figure 9. Effect of Advance Ratio on System Damping, k = .05, γ = 6, P = 1.0

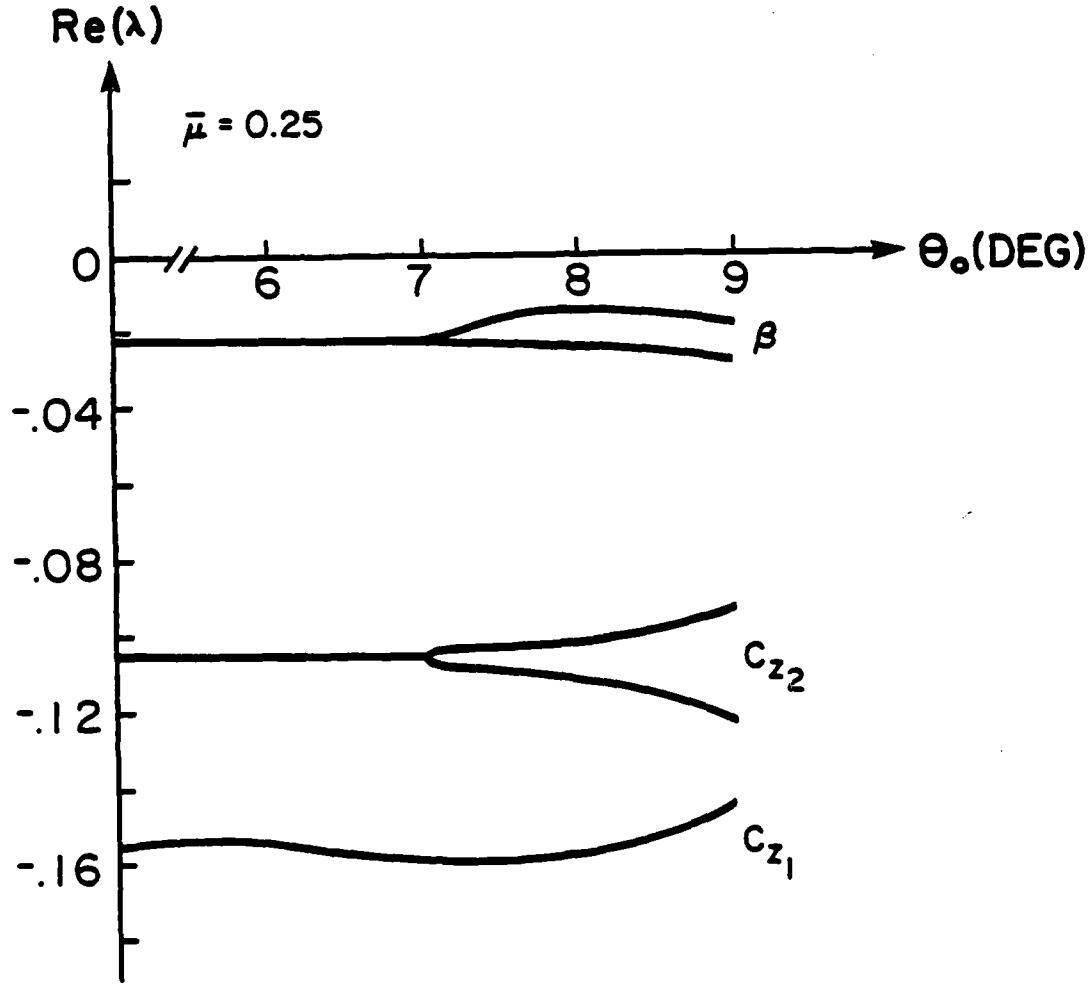

Figure 10. Effect of Collective Pitch on System Eigenvalues, k = .05, γ = 6, P = 1.0, $\bar{\mu}$ = 0.25

List of Figures

Figure 1. Difference between the Linearized Lift Coefficient and the Actual, Nonlinear Static Lift Coefficient

Figure 2. Lift Hysteresis Loops at Various Mean Angles of Attack, M = .30, k = .05

Figure 3. Effect of $\overset{*}{\theta}$ and $\overset{**}{\theta}$ Terms on Lift, k = .05

Figure 4. Effect of Apparent Mass Terms on Lift, k = .05

Figure 5. Rotor Blade Model

Figure 6. Forced Response of Baseline Configuration

Figure 7. Hover Transients, k = .05, γ = 6, P = 1.0, μ = 0.0

Figure 8. Flap Eigenvalue Root Locus, k = .05, γ = 6, P = 1.0, μ = 0.0

Figure 9. Effect of Advance Ratio on System Damping, k = .05, γ = 6, P = 1.0

Figure 10. Effect of Collective Pitch on System Eigenvalues, k = .05, γ = 6, P = 1.0, $\bar{\mu}$ = 0.25

NINTH EUROPEAN ROTORCRAFT FORUM

Paper No. 58

COMPARISONS OF THREE NUMERICAL TRIM METHODS FOR ROTOR AIR LOADS

James A. O'Malley, III

US Army Aviation Research and Development Command
St. Louis, Missouri
USA

and

Amir P. Izadpanah and David A. Peters

Washington University
St. Louis, Missouri
USA

September 13-15, 1983
Stresa, Italy

Associazione Industrie Aerospaziali

Associazione Italiana di Aeronautica ed Astronautica

COMPARISONS OF THREE NUMERICAL TRIM METHODS FOR ROTOR AIR LOADS

James A. O'Malley, III

US Army Aviation Research and Development Command
St. Louis, Missouri
USA

and

Amir P. Izadpanah and David A. Peters

Washington University
St. Louis, Missouri
USA

ABSTRACT

Most rotor air loads programs are trimmed by an iterative process with two steps per iteration. In the first step, controls are guessed and the equations are integrated in time until all transients are decayed. In the second step, the controls are improved based upon the difference between the desired hub loads (thrust, propulsive force, side force) and the computed loads. As an alternative to numerical integration, however, recent papers have suggested a procedure called periodic shooting. The numerical shooting procedure can be used sequentially in the above, 2-step process; or it can be used in parallel with the control strategy as a unified trim method.

In this paper, these three trim methods (conventional, sequential shooting, parallel shooting) are applied to production-version rotor air loads programs. The convergence and efficiency of the methods are studied, and the converged results are compared with wind-tunnel data.

1. Introduction

Any calculation of rotor air loads requires the periodic solution to the rotor aeroelastic equations with a known set of control settings. Similarly, most dynamic stability calculations are based on perturbation equations written about a periodic equilibrium position. Therefore, calculation of rotor control settings and periodic response is a fundamental aspect of rotor analysis.

This calculation is not at all trivial, however. Even when the controls are known, it is not always easy to solve for the periodic solution. This is especially true when one or more system modes has small damping. In fact, however, the rotors controls are not known. Instead, what is known is the lift force, propulsive force, and side force desired for a flight condition. The pilot controls, therefore, also appear as unknowns in the problem.

In general, there are three categories of methods to solve for the periodic rotor response. These are: 1) Numerical Integration, 2) Periodic Shooting, and 3) Harmonic Balance. There are also three categories of methods for finding the control settings. These are: 1) Automatic Pilot, 2) Newton-Raphson,

and 3) Algebraic Control Equations. Each of the three response methods (1,2,3) is particularly suited for one of the three control methods (1,2,3) in the sense that they are compatible for application in a parallel strategy. For example, numerical integration and automatic pilot are applied in Reference 1; Shooting and Newton-Raphson are applied in Reference 2; and Harmonic Balance with Algebraic Control Equations is applied in Reference 3.

Despite this compatibility, however, most production version air loads programs use numerical integration coupled with Newton-Raphson (a rather incompatible combination). The purpose of this paper is to compare three methods: 1) the conventional numerical integration with Newton-Raphson, 2) the sequential application of periodic shooting with Newton-Raphson (without capitalizing on their compatibility), and 3) the parallel application of the two methods.

2. Background

2.1 The Transition Matrix

The first step in solution of a system of linear differential equations is the determination of the transition matrix $[\phi]$. Given a set of n linear equations of the form

$$\{\dot{x}\} = [A(t)]\{x\} + b(t) \tag{1}$$

where A(t) and b(t) are periodic with period, τ, the transition matrix, $[\phi]$, is defined such that, for b(t) = 0,

$$x(t) = [\phi(t)]\{x(0)\} \qquad 0 \leq t \leq \tau \tag{2}$$

This further implies that

$$[\dot{\phi}] = [A][\phi] \tag{3}$$

In practice $[\phi]$ can be found by numerical integration of equation (1) with b(t) = 0. For nonlinear systems, the equation of state will have the form

$$\{\dot{x}(t)\} = \{F(x,t)\} \tag{4}$$

It is often helpful to linearize these equations around a nominal or periodic equilibrium position $\{x_p\}$. This solution solves the equations

$$\{\dot{x}_p\} = \{F(x_p,t)\} \tag{5a}$$

$$\{x_p(0)\} = \{x_p(\tau)\} \tag{5b}$$

Now, we write equations for perturbations about $x_p(t)$.

$$x(t) = x_p(t) + \delta x(t) \tag{6}$$

where higher powers of δx are negligible compared to δx. Now if F(x,t) is smooth enough to have a Taylor series representation, then

$$\{F(x,t)\} = \{F(x_p,t_p)\} + \left[\frac{\partial f_i}{\partial x_j}\Big|_{x=x_p}\right] \{\delta x(t)\} \tag{7}$$

This leads to the equations

$$\{\delta\dot{x}\} = \left[\frac{\partial f_i}{\partial x_j}\right]_{x=x_p} \{\delta x\} \tag{8}$$

Then the transition matrix $[\phi(t)]$ can be found from sequential perturbations of each element of $\{x(0)\}$ by a small amount, say Δ away from $\{x_p(0)\}$. The resultant perturbed initial conditions can be used in Equation (4a), and integration through one period gives a solution $\{x(t)\}$ from which $\{\delta x(t)\}$ may be obtained by

$$\{\delta x(t)\} = \{x(t)\} - \{x_p(t)\} \tag{9a}$$

or

$$\{x(t)\} = \{x_p(t)\} + \{\delta x(t)\} \tag{9b}$$

The transition matrix may be formed by dividing the $\{\delta x\}$ columns by Δ and assembling them in $[\phi]$ such that

$$\{x(t)\} = \{x_p(t)\} + [\phi(t)]\ \{\delta x(0)\} \tag{10}$$

as in Equation (7).

2.2 Periodic Shooting

The method prescribed here, periodic shooting, utilizes the transition matrix $[\phi]$ to find a periodic solution in a direct way. The first step in this procedure (once $[\phi]$ is known) is to integrate Equation (1) through one period with zero initial conditions but with $\{b(t)\}$ retained. The resultant, non-periodic solution will be called $\{x_f\}$.

It follows from linearity that the general solution to Equation (1) is

$$\{x(t)\} = \{x_f(t)\} + [\phi(t)]\ \{x(0)\} \tag{11}$$

Now a periodic solution, $\{x(0)\} = \{x(\tau)\}$ can be immediately achieved from the initial conditions

$$\{x(\tau)\} = \{x_f(\tau)\} + [\phi(\tau)]\ \{x(0)\} = \{x(0)\}$$

$$\{x(0)\}\ [I - \phi(\tau)] = \{x_f(\tau)\}$$

$$\{x(0)\} = [I - \phi(\tau)]^{-1}\ \{x_f(\tau)\} \tag{12}$$

The resultant periodic solution is obtained from substitution of Equation (12) into Equation (11). The calculation in Equation (12) is called "periodic shooting" because the initial conditions are "aimed" so as to hit the target $\{x(\tau)\} = \{x(0)\}$. We should mention here that the calculation in Equation (12) is conceptually identical (but computationally much simpler) than the method described in Reference (4).

In the case of a nonlinear system, Equation (5a), the procedure is similar to that outlined above. For example, estimated initial conditions, $\{x_E(0)\}$, can be assumed and an integrated solution found $\{x_E(t)\}$, that is not periodic but is a first estimate of $\{x_p\}$. Thus the initial conditions can be modified in an attempt to make $\{x_E\}$ periodic.

$$\{x_p(0)\} = \{x_2(0)\} + [I - \phi(\tau)]^{-1}\{x_2(\tau) - x_2(0)\} \qquad (13)$$

The procedure can then be repeated with $x_2(0)$ generating a new estimate $x_2(t)$. Thus, the above algorithm can be utilized to find the periodic solution $x_2(t)$ to a nonlinear system. It should be noted that this is equivalent to a modified Newton-Raphson procedure to find the initial conditions that will result in a periodic solution.

Thus, the above method and time-wise integration (until all transients decay) stand as two alternative methods for the periodic response. The third method, harmonic balance, is not treated in this paper. Now, the complete rotor trim involves calculation of control settings and periodic response. Three possible means of effecting trim are outlined below.

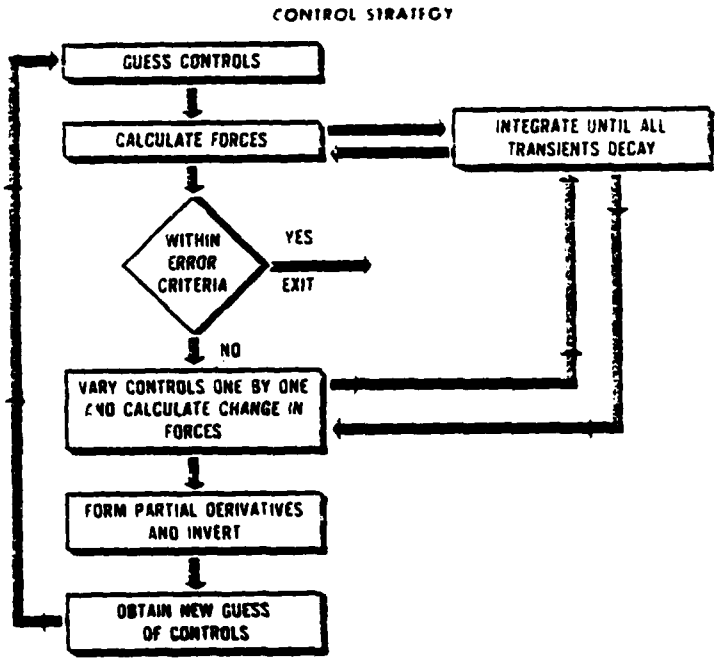

Figure 1. Flow Chart for Conventional Method

2.3 The Conventional Method

This is a method which uses a Newton-Raphson iteration procedure for convergence on controls (called control strategy) and integrates through time until a steady-state solution is found for the given initial conditions. A flow chart of this method is shown in Figure 1. It can be seen that, first, the controls are guessed. Second, the equations are integrated in time until a periodic solution is obtained (until all transients decay). Third, the forces are found. If they are within a certain error criteria, the program stops. If not, each control is perturbed; and, for each perturbation, integration in time is performed until transients decay. Fourth, a partial-derivative matrix is formed and new values for controls are found using a modified Newton-Raphson procedure.

$$\{\theta\}_{new} = \{\theta\}_{old} + \left[\frac{\partial F_i}{\partial \theta_j}\right]^{-1}\{F_{desired} - F_{actual}\} \qquad (14)$$

In some airloads programs only an approximate version of $[\partial F_i/\partial \theta_j]^{-1}$ is used. Approximations include: 1) neglect of diagonal terms, 2) closed form approximations, and 3) pseudo inverses. These approximations may save computation for each iteration, but at the possible expense of requiring more total iterations.

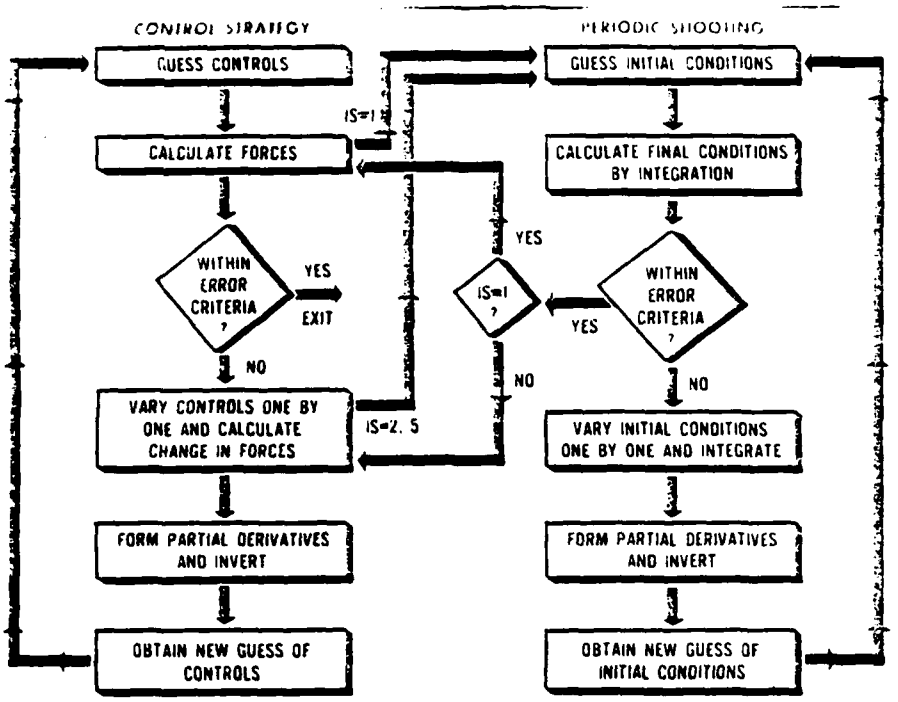

Figure 2. Flow Chart for Sequential Method

2.4 The Sequential Method

In the sequential method of periodic shooting, the right block in Figure 1 is replaced by the shooting algorithm described previously. This is depicted in Figure 2. A convergence criteria must be applied to the shooting algorithm. This is done as follows. A solution is considered to be converged when the error between each of the state variables at $\Psi = 0$ and $\Psi = 2\pi$ is less than some chosen value. Thus, every time the block diagram calls for a periodic solution (i.e., at every control perturbation), a new convergence is required on initial conditions.

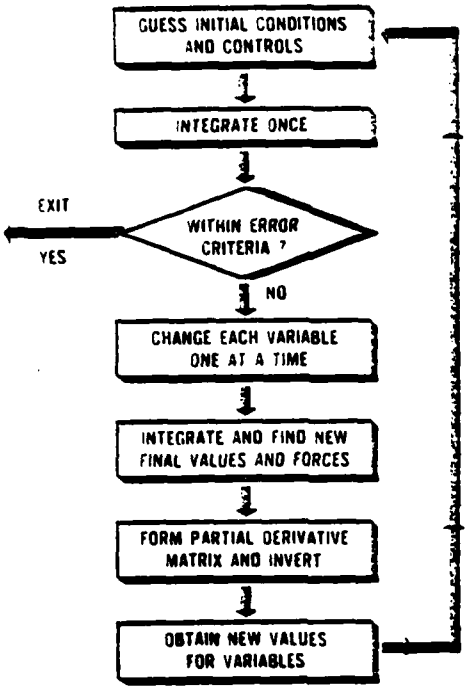

Figure 3. Flow Chart for Parallel Method

2.5 The Parallel Method

In this method the iterations on control variables and initial conditions in Figure 2 are combined into one scheme that iterates simultaneously on controls and periodicity. The procedure is similar to the former algorithm except that a single partial derivative matrix is obtained that includes the changes in forces and periodicity with respect to control settings and initial conditions. The flow chart for this refined method is given in Figure 3. Here, we have capitalized on the fact that both strategies (controls and periodic solution) are Newton-Raphson procedures. Thus, it makes sense to combine these into a single Newton-Raphson scheme with both controls and initial conditions as unknowns.

3. Application to Production Program

3.1 Discussion of Rotor Loads Basis

A test of the above described methods is provided by application to a rotor loads and performance analysis that has been developed as a subroutine for use within the AVRADCOM, Applied Technology Laboratory (ATL) V/STOL Preliminary Design Program. The importance of an efficient iteration method within a preliminary design process becomes evident as the analysis is permitted to allow more and more design variables to be considered. The basis for the applied rotor analysis is documented in the cited References 5, 6.

The basic equations are for a rigid hinged blade with hinge offset. Only flapping dynamics are considered. Calculation of the rotor loads requires the airfoil section lift and drag characteristics as well as the resultant velocity. The airfoil section characteristics are provided for section angles of attack from -180° to 180° for Mach numbers from 0. to 1.0. The use of basic steady airfoil lift and drag measured as a result of 2- dimensional transonic wind

tunnel tests is done with confidence along most of the rotor blade span. However, three separate adjustments are required to account for air flow and blade motion which can become significant depending upon the rotor operating regime. The first of these adjustments is a so-called tip relief model, derived in Reference 7, which accounts for the reduced compressibility existing in the 3-dimensional flow near the tip of a lifting surface. The tip relief model is based upon the potential representation of the thickness effect of an airfoil by a source-sink distribution. The thickness effect can be thought of as a qualitative explanation for tip relief in the sense that 2-dimensional flow requires greater displacement in a perpendicular direction than 3-dimensional flow about a finite tip. Therefore, there results a relief in the flow about the tip as compared to the 2-dimensional flow. The potential function is formulated for a finite wing by subtracting the functions for complementary wings on both sides from the function for an infinite wing (2-dimensional airfoil). Formulation in this manner relates the velocity on the 2-dimensional airfoil to that on the finite wing.

The second adjustment to the 2-dimensional airfoil data is intended to account for the radial flow conditions that exist on a rotor blade due to its yawed position present for much of the azimuthal circuit. The significant features of this method (Reference 8) include an estimate for the increased skin friction drag due to the use of the resultant velocity acting at a yaw angle to the blade element and a stall delay due to an increased lift capability evidenced in yawed flow experiments on various wings.

The third adjustment to the basic wind tunnel tested airfoil data is an approximation of the stall hysteresis with lift overshoot that occurs as a result of an airfoil oscillating near stall. The cyclic pitch variation required by a conventional rotor system causes this unsteady airfoil characteristic to have a significant effect upon calculations when the operating condition allows appreciable stall. The formulation, detailed in Reference 8, is based upon tests of four airfoil sections from 6% to 12% thick. Derived from these tests are the stall delay angles as a function of a dimensionless parameter, $\sqrt{C\dot{\alpha}/2V}$ (analogous to the reduced frequency parameter) where C = blade chord and V = local velocity. Linear functions have been developed for a stall delay parameter which depend on the airfoil thickness, Mach number, $\sqrt{C\dot{\alpha}/2V}$ parameter, and whether it is lift or moment stall which is being examined. The moment stall formulation is used to determine the unsteady drag coefficient. Reference 9 shows this to be a good approximation.

The non-dimensional integral expressions for the three rotor forces (thrust along rotor shaft, and propulsive force and side force, perpendicular to each other and the rotor shaft) are derived from the resolution of the airfoil force coefficients as they vary along the rotor blade. The integral spans the distance from the root cutout $\bar{r}_c$ to the tip (1). Tip losses, or the approximation of the loss of lift due to the finite blade, are approximated by

setting lift = 0.0 at $\bar{r}$ = 1 and assuming a linear variation in the lift from $\bar{r}$ = .97 to $\bar{r}$ = 1. The drag force coefficient used at $\bar{r}$ = 1 is that which has been calculated as a result of applying the above summarized tip relief method at lift = 0.0.

3.2 Application of Iteration Methods

The application of the procedure summarized above requires an iteration method to solve for the required rotor forces and the accompanying steady-state rotor blade motion. Specifically, the ATL V/STOL Preliminary Design Program requires rotor torque and tip path-plane inclination when given the rotor forces. The iteration method must provide convergence of magnitude and direction upon the resultant of rotor lift, propulsive force and side force (Figure 4). This is done by adjusting collective pitch (θ_o), longitudinal cyclic angle (θ_s), and lateral cyclic (θ_c). Steady state blade flapping magnitude and velocity must be attained. Three methods of iteration have been applied to investigate the relative efficiency of each in achieving convergence through the variation of the five variables.

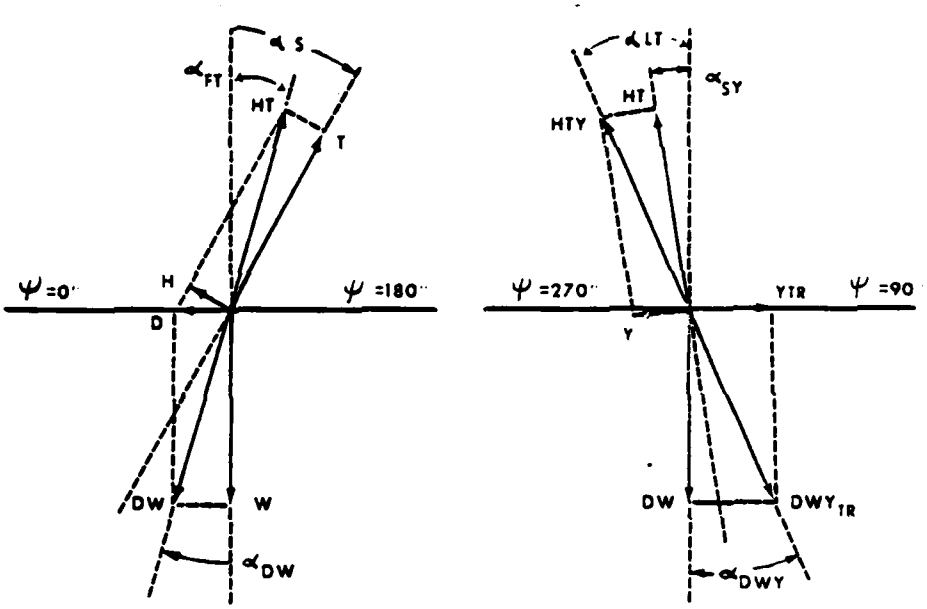

Figure 4. Force Vectors

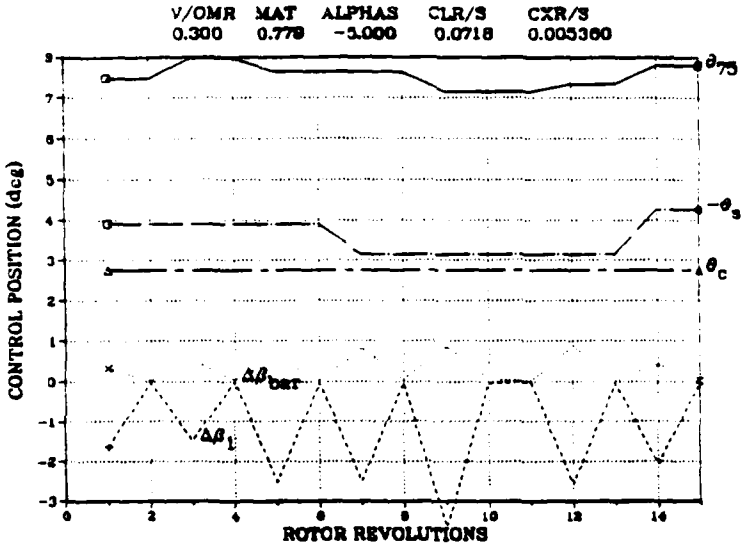

Figure 5. Step by Step Conventional Method

1) Step by step conventional method: This first method (Figure 5) steps through each one of the variables, insuring convergence within a specified tolerance before proceeding to the next variable. Steady State flapping is calculated first and then Θ_o is incremented toward the resultant vector magnitude convergence. Total force is not integrated until a steady state flapping is achieved. When the force magnitude is converged, Θ_s is incremented toward the vector direction required. The vector magnitude is then checked and then reiterated until it again is converged. This procedure is repeated until both magnitude and direction are correct. At this point, Θ_c is incremented and when the results of this perturbation are available, tests are made to check the previously achieved convergence on Θ_o and Θ_s. If this test shows non-convergence the procedure is repeated from the point of non-convergence. Extrapolation and interpolation are accomplished in small enough linear steps so as to approximate the non-linearities of the problem. When enough consistent perturbations have been accomplished, the step by step procedure is deviated upon, in that when one control is incremented, enough is known about the sensitivities so that the other controls can be changed at the same time. Thus the off-diagonal terms (coupling terms) of the inverse matrix can be included. Upon changing Θ_s:

$$\theta_o = \theta_{o_1} + (\alpha_{DW} - \alpha_{FT_1})(\theta_{o_2} - \theta_{o_1})/(\alpha_{FT_1} - \alpha_{FT_2}) \qquad (15)$$

Upon changing θ_c:

$$\theta_o = \theta_{o_1} + (\alpha_{DWY} - \alpha_{LT_1})(\theta_{o_2} - \theta_{o_1})/(\alpha_{LT_2} - \alpha_{LT_1}) \qquad (16)$$

$$\theta_s = \theta_{s_1} + (\alpha_{DWY} - \alpha_{LT_1})(\theta_{s_2} - \theta_{s_1})/(\alpha_{LT_2} - \alpha_{LT_1}) \qquad (17)$$

where 1 and 2 are from magnitude or direction converged conditions.

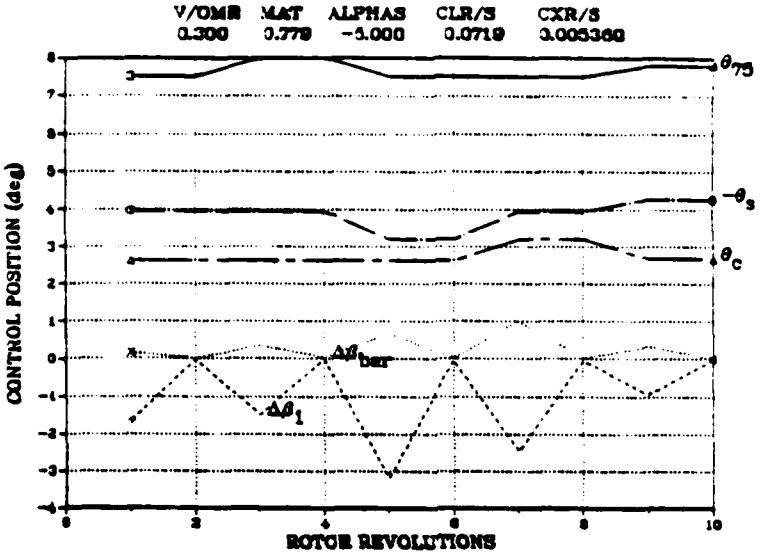

Figure 6. Newton-Raphson Sequential Method

2) Sequential Newton-Raphson: This method (Figure 6) requires the establishment of a matrix of slopes representing the sensitivity of the rotor forces to the isolated perturbation of each of the control variables. This matrix is applied, through inversion, to the Newton-Raphson equation to achieve simultaneous convergence. The method is termed Sequential because each perturbation requires first the convergence of flapping displacement and velocity. Flapping convergence is achieved through periodic shooting with the first perturbation being the value found from numerical integration. If an accurate first estimate is possible for the flap motion, numerical integration will yield a periodic solution within two revolutions for a practical articulated rotor. For the two variables included in this problem, sequential periodic shooting would require four rotor revolutions to establish the required matrix and then another (minimum) to converge, for a total of five revolutions. Because convergence is tested for every perturbation, the Newton-Raphson sequential integration (conventional method) is superior, in this application, to the Newton-Raphson sequential shooting technique. Sequential shooting would be advantageous for more blade motion degrees of freedom. When all the control variables are perturbed and the simultaneous solution of all the variables does not result in convergence, two variations of matrix update are possible. The first variation checks to see which parameter is furthest from convergence and then allows a perturbation of this single variable in order to update only the one affected matrix column. A new estimation is then made for all the variables and convergence is retested. The second variation requires perturbation of each of the variables when convergence is

not achieved, thus resulting in a completely updated matrix. This second variation is the procedure for which results are presented.

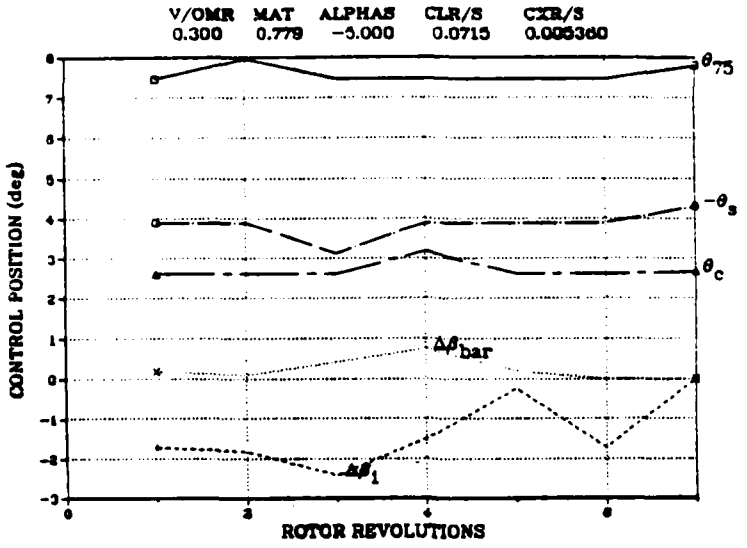

Figure 7. Newton-Raphson Parallel Shooting

3) Parallel Newton-Raphson shooting: This method (Figure 7) extends the sequential method to include in the Newton-Raphson formulation, the periodic blade motion variables. Isolated perturbation of each of the variables is used to construct a combined matrix of slopes representing the sensitivity of both the forces and periodic blade motion. The term "parallel" then, refers to the fact that the periodic blade motion is being iterated upon at the same time as the integrated force magnitude and direction.

3.3 Method of Application

Each of the above three methods has been used, on an equal basis, in conjunction with the rotor loads and performance method summarized above. An equal basis of comparison is assured by the use of the same estimates for the starting values of the control variables. For each series of calculations (each rotor shaft angle at a particular advance ratio) the first point uses the estimates for control angles and blade motion based on a closed form solution. The subsequent points use this same closed form solution for the angles, but the estimate is modified based on the differences between the initial values and the converged values for the previous point. Improvements to this scheme would include extrapolating the converged controls (angles and blade motion) based on the previous two values. The convergence criteria is the same for all cases: 1% of resultant force magnitude; 1% of resultant force direction; 10% of rotor side force; 1% of blade flapping angle and velocity (except for small angles the tolerances for which is .001 radians). These convergence criteria are small enough such that a consistent set of data can be calculated. Overall rotor performance is relatively insensitive to side force, so the larger tolerance is acceptable.

Each perturbation includes a tolerance test on every required variable, so each time a perturbation is required, the control is perturbed in the direction toward convergence. Each time the controls are calculated as a result of the complete matrix update, they are saved to be used with their previous counterparts to predict the next value used during the subsequent perturbations. An important consideration during calculation for cases near the analytical lift limit for the rotor is to limit the extrapolated control predictions in order to avoid a condition too far into stall (beyond the required condition). The two Newton-Raphson methods which produced the results shown here do not include specific tests to contend with predictions which overshoot the target and end up too far into stall. This would be a problem only if the predicted controls required calculations in the area of the second lift rise at very high angles of attack, since the slopes would indicate iterations to even higher angles of attack. The overshoot at conditions near "maximum" lift is most critical for the step-by-step conventional method since convergence is accomplished for each individual control variable (its related force, direction, or motion) while the remaining variables are held constant. This means that, if, for some reason, the combination of controls becomes unreasonable, a false indication of lift required being greater than lift available will result. For this reason some checks are required which result in a restart at a more reasonable value for the step-by-step method.

4. Results

4.1 Preliminary Investigations

Before proceeding to the results for a production airloads program, it is interesting to compare results for a research oriented response problem as given in Reference 2. Three separate assumptions can be established for a comparison of periodic shooting with numerical integration (solution of equations of motion until tranients decay). Figure 8 illustrates the boundaries established when these assumptions are coupled to a knowledge of the stability of problem. For the sake of comparison, it is assumed that each method starts with a first guess of the initial conditions (often zero), having an error, E_0. Each method must then be pursued until a desired error, E is reached. It is also assumed that the equations are nonlinear so that the shooting method requires several iterations. For the controls known case, Figure 8 shows that for 10% damping, such as is typical of articulated rotors with dampers, direct numerical integration is always preferred, even for only one degree of freedom. For hingeless rotors, however, for which as little as 1% damping is typical, direct integration is superior only when more than 16 degrees of freedom are present. For damping less than 0.1%, as is typical in stability work, direct integration is generally inferior to the present method of periodic shooting.

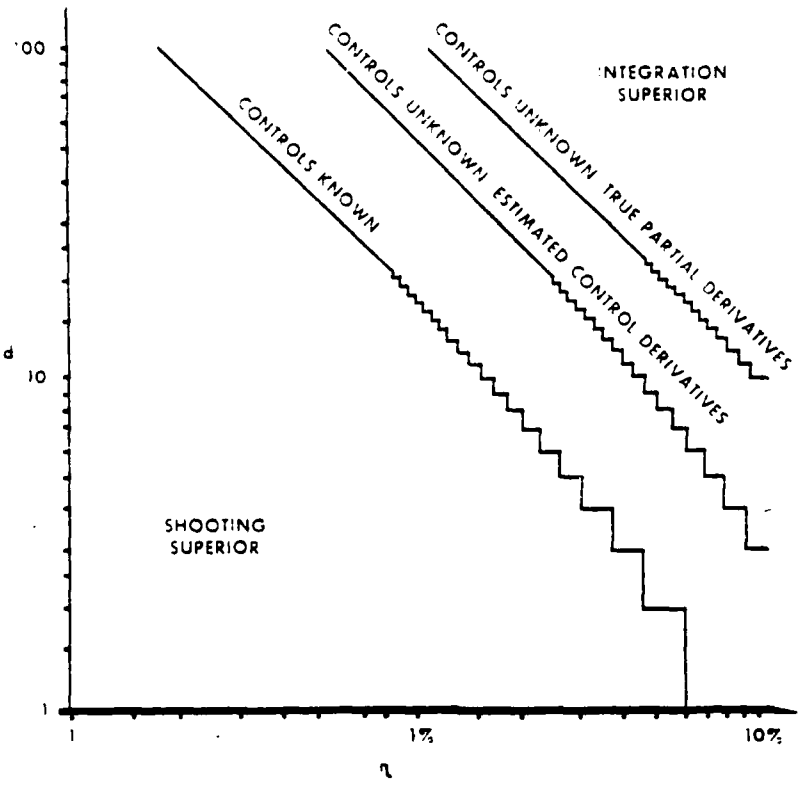

Figure 8. Comparison of Numerical Integration and Periodic Shooting

For the case when the controls are not known, the above comparison must be modified to include the fact that controls and initial conditions are found simultaneously by the combined Newton-Raphson shooting method, but are found sequentially when Newton-Raphson is coupled with direct integration. Figure 8 shows for the comparison between shooting and direct integration becomes more favorable for periodic shooting when the controls must be found. For typical articulated rotors (damping 10%) shooting is superior for less than 10 degrees of freedom and for typical hingeless rotors (damping 1%)shooting is superior for less than 100 degrees of freedom. Thus there is a great potential advantage of the shooting method over numerical integration even for large problems.

Finally, it might be argued that the potential advantage of direct integration would increase if direct integration were used with only an estimated set of partial derivatives. However, as seen in Figure 8, even for estimated derivatives, it has been found that there is still a favorable trade-off between shooting and integration.

Thus, the relative advantage of shooting is enhanced for systems with low damping. For unstable systems, (damping less than 0.0) direct integration cannot be used and so, periodic shooting (or some other method) is necessary.

4.2 Direct Applications

In order to provide a comparison of the relative efficiencies of the iteration procedures which would be indicative of what is required to undertake a complete rotor loads and performance analysis, calculations have been made of an advanced rotor design for which wind tunnel data is available (References 10, 11, 12). The simulation of the rectangular planform rotor (baseline) requires the ability to include three airfoil data tables with interpolation between adjacent ones to represent transition section characteristics (Figure 9). The airfoil data tables consist of data measured in a transonic wind tunnel at Reynolds numbers which are representative of the full scale rotor test.

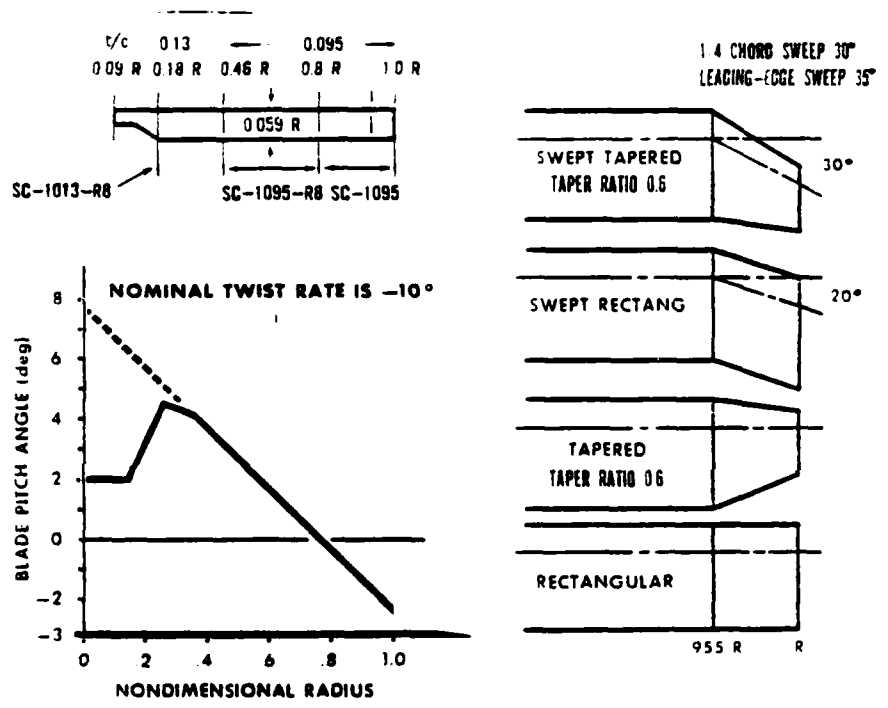

Figure 9. Blade and Tip Geometry

Figures 10, 11 and 12 illustrate the range of rotor test conditions and the number of points which were calculated to provide a comparison. The actual reported test point values (lift, drag, side force and shaft angle) are used as the calculated trim valves. This not only exercises the trim procedures to the maximum possible extent for this analysis, but also insures the calculation of the actual rotor condition as measured in the test. Although the calculated value of the relative rotor power does not, in all cases, correlate well with the test value, the trends are quite representative for the range from the autorotative to the propulsive state of the rotor.

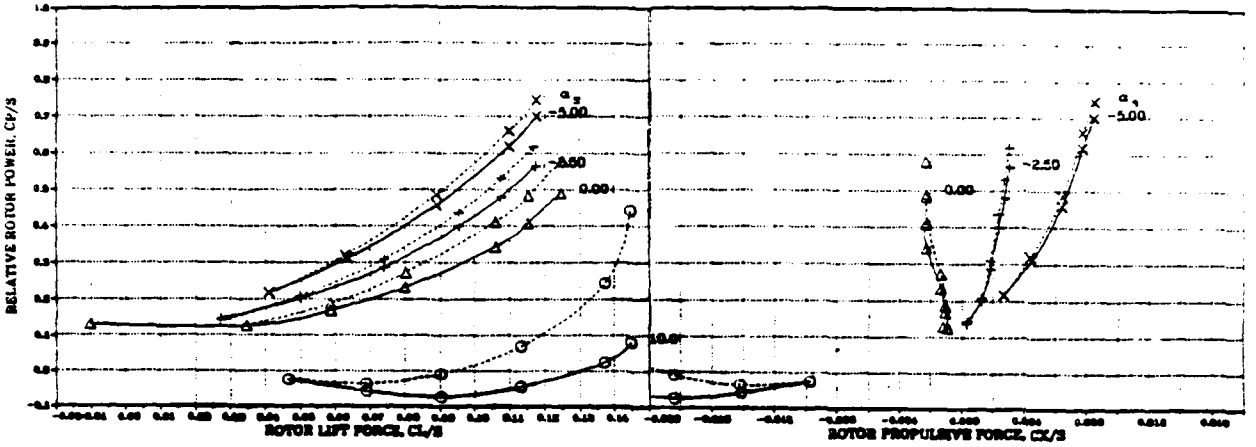

Figure 10. Advance Ratio = .2, Advancing Tip Mach Number = .72

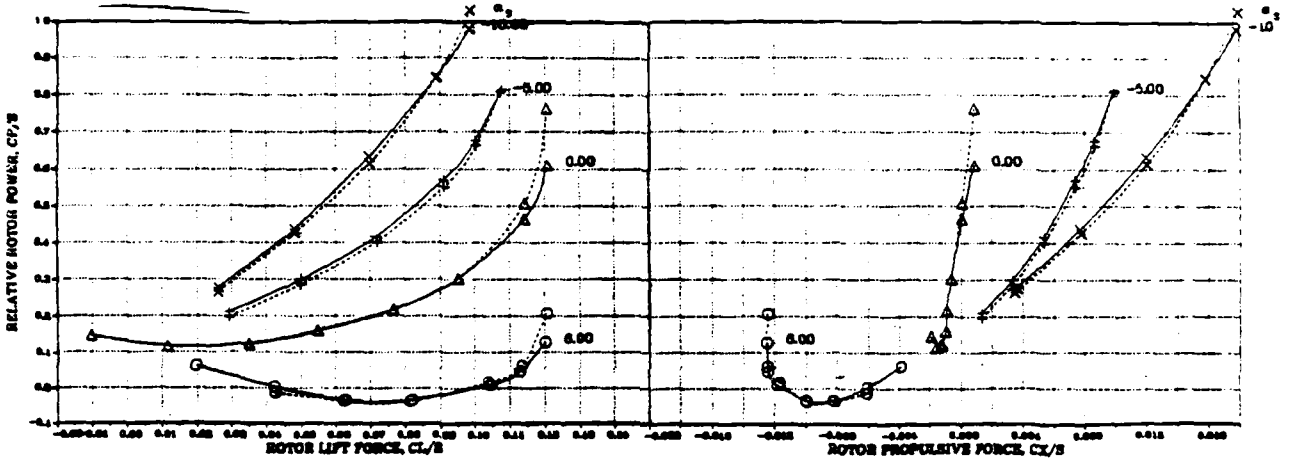

Figure 11. Advance Ratio = .30, Advancing Tip Mach Number = .78

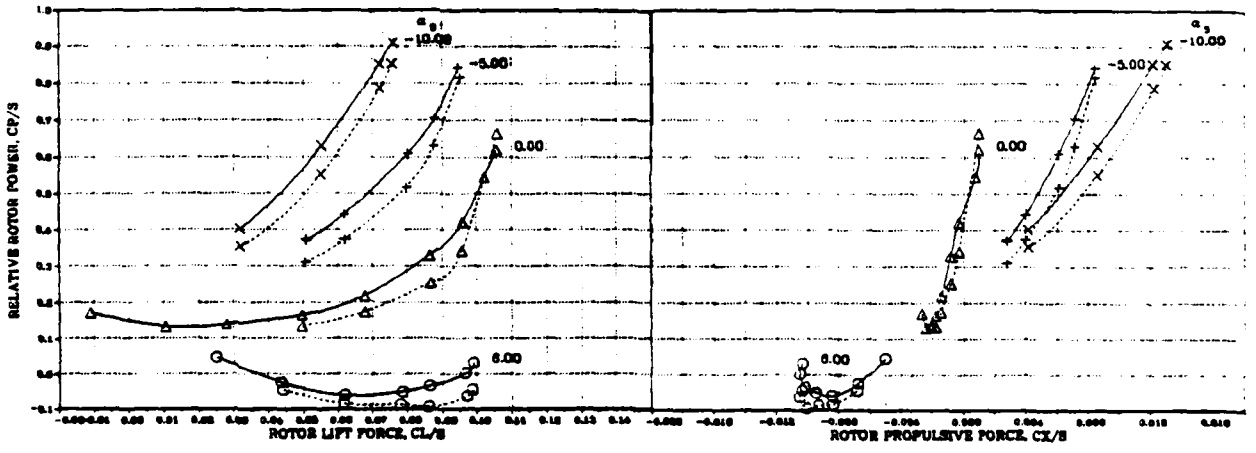

Figure 12. Advance Ratio = .375, Advancing Tip Mach Number = .825

Correlation can be obtained through the adjustment of profile drag and inflow velocity. The profile drag increment would account for the differences between the wind tunnel airfoil and the full scale section (small imperfections). The inflow velocity varible adjustment can be used (References 13, 14) to adjust the slope of the variation of relative rotor power with advance ratio. Through the comparison of the analysis with the full range of the test results, it is insured that the trim iteration methods are exercised to their useful limits. The test results represent a helicopter rotor at its maximum lift and propulsive force limits (within the power required limit of the test facility) for a wide range of inflow conditions.

A summary of the rotor revolutions required for each case is shown in Figure 13 for a comparison of each of the trim iteration methods. It is apparent that for this analysis, the Newton-Raphson and Shooting methods are superior in an overall reliability and efficiency sense. However, it is interesting to note that the parallel shooting method fails to converge at some isolated cases for a very high lift condition, where the other two methods are successful.

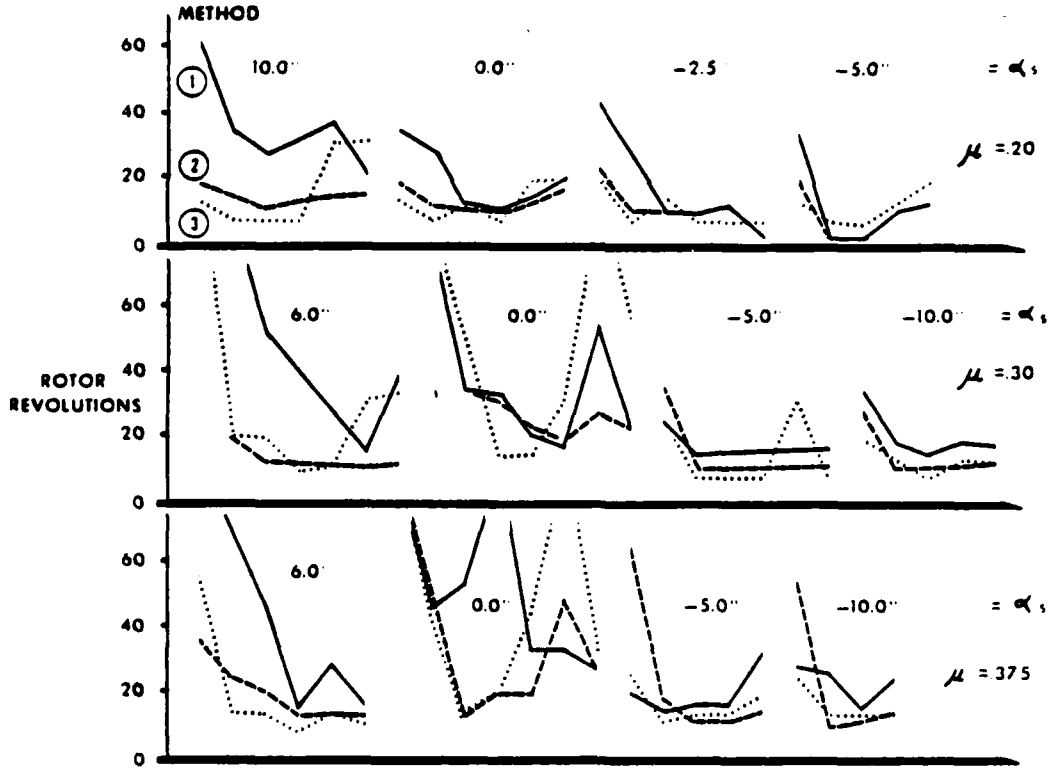

Figure 13. Summary of Convergence

5. Conclusions

The shooting method can be applied to an existing airloads program with a moderate amount of program changes. Many airloads programs are set up to remain in the azimuth loop until blade motion transients decay. This loop must be interrupted to allow only one revolution per perturbation and the resulting partial derivative then added to the matrix for the Newton-Raphson method.

For this example, parallel shooting is superior to the conventional method for about 50% of the cases. This is consistent with earlier estimates for a system with 1 Degree of Freedom and 14% damping.

The use of an approximate Partial Derivative Matrix is not satisfactory and requires an average of 2 - 8 times as many iterations as when using the full matrix.

No unusual convergence problems were encountered. The parallel shooting method and the conventional method generally failed to converge for the same cases (about 6% of the time).

The sequential application of shooting is generally much less efficient than the parallel application, requiring 3 to 4 times as many rotor revolutions.

The periodic shooting technique can be successfully applied to a rotor airloads program which includes detailed aerodynamics and dynamic stall, to calculate the full range of performance of an advanced technology operational helicopter rotor.

6. References

1) David A Peters, Byung S. Kim and Han-Sheng Chen: Calculation of Trim Settings for a Helicopter Rotor by an Optimized Automatic Controller. Journal of Guidance, Control and Dynamics Vol. No. 1, July 1983.

2) David A Peters and Amir P. Izadpanah: Helicopter Trim by Periodic Shooting with Newton-Raphson Iteration. Proceedings of the 37th Annual National Forum of the American Helicopter Society, New Orleans, May 1981, Paper 81-23.

3) Tung-Kuang Hsu and David A. Peters: Coupled Rotor/Airframe Vibration Analysis by a Combined Harmonic-Balance, Impedance Matching Method. Journal of the American Helicopter Society, Vol. 27, No. 1, January 1982, pp 25-34.

4) S.B.R. Kottapalli and P.P. Friedmann: Aeroelastic Stability and Response of Horizontal Axis Wind Turbine Blades. Presented at the 2nd International Symposium on Wind Energy Systems, Amsterdam, October 3-5, 1978.

5) Harris, et al: Helicopter Performance Methodology at Bell Helicopter Textron. Proceedings of the 35th Annual National Forum of the American Helicopter Society, Washington, May 1979.

6) Gessow, A. and Meyers, Garry C.: Aerodynamics of the Helicopter. Frederick Unger Publishing Co., New York, 1967.

7) J.M. LeNard and G.D. Boehler: Inclusion of Tip Relief in the Prediction of Compressibility Effects on Helicopter Rotor Performance. USAAMRDL Technical Report 73-71, December 1973.

8) R.E. Gormont: A Mathematical Model of Unsteady Aerodynamics and Radial Flow for Application to Helicopter Rotors. USAAMRDL Technical Report 72-67, May 1973.

9) K.W. McAllister et al: An Experimental Study of Dynamic Stall on Advanced Airfoil Sections, Vol. 2 Pressure and Force Data. USAAVRADCOM TR-82-A-8, September 1982.

10) R.H. Straub, et al: Rotor Blade Tip Shape Effects on Performance and Control Loads From Full-Scale Wind Tunnel Testing. Journal of the American Helicopter Society, October 1979.

11) D.T. Balch: Correlation of Full Scale Wind Tunnel Test Data with Model Rotor Test Data and Theory for a Modern Helicopter Main Rotor. Journal of the American Helicopter Society, July 1979.

12) W. Johnson: Performance and Loads Data From a Wind Tunnel Test of a Full-Scale Rotor with Four Blade Tip Planforms. USAAVRADCOM TR 80-A-5, September 1980.

13) W. Johnson: A Comprehensive Analytical Model of Rotorcraft Aerodynamics and Dynamics, Part I: Analysis Development. USAAVRADCOM TR 80-A-5, June 1980.

14) C.N. Keys: Rotary Wing Aerodynamics, Vol II - Performance Prediction of Helicopters. NASA Contractor Report 3083, January 1979.

Acknowledgement: This work was sponsored by the United States Army Research Office, Grant No. DAAG-29-80-C-0092. The view, opinions, and/or findings of this report are those of the authors and should not be construed as an official Department of the Army position, policy, or decision, unless so designated by other documentation.

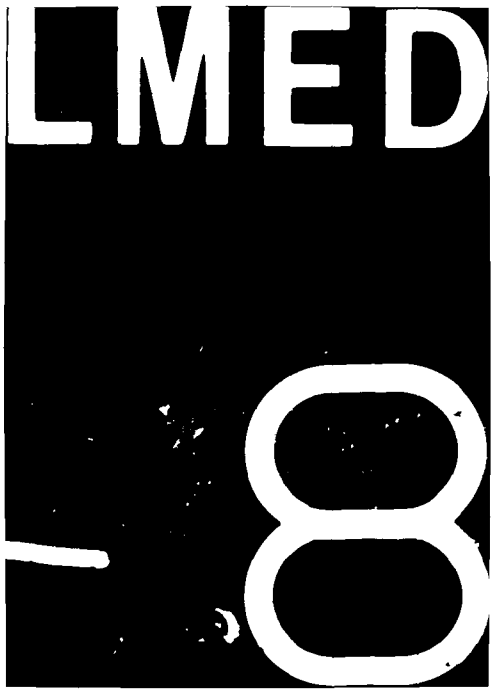
LMED
8